EVALUATION OF WHEEL LOADING IN THE GRINDING OF STEELS, BRASS AND ALUMINIUM

By

R. S. SHAH

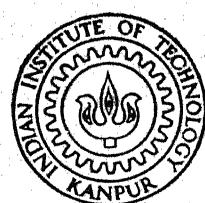DEPARTMENT OF MECHANICAL ENGINEERING
INDIAN INSTITUTE OF TECHNOLOGY, KANPUR
SEPTEMBER, 1977

EVALUATION OF WHEEL LOADING IN THE GRINDING OF STEELS, BRASS AND ALUMINIUM

A Thesis Submitted
In Partial Fulfilment of the Requirements
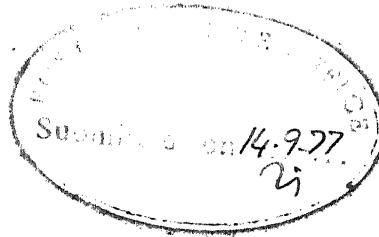for the Degree of
MASTER OF TECHNOLOGY

By
R. S. SHAH

to the
DEPARTMENT OF MECHANICAL ENGINEERING
INDIAN INSTITUTE OF TECHNOLOGY, KANPUR
SEPTEMBER, 1977

ME-1977-M-SHA-EVA

CERTIFICATE

     This is to certify that the present work entitled 'Evaluation of Wheel Loading in the Grinding of Steels, Brass and Aluminium', has been carried out by Mr.R.S. Shah under my supervision and has not been submitted elsewhere for the award of a degree.

Rakesh Chawla

(R. Chawla)
Assistant Professor
Mechanical Engineering Department
Indian Institute of Technology
Kanpur

September, 1977

ACKNOWLEDGEMENTS

CONTENTS

LIST OF FIGURES

LIST OF TABLES

LIST OF PLATES

NOTATIONS

C	No. of cutting points/unit length of wheel surface.
d	Dept. of cut, or down feed (mm).
D	Wheel diameter (mm)
F_n	Normal force (Kgf)
F_t	Tangential force (Kgf)
r	Width-to-depth ratio of an average cut
t	Undeformed chip thickness (mm)
v	Table speed (m/min)
V	Wheel speed (m/min)
$V_{\ell 55mm^3}$	Loaded volume corresponding to 55 mm^3 of material removal (mm^3)
$V_{\ell 150mm^3}$	Loaded volume corresponding to 150 mm^3 of material removal (mm^3)
$V_{\ell 40mm^3}$	Loaded volume corresponding to 40 mm^3 of material removal (mm^3)
$V_{\ell 150 P}$	Loaded volume corresponding to 150 passes (mm^3)
$V_{\ell 40 P}$	Loaded volume corresponding to 40 passes (mm^3)
$V_{\ell 15 sec}$	Loaded volume corresponding to 15 secs. of grinding (mm^3)
$V_{\ell 4 sec}$	Loaded volume corresponding to 4 secs. of grinding (mm^3)
V_r	Volume of material removed (mm^3).

ABSTRACT

Using radiotracer methods, wheel loading studies have been conducted in the grinding of steel, brass and aluminium workpieces, with both alumina and silicon carbide wheels.

The possibility of generating alternative radiotracers for such studies was established, for each material, by using two different methods of neutron activation of the workpieces, viz. thermal neutron irradiation in a research reactor and 14 MeV neutron irradiation using an accelerator source.

Grinding experiments were conducted for each work/wheel combination over a range of table speeds and depths of cut, under dry plunge-cut conditions. Absolute loading results were deduced by applying an extrapolation method to singles γ-counting of the activity on the wheel's cutting surface.

For steel and brass work specimens, the amount of loaded material was found to increase rapidly at first and then at a slow, steady rate. For aluminium, on the other hand, there was rapid increase of the loaded volume to a very much higher value.

In order to study the variation of wheel loading with grinding parameters, three different criteria were considered for each work/wheel combination, viz. corresponding to a fixed

volume removed, a fixed number of passes, and a constant
grinding time. The last mentioned criterion was found to
yield more consistent results than the other two.

CHAPTER I

INTRODUCTION

Grinding is one of the most important manufacturing processes by which metal may be removed and a good surface finish obtained. In precision-production grinding operations, the objective is to obtain the product to close size tolerances with a specified degree of surface finish, and at minimum cost. In order to achieve this objective, it is necessary to develop techniques for the accurate measurement of process variables such as wheel wear, chatter vibration, surface finish, wheel loading, etc., so that optimum grinding conditions may be established for a given operation. Wheel loading phenomena have been studied in the present work, in the grinding of steels, brass and aluminium, by applying radiotracer techniques of measurement.

1.1 Grinding Wheel Loading:

During grinding, the cutting surface of the wheel and the workpiece surface are in a state of active physical and chemical interaction with each other and with the ambient medium (air or cutting fluid). In the course of the operation, the cutting efficiency decreases due to attritious wear of the abrasive grits (formation of 'flats') and/or the loading

of foreign material into the porous surface of the grinding
wheel.

The wheel loading may be of two types, viz.
(a) gum loading, with the cutting fluid depositing a gummy
deposit on the wheel surface, (b) metallic loading, wherein
pores on the cutting surface are filled with metal particles,
leaving insufficient space for chip clearance.

Increased loading leads to several undesirable effects,
such as reduction in material removal rate, generation of
excessive heat, surface deterioration of the workpiece and
increased instability due to chatter vibration. The life of
a grinding wheel is thus directly affected by excessive loading.

Several conventional methods have been reported for the
measurement of wheel loading, but these are found to have
certain drawbacks, such as painstaking sample preparation
and the difficulty of obtaining accurate absolute results.
These drawbacks are absent in the radiotracer technique, wherein
neutron-activated work samples are employed.

1.2 The Present Work:

In the present study, wheel loading measurements have
been carried out, using the radiotracer technique, in grinding
experiments for steel, brass and aluminium workpieces, with
both alumina and silicon carbide wheels.

The generation of γ-emitting radiotracers was carried out in two different ways for each work material, viz. thermal neutron activation using reactors at BARC and 14 MeV neutron activation using the Van de Graaf at IIT Kanpur. The two different methods of radiotracer generation were found to have their own, respective advantages. A few experiments were conducted to establish the equivalence of loading results deduced from measurements with the two 'alternative' radiotracers generated for each work material.

Grinding experiments were conducted for each work/wheel combination over a range of table speeds and depths of cut, under dry plunge-cut conditions. The growth of loaded material on the wheel surface was studied by singles γ-counting of the wheel activity. Absolute loading results were deduced, in each case, by an extrapolation method involving the use of small, reference pieces of work material.

For steel and brass work specimens, it was found that the amount of loaded material increases rapidly at first and then at a much slower, but steady, rate. In the case of aluminium, however, it was found that the volume of loaded material increases rapidly to a very much higher value than for steel or brass, indicating an approach to 'saturation' of the wheel's porous surface.

The variation of loading with various parameters, viz. table speed, depth of cut, material removal rate, chip thickness and grinding forces, was studied. For doing this, a suitable criterion for loading had to be established. Accordingly, for each work/wheel combination, three different loading parameters were considered - one corresponding to a fixed volume removed, a second to a fixed number of passes, and the third to a constant grinding time. The experimental results have indicated that a loading criterion corresponding to a constant grinding time is probably the most appropriate for such studies.

CHAPTER II

GENERAL REVIEW AND ADOPTED EXPERIMENTAL PROCEDURES

2.1 Grinding:

In grinding, metal is removed by a shearing process.
It may be described as a multi-tooth operation in which a
large number of abrasive grits, held by a bonding material,
perform the cutting. Grinding is usually applied in removing
small amounts of material from previously machined parts to
achieve desired tolerances. However, improvements made in
recent years in the quality of wheels and machines and
developments in the manufacture of blanks (rolling, drop-
forging, investment and other precision-casting processes)
have resulted in grinding being applied for stock removal, as
well as finishing.

When compared with other metal-cutting processes, grind-
ing is seen to have certain unique characteristics, e.g. the
random grit geometry, high cutting speeds and small depths
of cut, which make the mechanisms involved very complex
and difficult to evaluate.

2.1.1 Grinding Wheel Types:

A grinding wheel is a bonded abrasive body consisting
usually of aluminium oxide or silicon carbide abrasive grits

in a matrix of ceramic, resionoid or rubber bond. The ceramic
or vitrified bond is the most common type. Silicon carbide
crystals are very sharp and extremely hard, but their general
usage as an abrasive is limited by their brittleness. Thus,
SiC grinding wheels are recommended for material of low tensile
strength, e.g. cast iron, brass, bronze and cemented carbides.
While alumina is slightly softer than silicon carbide, it is
much tougher and possesses high shock resistance. It is re-
commended for materials of high tensile strength, e.g.
hardened steel, high-speed steel and other alloy steels.

The grade of a wheel is a measure of the amount of bond
supporting the grinding grits and is thus also a measure of
bond-post strength. It follows that a harder grade wheel
will permit the abrasive grains to become duller prior to
bond-post rupture, hence causing the wheel to assume a less
free cutting equilibrium condition than would be the case
for a softer wheel. The grade of a wheel is denoted by a
letter of the alphabet (A to Z, in order of increasing
hardness).

The structure of a grinding wheel is related to the
grit-spacing, and thus to available chip clearance space.
For the same amount of bond material (same grade), a more
dense wheel will tend to act somewhat harder than one of
open structure. Opening the structure of a wheel will cause

it to cut more efficiently. The maximum grit spacing is, however, limited by bond-post strength since a wheel with too open a structure will be too soft and will wear rapidly making it uneconomical to use. Wheel structure is designed by a number between 1 (dense) and 12 (open).

The other important specification for a grinding wheel is the mean grit size, denoted by a number in the range 6 to 24 (coarse), 30 to 60 (medium), and 70 to 600 (fine).

As an example of wheel designation, one may consider the following wheel, manufactured by Grindwell-Norton

38A	60	K	5	V	BE
Identifies the type of abrasive grit (alumina)	Grit size	Grade	Structure	Vitrified	Specific Type of Vitrified bond

2.1.2 Truing and Dressing of Grinding Wheels:

After a certain period of use a grinding wheel becomes" lo
At this stage, the wheel's circular contour has to be regenerate
This is usually termed 'truing' the wheel. During a truing operation, the wheel is subjected to very severe con-ditions, which result in removal of abrasive grits and bond material and in the exposure of now cutting edges. A secondary effect is the weakening of the adhesive forces between the bond and abrasive grains which are retained on the wheel's cutting surface. Final 'spark-out' passes without downfeed are provided, causing the grits to be machined flush with the bond. This results in there being

little or no clearance between the bond material and the abrasive grains.

In order to enable the wheel to remove material efficiently, the bond material between the grains must be removed preferentially so that adequate space is available for chips to be accommodated during cutting. Also, the grits must be fractured so as to reduce dullness. These are the functions of the dressing operation, after which the wheel is obtained in an 'open' and 'sharp' condition [1].

2.1.3 Grinding Performance:

When the material to be ground is narrower than the width of the wheel, the operation is called plunge grinding. This is a special type of surface grinding operation, represented schematically by Fig. 2.1 which indicates the important grinding variables - wheel speed (V), table speed (v), down feed or depth of cut (d), wheel diameter (D), and undeformed chip thickness (t). The other variables are the number of cutting points per unit length of wheel surface (C) and the width-to-depth ratio of an average cut (r).

The performance of a grinding wheel can be assessed in terms of its 'grindability', a term used to describe the relative ease of grinding. Grindability is concerned with the forces, power required in grinding, wheel wear and stock removal rate, as well as the surface finish produced.

A material is said to have good grindability if the forces, power required and wheel wear are low, the stock removal rate is high and the surface finish is good. Most of the factors affecting grindability can be shown to be related to the undeformed chip thickness [2], given by the equation

$$t = \sqrt{((4v/VCr)\sqrt{(d/D)})} \qquad (1)$$

The ease of grinding is mainly assessed in terms of the following three indices.

(1) Volume ratio or Grinding ratio $= \dfrac{\text{Volume of metal removed}}{\text{Volume of wheel worn}}$

(2) Grinding characteristic $= \dfrac{\text{Grinding ratio}}{\text{Net horse-power}}$

(3) Grinding Rating $= \dfrac{\text{Grinding ratio}}{(\text{Power per unit volume removal rate}) \times \text{Surface finish (RMS)}}$

For good grinding conditions, the above three indices should be as large as possible.

Another useful parameter is the Grinding Coefficient, defined as the ratio of tangential to normal forces acting during the grinding operation.

2.2 Wheel Loading:

2.2.1 Past Work:

The loading of chips into the porous cutting surface of a wheel is one of the main factors which affect precision grinding performance. The metal build-up on abrasive grits is detrimental to the life of the grinding wheel, since it affects the surface integrity and finish of the workpiece and induces chatter and excessive heat generation. In practice, it is necessary to carry out truing and dressing operations for the wheel when the loaded amount reaches a value high enough to cause serious deterioration of the cutting efficiency.

From the available literature, it appears that due to experimental difficulties, little attention has been paid in the past to the quantitative study of the wheel-loading phenomenon. A brief review of the reported work, to date, is given below:

(i) In the early fifties, Shudolz et al. [3] studied the effect of cutting fluid conditions on wheel loading, using a chemical detection method. The degree of wheel loading was estimated by considering two different positions on the wheel surface where maximum loading was apparent.

(ii) Khudobin [4] developed a colorimetric method for measuring the loading of ferrous metals. In this method, samples of loaded material were scraped from five different points on

the wheel surface and chemically treated. The colour of
the resulting solution was compared with a standard solution
to yield a measure of the wheel loading. It was observed
that loading increases with the grinding time in the manner
indicated in Fig. 2.2(a).

(3) Pandey et al [5] have reported a method wherein samples
of loaded metal are chemically treated and the transmittance
of the resulting solution measured using a spectro-photometer.
They have studied wheel loading for several work/wheel combi-
nations for different grinding conditions, and some of their
results, e.g. Fig. 2.2(b), will be discussed later.

(4) Sata et al [6] used an eddy-current sensor for inprocess
measurements of wheel loading (Fig. 2.2(c)). Using this method,
Suto et al,[7] have reported results for the distribution of
loaded metal particles, area growth rate, loading duration,
etc.

(5) Yamamoto and Maeda [8] have developed a d.c. magnetizing
method for in-process measurement of wheel loading. Their
results are exemplified by Fig. 2.2(d).

(6) Recently, Gohad [9] applied radiotracer techniques for
obtaining quantitatively accurate results in wheel loading
experiments. Since this is the basic approach adopted for
the present work, it would be appropriate to review the
method separately.

2.2.2 The Radiotracer Method:

The available conventional methods for measuring grinding wheel loading, i.e. (1) to (5) above, have one or more of the following drawbacks:

(i)   Difficulties in obtaining accurate absolute results,

(ii) Sampling of only a small part of the loaded wheel surface,

(iii) Painstaking sample preparation involving chemical separation, etc.

The radiotracer method does not offer any of these difficulties.

The workpiece material chosen by Gohad for the development of the method was annealed HSS containing $\sim 0.1\%$ cobalt. The workspecimen were irradiated, along with accurately weighed reference samples of workpiece material, in the CIRUS reactor at BARC in a thermal neutron flux of $\sim 10^{12}$ cm^{-2} sec^{-1} for 2-3 hours. The radiotracer activities generated were ~ 1 µCi/gm of ^{59}Fe and ~ 0.2 µCi/gm of ^{60}Co. Figs. 2.3, 2.4 show NaI and Ge(Li) γ-energy spectra of the irradiated samples.

Gohad used two separate techniques for normalising the relative loading curves obtained through single γ-counting of the activity of loaded material on the wheel cutting surface, viz.,

(a) γ-γ coincidence counting of the ^{60}Co activity, and

(b)   an extrapolation method applied to singles γ-counting of the ^{59}Fe/^{60}Co activity.

Consistency obtained between these two methods was within statistical errors (typically $\pm$ 4%). Results from the nuclear techniques were also compared with some conventional measurements of wheel loading involving chemical separation of abrasive grits from dressed debris. The agreement obtained was satisfactory.

For the γ-γ coincidence method to be applicable, the basic requirement that the radiotracer should emit two coincident γ-rays is rather limiting. Also, this method needs relatively long counting times (typically 12 hours) to obtain adequate statistical accuracy. On the other hand, the extrapolation method of normalisation, being based on singles γ-counting alone, can be used when any γ-emitting radiotracer is available, e.g. ^{59}Fe for mild steel, ^{65}Zn for brass, etc. For the present work, it was this latter method, viz. extrapolation, that was applied throughout.

Fig. 2.5 is typical of the results obtained by Gohad who concluded that, for the work/wheel combination considered, the loaded amount increased rapidly at first and then approached a steady-state value which was dependent on the grinding conditions.

2.3 Presently Adopted Experimental Procedures:

2.3.1 Experimental Set-up:

The grinding set-up used in the present study is shown in Plate 2.1. A 1 H.P., surface-grinding machine with horizontal spindle was used for the experiments, conducted under dry, plunge-cut conditions. Various experimental particulars are given in Table 2.1.

Table 2.1

Machine Specifications:	Make: Jaymes Engineering Co., Bombay
	Stepped-pulley two-speed belt drive.
Grinding Wheels:	Make: Grindwell-Norton
	Dimensions: 150 mm x 31.75 mm x 13 mm
	(1) 38 A 60 K 5 VBE (White, Alumina)
	(2) 39 C 60 L 5 VK (Green, Silicon carbide)
	(3) A 60 P 5 V (Brown, Alumina)
Wheel Speed:	3000 rpm, for annealed HSS, brass and mild steel,
	2000 rpm, for aluminium
Table Speeds:	2 - 8 m/min.
Depths of Cut:	.00325 - .0195 mm
Work Materials:	Annealed HSS (BHN ∼ 240)
	Rolled brass (60:40) (BHN ∼ 100)
	Mild Steel (BHN ∼ 88)
	Rolled Aluminium (BHN ∼ 23)
Workpiece dimensions:	10 mm x 10 mm x 20 mm

In order to enable measurements of normal and tangential force components to be made during the grinding experiments, the workpiece was mounted on a 2-component, extended, octagonal-ring type, strain-gauge dynamometer (Fig. 2.6). Outputs from the dynamometer were fed to a 2-channel 'Encardiorite' recorder.

The measurement of volume of material removed during the grinding experiments was carried out using a 'Starrett' dial gauge.

For the γ-counting of the grinding wheel, reference samples, etc. a lead-shielded, twin NaI scintillation counter system was used (Plate 2.2). The electronics modules were of ECIL design [9]. A block diagram is shown in Fig. 2.7.

2.3.2 A Typical Experiment:

Table 2.2 gives the sequence of operations followed for truing and dressing the grinding wheel before the start of an experiment. Apart from achieving the removal of loaded material from any previous experiment, the use of this standard sequence ensured consistency of results in that similar initial wheel surfaces were generated for the different experiments. A precaution taken during the truing/dressing operations was the use of thin rubber sheets to cover the faces of the grinding wheel, so as to minimise contamination by the previously loaded material [9].

Table 2.2:   Dressing Sequence Employed.

Diamond Tool: 1.0 Carret, pyramidal shape.

Wheel Speed: 3000 rpm

Average Linear Speed of Diamond
Dresser During Each Pass: .02 m/min.

I. Standard Procedure for Wheel Truing:

    (a) Several passes of diamond tool with down feed
        .013 mm/pass until all traces of loaded material
        were removed.

    (b) One pass with down feed .026 mm.

    (c) One pass of .0065 mm.

    (d) Finally two passes with zero in-feed.

II. Standard Procedure for Wheel Dressing:

    (a) Two passes of diamond tool with down feed of
        .026 mm per pass.

    (b) Two passes of diamond tool with down feed of
        .013 mm per pass.

    (c) Two passes of diamond tool with zero in-feed.

In order to obtain a repeatable mounting position for
the grinding wheel, the front face of the spindle casing, the
rear and front flanges, as well as the faces of the grinding
wheel were suitably marked.

Before starting the experiment, window settings for
the single channel analysers were suitably adjusted using a
multichannel analyser (Fig. 2.7), so that an appropriate
region of the γ-spectrum of the activated workpiece would be
counted. The wheel background was then taken by counting the
newly dressed wheel. An initial dial gauge reading was also
taken for the mounted workpiece.

To obtain the first point on the loading curve, grinding
of the activated workpiece was carried out for a certain
number of passes, say n (typically n = 30). The wheel was
then removed and singles γ-counted on the NaI counting set-up
for 200 secs. A perspex box was used for holding the wheel
in position during the counting (plate 2.2). The sum of the
two single-channel count rates obtained, after appropriate
background subtraction (initial wheel reading), was taken as the
relative measure of the loaded amount of work material. At this
stage, a dial gauge reading of the workpiece was also taken to
indicate the volume of material removed. After mounting the
wheel back on the grinding machine, the grinding operation
was then continued with the partially loaded wheel for another
n passes. The wheel was then removed and counted once again
to yield the second point on the loading curve (corresponding
to now, 2n passes). In this way, successive points on the
loading curve were generated till the desired volume of
material had been removed (typically 300 mm^3, in the present

work). Periodically, a reference sample of the activated work material was counted during the experiment, to monitor any electronic drift of the counting system.

Since the workpiece was mounted on a 2-component dynamometer during the grinding (Sec. 2.3.1), measurement of normal (F_n) and tangential F_t) forces was achieved in parallel with the loading measurements.

As mentioned earlier, normalisation of the relative count rates from the wheel loaded surface was presently achieved by applying the extrapolation method (Sec. 2.2.2). The method involved sticking three, similar-weight reference pieces of the activated work material on the wheel surface to form an equilateral triangle. The sum of the two back-ground-corrected single channel count rates, with the samples in this position, was taken as the singles count-rate corresponding to a wheel/sample spacing equal to the half-thickness of the samples. A second singles count rate was obtained with a dummy spacer of non-radioactive work material stuck between each of the reference pieces and the cutting surface. This count rate corresponded to a wheel/sample spacing equal to the sample half-thickness plus the dummy spacer thickness. The counting was repeated with two, and then three spacers stuck between each reference sample and the wheel cutting surface. In this way, the dependence of the singles count

rate from the reference samples on the wheel/sample spacing was established. Graphical extrapolation of this count rate to zero wheel/sample spacing yielded the singles count rate (say, C_{so}) which would be obtained if the total mass of the reference samples (say, y gm.), were embedded in the pores of the wheel's cutting surface. This type of extrapolation essentially takes into account:

(i)   the slightly different geometry offered by the reference samples,

(ii) self-absorption effects in the γ-counting of the samples.

Thus, if at the end of an experiment the singles count rate obtained from the wheel was C_w, the finally loaded amount was given by [9]:

$$M_{l.f} = [(\frac{C_w}{C_{so}}) \ y] \quad gm \qquad (2)$$

Fig. 2.8 gives a typical 'extrapolation curve' (for the ^{65}Zn 1.12 MeV γ-ray counting in an experiment for brass), indicating an extrapolation correction of $\sim 2\%$.

2.4 Health Physics Considerations:

A fundamental aspect of radioisotope applications is the need to protect the users, as well as other people in the vicinity, against the harmful effects of exposure to nuclear radiation. The radiological hazards can arise from an external

source or internally through inhalation/ingestion of radio-
active material. Suitable precautions are necessary at
every stage of experimentation.

The specific activities of the workpieces used in
the present work were in the range 0.1 - 1.0 μCi/gm, so that
source shielding during the experiments was not necessary.
But, as the radioactive chips were of particulate size, there
was danger of activity being airborne to cause equipment
contamination and accidental inhalation of radioactive dust.
Special care was taken during truing/dressing operations,
as well as the grinding experiments, to confine all the chips
to within a double-walled perspex box (Plate 2.1), internally
lined with petroleum jelly [9]. The jelly containing dressed
debris and collected chips was periodically scraped from the
inner walls of the box into pill boxes. This was done in a
special tray which was periodically monitored and cleaned
carefully. The floor area was covered with rubber sheets
to minimise the spread of any loose activity while cleaning
the debris-collection box, etc.

An apron and hand gloves were worn during experimentation.
Handling of the workpieces was carried out using 30 cm,
electroplated tongs. An air-contamination monitor and an
area survey meter were used regularly to check the dose
levels during the experiments. A regular film-badge service

was utilized for maintaining a record of dose received during the course of the entire work.

For counting purposes, the grinding wheel was wrapped in a thin polythene bag, before being inserted into the perspex box which held it in position between the detectors (Sec. 2.3.2.).
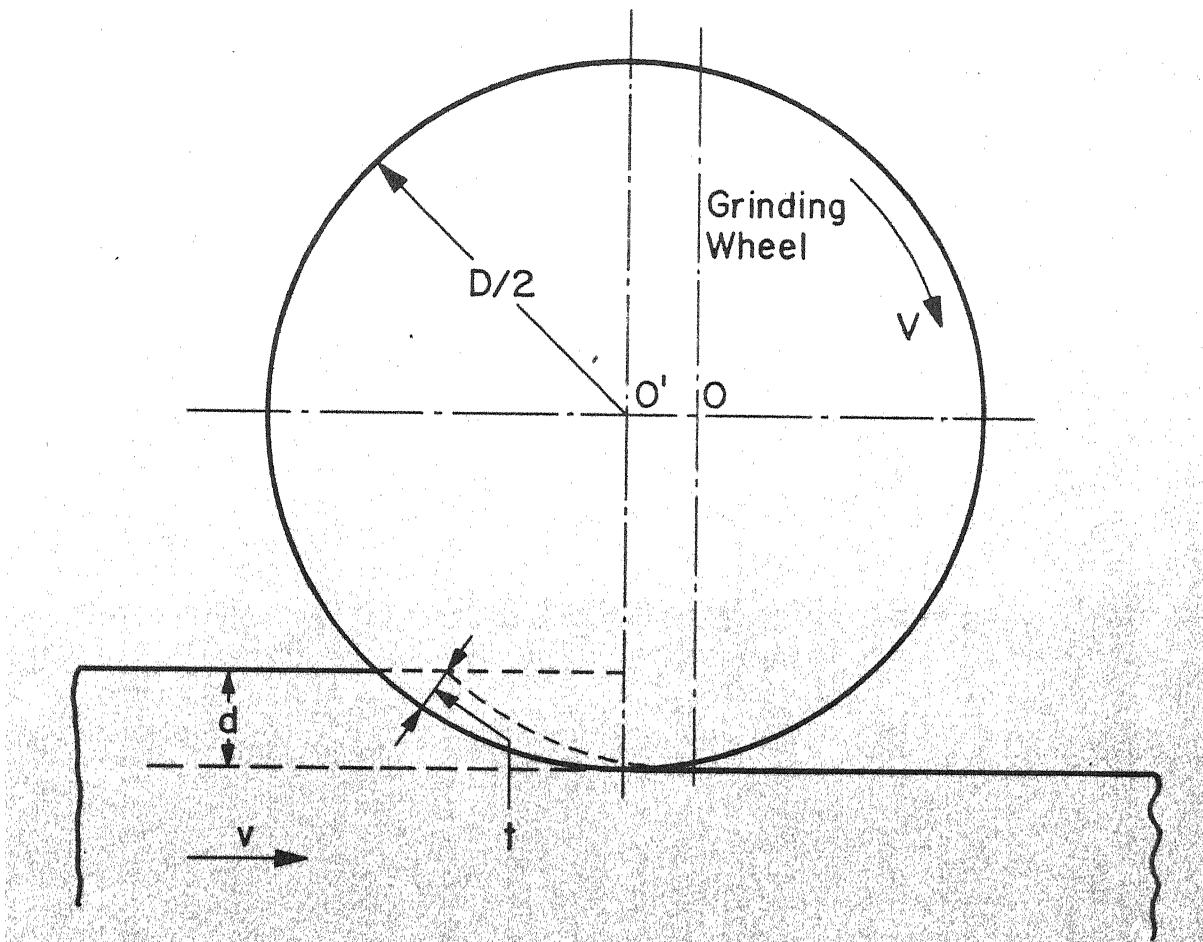
v = Table Speed
d = Depth Of Cut (Down Feed)
V = Wheel Speed
t = Chip Thickness
D = Wheel Diameter

Fig. 2·1   Variables In Surface Grinding

(a)

E9A16SM2K5

EB40SN1K

Loaded Amount(Relative)

Grinding Time(min.)

(b)

Wheel   A46Q5V
Down Feed   0.02 mm
Table Speed 10m/min
Work .   Cast Iron

Specific Loading

Grinding Time(min.)

(c)

Metal Removal
Rate 1.0mm^3/mm−Sec

0.5 mm^3/mm−Sec

Work; Stainless
Steel

Loaded Surface (%)

Metal Removal (mm^3/mm)

(d)

○ A46 KmV
● A46 ImV
◐ A46OmV

Loaded Amount (Relative)

Grinding Time(min.)
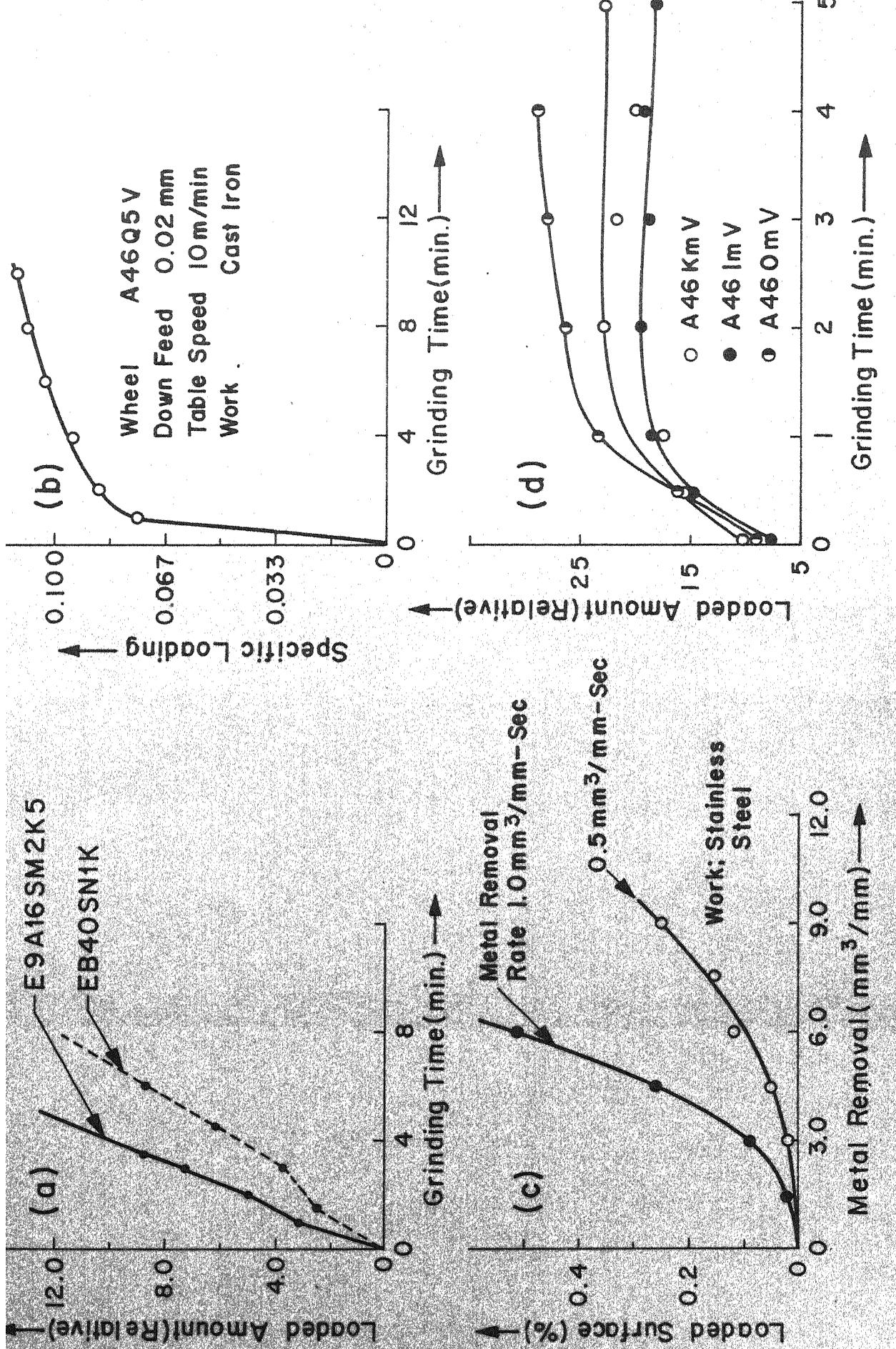
Fig. 2.2 Loading Curves From Reference No. (a)4,(b)5,(c)6,(d)8
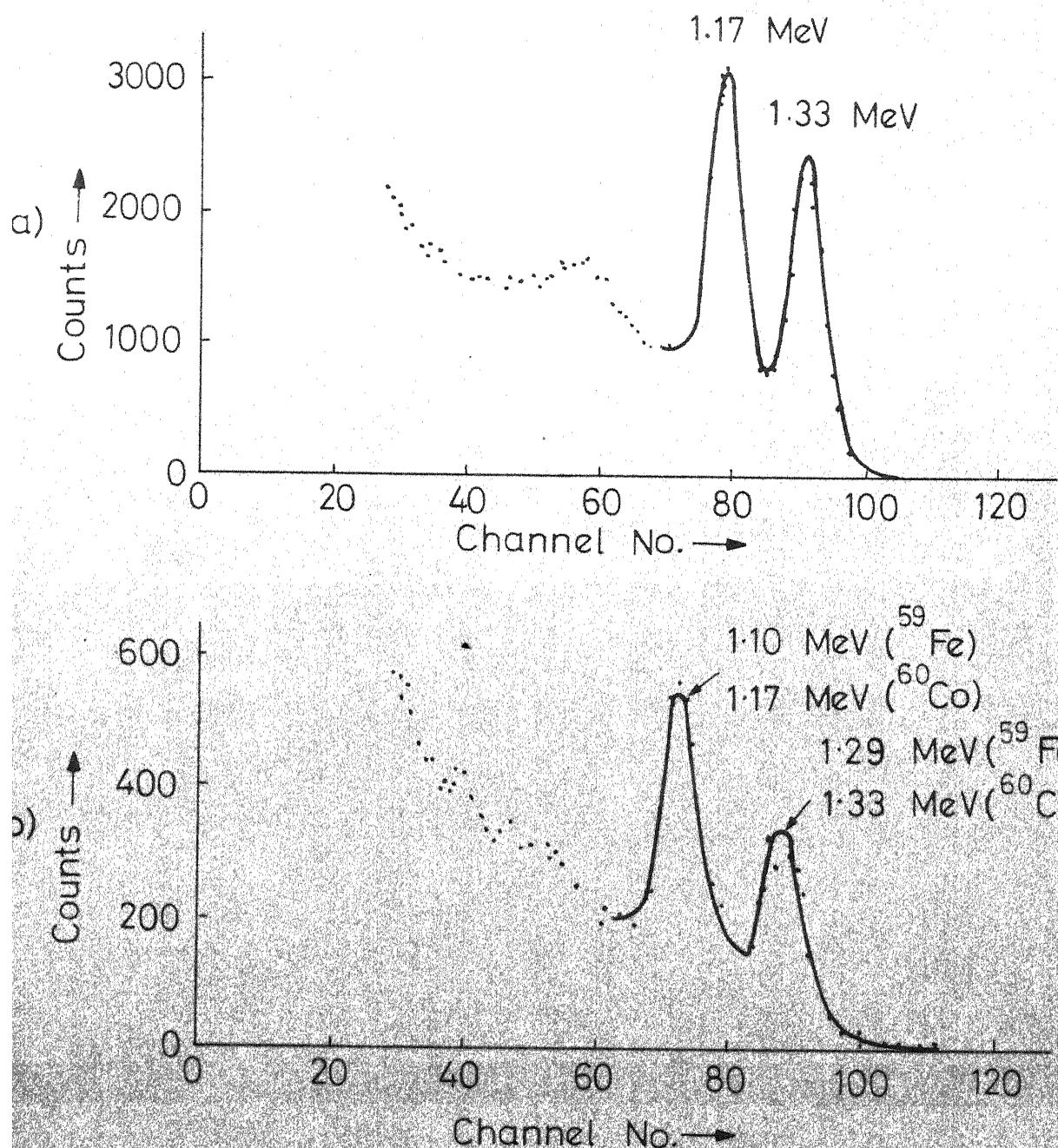
Fig. 2·3 Comarison Of NaI Spectra Of
(a) Standard [60]Co Source and
(b) Irradiated Annealed HSS
Sample [9]
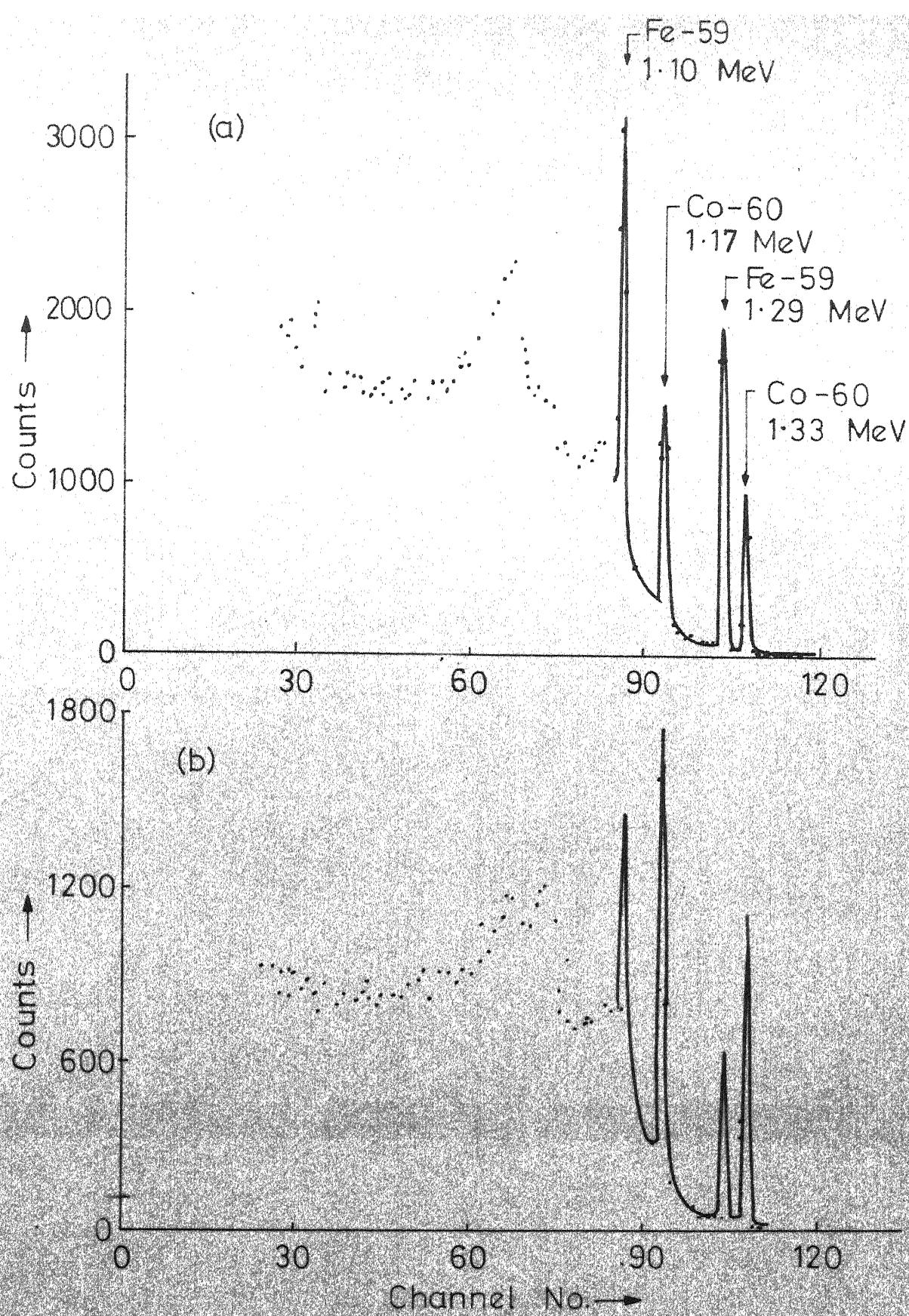
Fig. 2·4   Ge (Li) Spectra Of Irradiated Ann HSS
Samples
(a) 2 Weeks   (b) $4\frac{1}{2}$ Months After
Irradiation
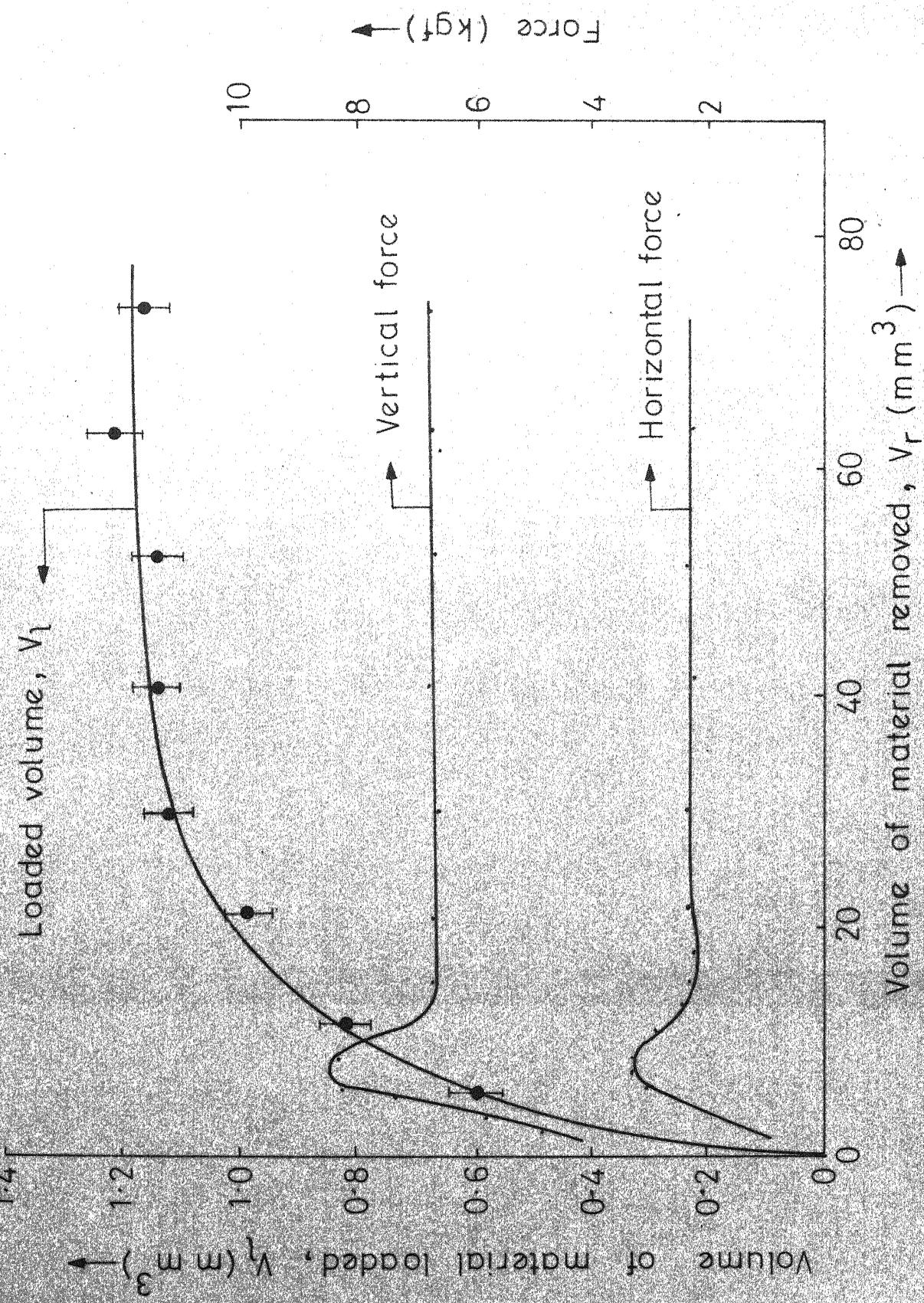
Fig. 2·5 Typical Curve For Annealed HSS From Reference No.9 (Wheel:38A 46 J8 VBE)
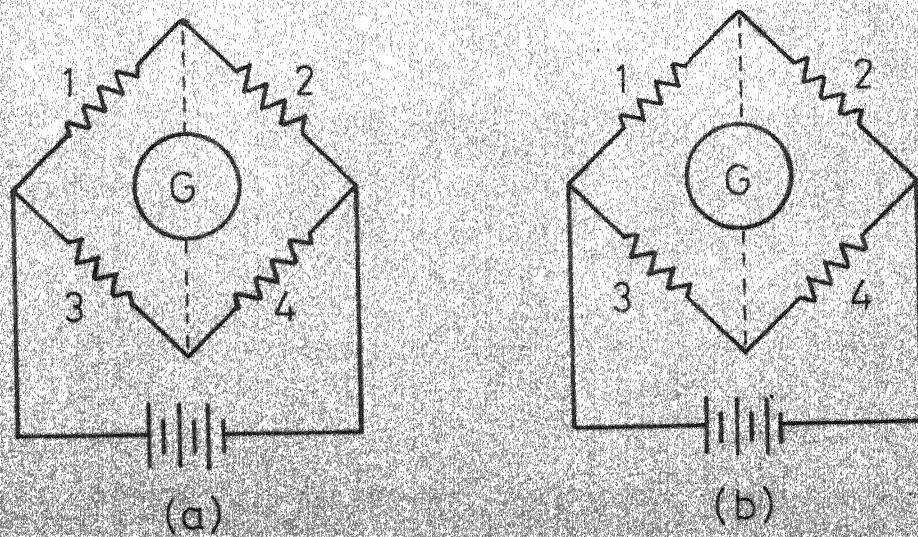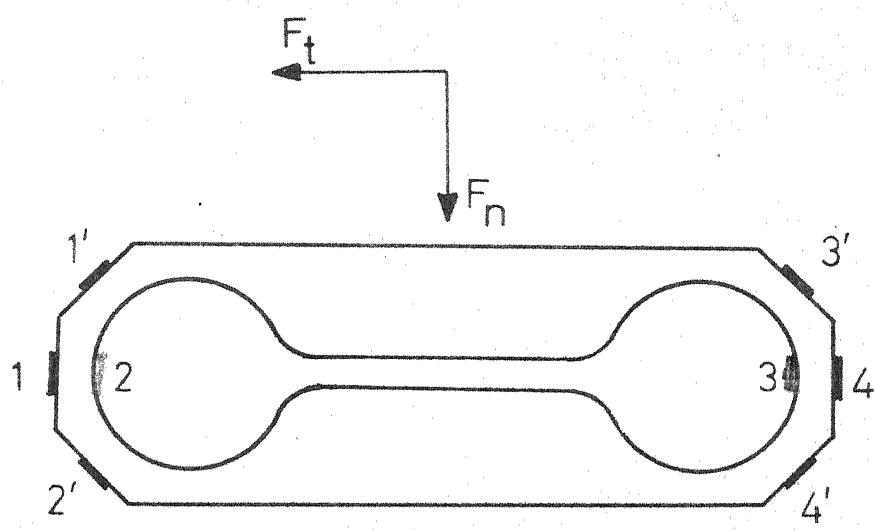
Fig. 2·6 Extended Octagonal Ring Type
Dynamometer
(a) Wiring Diagram For Normal Force
(b) Wiring Diagram For Tangential Force
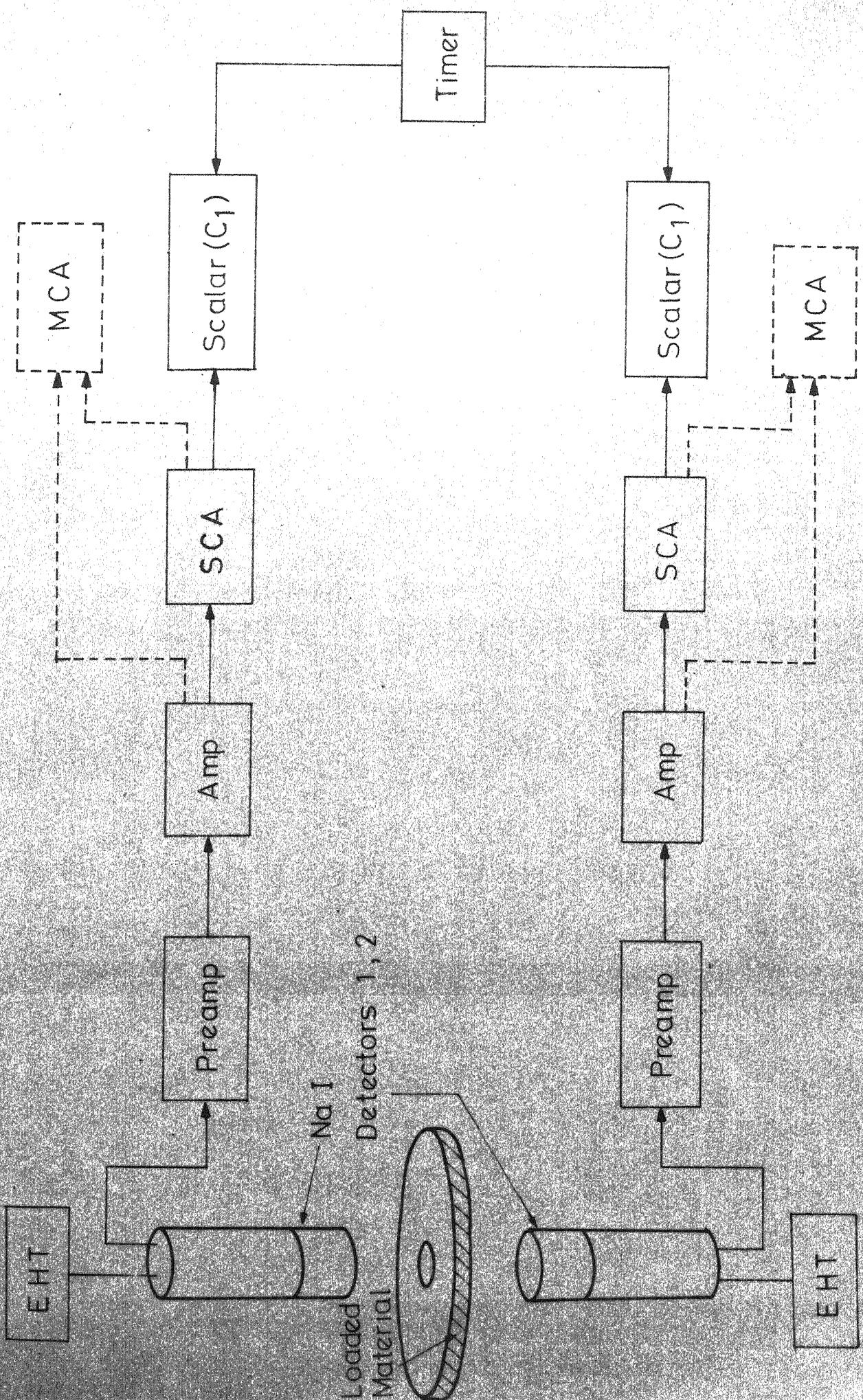
Fig. 2·7 Block Diagram Of Twin Na I Scintillation Counter Set-Up

Fig. 2.8 Extrapolation Curve For A Typical Experiment With Brass
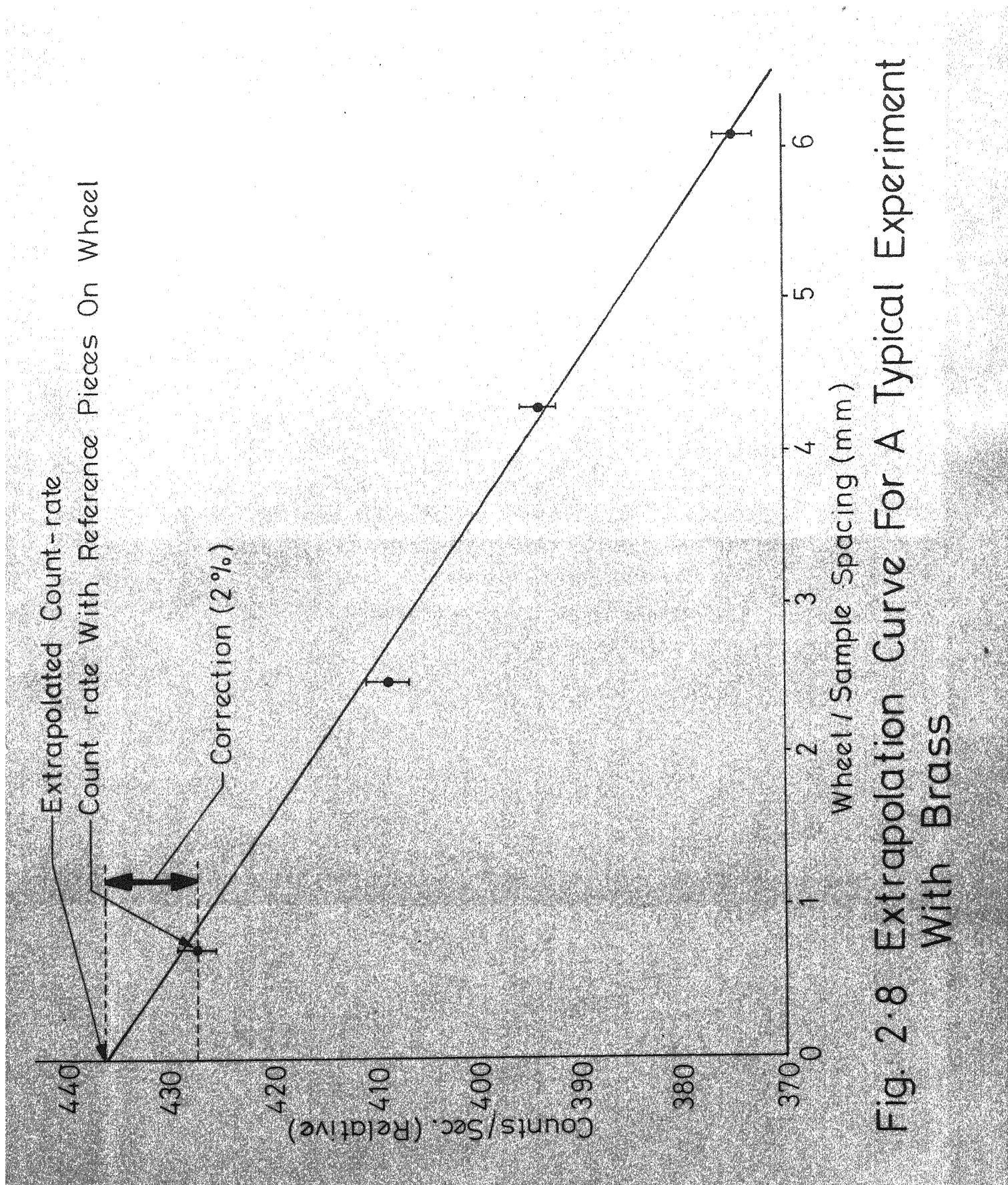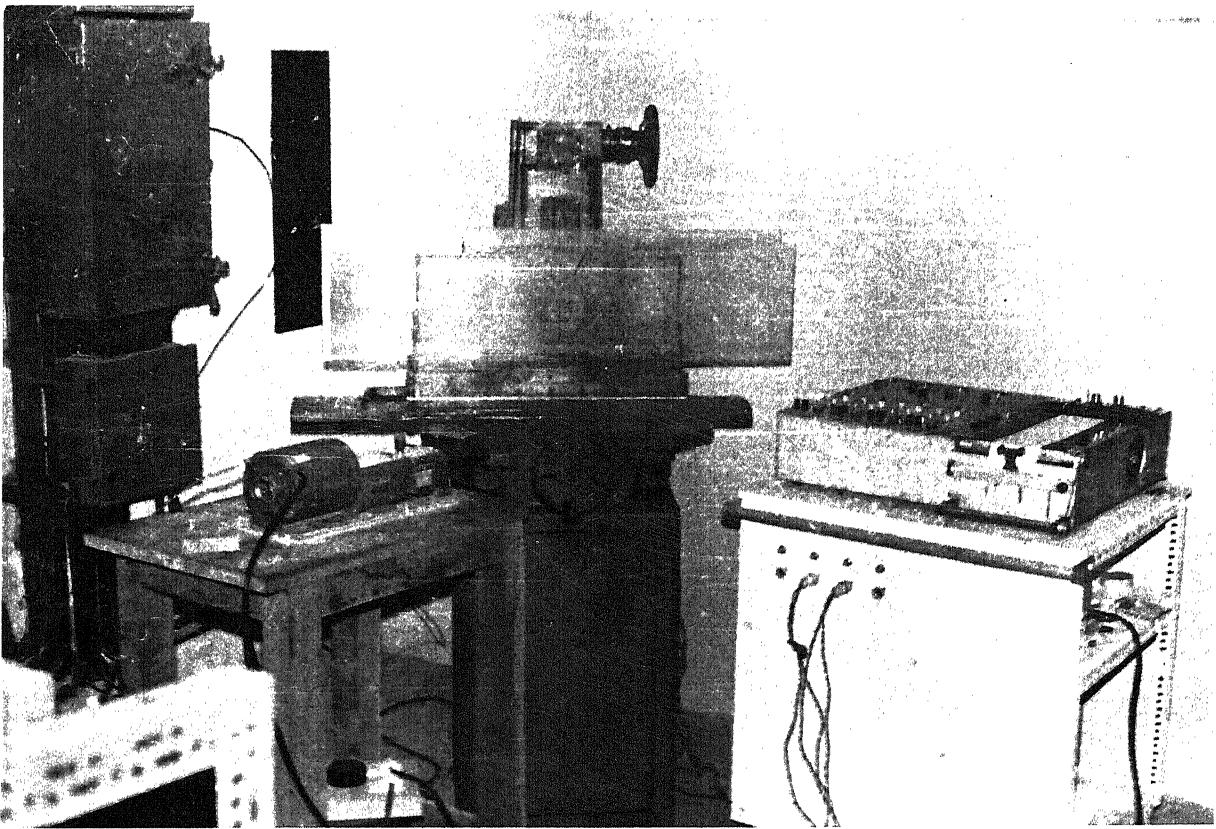
2.1   The Grinding Set-up.
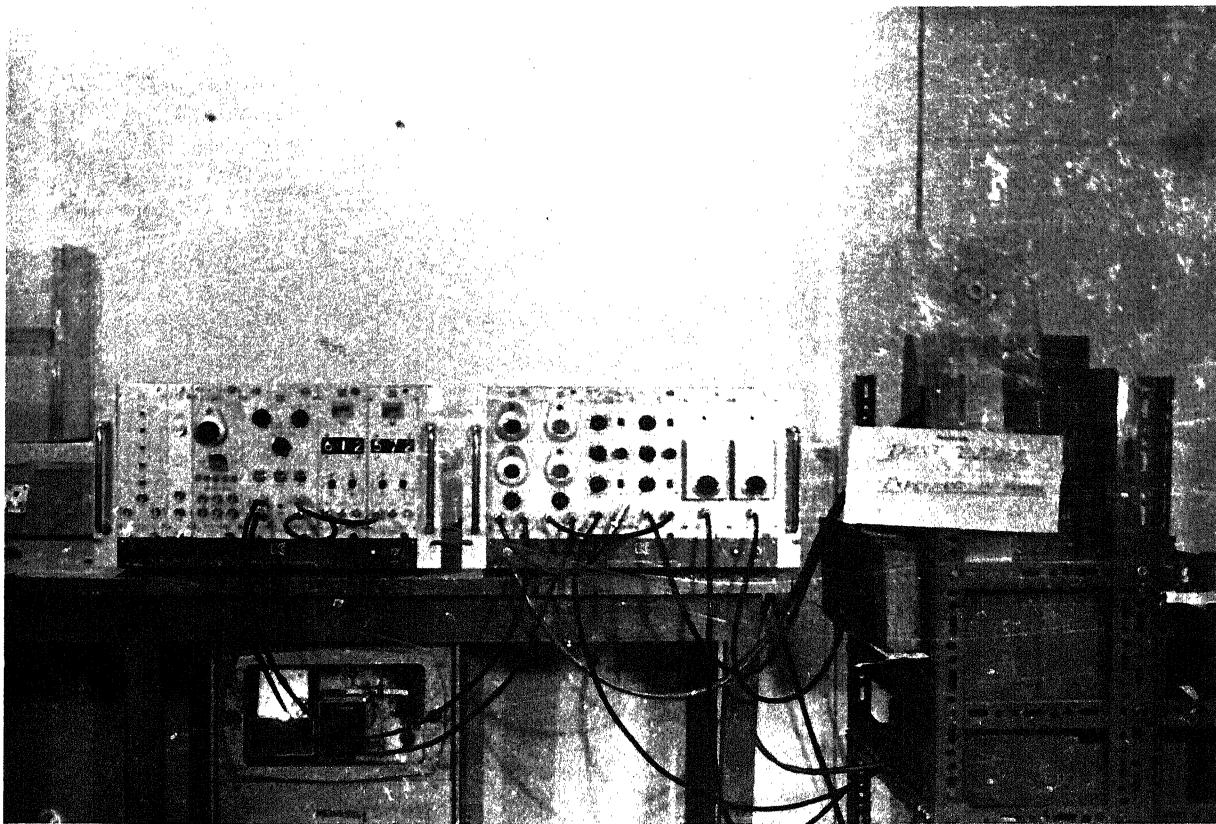
2.2   The γ-Counting Set-up.

CHAPTER III

GENERATION OF RADIOTRACERS

3.1 Introduction:

Since a uniform distribution of the radiotracer activity within the workpiece is an important requirement for wheel loading studies, the generation of the radiotracer by neutron irradiation of work samples is the appropriate method, provided a suitable activation reaction can be identified. Thus, Gohad [9] used thermal neutron activation for generating $^{60}Co/^{59}Fe$ as the radiotracers for cobalt-containing, annealed HSS work samples. For aluminium workpieces, however, he has reported that fast neutron activation is necessary, since thermal neutrons only induce the (n, γ) reaction producing ^{28}Al which has too short a half life (~ 2 mins.). He established the possibility of using ^{24}Na ($T_{\frac{1}{2}} \sim 15$ hrs.) as the radiotracer for grinding experiments with aluminium, generated via the $^{27}Al(n, \alpha)$ reaction with 14 MeV neutrons from a Van de Graaf source.

If one considers an activation reaction of, say the (n, γ) type, namely,

$$^{A}_{Z}X + n \longrightarrow ^{A+1}_{Z}X + \gamma \tag{1}$$

then the activity of the radioisotope $^{A+1}_{Z}X$ may be expressed by the relation:

$$\text{Activity} = [(\frac{0.693}{T_{\frac{1}{2}}}) \times p \times (\frac{0.602 \times 10^{24} \times \sigma_a \times \emptyset \times t}{A \times 3.7 \times 10^{10}})]Ci/gm$$

(2)

where,

$T_{\frac{1}{2}}$ = half-life of the radioisotope in secs,

p = fractional abundance of stable parent,

σ_a = microscopic neutron cross-section of parent in cm^2,

A = mass number of parent,

$\emptyset$ = neutron flux in n/cm^2-sec,

t = irradiation time in secs.

This relation is valid for radioisotopes whose $T_{\frac{1}{2}} \gg$ duration of the irradiation. This was the case for the workpieces presently irradiated in thermal reactors at BARC. However, the radiotracers generated by fast neutron activation were of relatively short half-life, for which equation (2) has to be modified.

3.2 Thermal Neutron Activation:

The work materials considered in the present study were annealed HSS, mild steel, brass and aluminium.

3.2.1 Annealed HSS:

These workpieces, containing ~ 0.1% Cobalt, were the same as used by Gohad in his experiments. They had been irradiated in the CIRUS reactor at BARC in a thermal neutron flux of ~ 10^{12} n/cm^2-sec. for a duration of 2-3 hours, generating radiotracer activities of ~ 1 μCi/gm of ^{59}Fe and ~ 0.2 μCi/gm of ^{60}Co. At the time of present experiments (~ 16 months after the original irradiation), the ^{59}Fe ($T_{\frac{1}{2}}$ ~ 45 days) had almost completely decayed, but the ^{60}Co activity ($T_{\frac{1}{2}}$ ~ 5.2 yrs.) was still ~ 0.2 μCi/gm and quite adequate for use as radio-tracer. Fig. 3.1 shows the NaI, Ge(Li) spectra of the annealed HSS samples at the time of the present experiments and confirms the absence of ^{59}Fe activity (cf. Fig. 2.4).

3.2.2 Mild Steel:

The mild steel workpieces presently used had been unintentionally irradiated during the course of Gohad's work [10] to a very high level of ^{59}Fe activity (~ 80 Ci/gm generated after 1 day's irradiation in a flux of ~ 5 x 10^{12}/cm^2-sec.) when these specimens were examined at the time of the present experiments (~ 16 months after the original irradiation), negligible ^{59}Fe activity was observed, but there was ~ 0.5 μCi/gm of ^{60}Co (Fig. 3.2). This, again, was easily usable as radiotracer.

3.2.3 Aluminium:

It is clear that the radiotracer presently used for mild steel had resulted from the activation of a certain amount of cobalt 'impurity' (of the order of ~ 0.002%). This led to the consideration of the possibility of activating known impurities in aluminium work specimens by thermal neutron irradiation. As already mentioned, (n, γ) activation of aluminium itself is not appropriate. However, if γ-emitting radiotracers of $T_{\frac{1}{2}} > 1$ week were to be generated by (n, γ) activation of impurities in the aluminium, these would be usuable. (A week is typically required for the transport of irradiated samples from BARC to Kanpur). The available data for the rolled aluminium samples used in the present study indicated impurities of ~ 0.3% iron, ~ 0.1% chromium and ~ 0.1% zinc. Of these, the iron impurities seemed to be the most promising. Accordingly, irradiation conditions of ~ 10^{13} n/cm^2-sec. for a duration of 5 days were chosen. ^{59}Fe activity of ~ 2 μCi/gm was thereby generated in an aluminium work sample. In actual fact, there was slight contribution to the γ-activity from other impurities also, viz. zinc and cobalt. This can be seen quite clearly from the Ge(Li) spectrum of the aluminium workpiece taken ~ 6 months after the irradiation (Figs. 3.3 and 3.4). At this time, the ^{59}Fe activity ($T_{\frac{1}{2}} \sim 45$ days) had decayed considerably as

compared to the other indicated 'impurity' activities of ^{65}Zn ($T_{\frac{1}{2}} \sim$ 245 days) and ^{60}Co ($T_{\frac{1}{2}} \sim$ 5.2 yrs.).

3.2.4 Brass:

For the rolled brass workpieces presently used (60% copper, 40% zinc), thermal neutron activation would result in the generation of ^{64}Cu, from ^{63}Cu(n,γ), and ^{65}Zn, from ^{64}Zn(n,γ), as the two main γ-emitting radiotracers. In the case of the former, however, the $T_{\frac{1}{2}}$ of 12.8 hrs. is too short to permit its use after $\sim$ 1 week, the time required for transporting the irradiated samples from BARC to Kanpur. Accordingly, the irradiation conditions were chosen to generate $\sim$ 0.5 μCi/gm of ^{65}Zn tracer ($T_{\frac{1}{2}} \sim$ 245 days, 1.12 MeV γ-ray) in the brass workpieces. From equation (2), these conditions were obtained as a thermal neutron flux of $\sim 10^{11}$/cm^2-sec for a duration of 2 hours. The irradiation was carried out in the APSARA reactor at BARC. Fig. 3.5 shows NaI, Ge(Li) spectra of one of the irradiated brass samples.

3.3 14 MeV Neutron Activation:

3.3.1 Introduction:

Fast neutrons from an accelerator source were used by Gohad to generate ^{24}Na as the radiotracer for aluminium via the ^{27}Al(n,α) reaction which has a threshold of $\sim$ 6 MeV.

This was done with the consideration that thermal neutron activation of aluminium itself is not applicable. While it has been presently shown that impurities in an aluminium workpiece can be successfully activated by thermal neutrons for carrying out loading studies (Sec. 3.2.3), there are certain advantages associated with the use of a tracer such as ^{24}Na. These are,

(i) On-the-spot activation for experiments to be conducted at an Institute, such as IIT/K, which has ready access to a 14 MeV neutron generator but does not have a research reactor.

(ii) A relatively short half-life of the radiotracer ($\sim$15 hrs. for ^{24}Na), resulting in there being no possibility of long-term contamination of any equipment or working area, as also no problem associated with storage/disposal of low-activity radioactive waste (grinding debris, used work specimens, etc.).

The main disadvantage is that the grinding experiment has to be conducted soon after the activation, i.e. a number of separate activations would be necessary for conducting a series of experiments.

The choice of the method of activation for aluminium work specimens to be used for loading studies, i.e. thermal neutron activation of impurities vs. 14 MeV neutron irradiation, would depend on the particular situation at hand. However, advantages (i) and (ii) above are quite seg-nificant. Consideration was, therefore given to the possibility of generating radiotracers for brass and steel work-pieces by fast neutron activation. If this were shown to be possible, one would have a choice in the method of generating tracers for these materials also.

The constraints on the use of 14 MeV neutron activation as a general method for radiotracer generation are the relatively low neutron fluxes that can be obtained from an accelerator source, the low neutron cross-section values for threshold reactions, as also practical limits on the length of the irradiation. For wheel loading studies, however, a γ-emitting radiotracer activity of ~ 0.1 μCi/gm is sufficient. The half-life of the activated isotope is an important factor since, if it is too short (say, a few minutes), it will not be usable as a radiotracer, while, on the other hand, if it is too long, the activity generated (inversely propor-tional to $T_{\frac{1}{2}}$) would be too low. A $T_{\frac{1}{2}}$ range of 2–20 hours would be appropriate.

3.3.2 Reactions for Brass and Steel Samples:

A variety of radiotracers would be generated by 14 MeV neutrons irradiation of brass via various threshold reactions with Cu, Zn isotopes. The important ones, with 14 MeV neutron cross-sections $>$ 100 mb, are listed in Table 3.1 [11,12]. From the earlier discussion (Sec.3.3.1), it is evident that the most suitable radiotracer for the grinding experiments would be ^{64}Cu ($T_{\frac{1}{2}} \sim$ 12.8 hrs, 0.51 MeV γ-ray) from the ^{65}Cu(n, 2n), ^{64}Zn(n,p) reactions.

For the case of steel samples, a similar consideration of the various possible threshold reactions indicated that the ^{56}Fe(n, p) reaction, with a 14 MeV neutron cross section of $\sim$ 100 mb, would be the only suitable one. This reaction generates ^{56}Mn of $T_{\frac{1}{2}} \sim$ 2.6 hrs, the principal γ-ray emitted being 0.85 MeV (99 % yield).

Table 3.1: Principal 14 MeV Neutron Reactions for Brass
(60 % Cu, 40 % Zn).

Isotope	Threshold reaction	Cross-section at 14 MeV(mb)	Radio-isotope generated	$T_{\frac{1}{2}}$	Main γ-rays
(a) Copper					
^{63}Cu(69%)	(n,2n)	450	^{62}Cu	9.8 min	0.51 MeV
^{65}Cu(31%)	(n,2n)	900	^{64}Cu	12.8 hr.	0.51 MeV
(b) Zinc					
^{64}Zn(49%)	(n,2n)	120	^{63}Zn	38 min.	0.51 MeV
^{64}Zn(49%)	(n,p)	200	^{64}Cu	12.8 hr.	0.51 MeV
^{66}Zn(28%)	(n,2n)	530	^{65}Zn	245 days	1.12 MeV

Initially, the activation of brass and steel samples was attempted by using a 5 Ci Pu-Be neutron source. Such a source has a yield $\sim 10^6$ n/sec-Ci, with an average neutron energy of $\sim$ 4 MeV [13]. Since the fraction of neutrons of energy above the thresholds for the earlier-mentioned reactions was small (e.g., the threshold for the ^{65}Cu(n, 2n) reaction is $\sim$ 10 MeV), and since the available flux was $\sim 10^5$ n/cm^2- sec, the ^{64}Cu and ^{56}Mn activities obtained were too low for carrying out loading experiments. The characteristic γ-spectra of these two isotopes, however, was clearly observable from the respective, irradiated samples.

3.3.3 Van de Graaf Irradiations:

When a charged-particle accelerator is available, the ^{3}H(d, n) ^{4}He reaction provides a relatively prolific source of 14 MeV neutrons [14]. This neutron energy is highly suitable for the threshold reactions discussed above, as may be seen from Fig. 3.6 which shows the neutron energy variation of cross-section for the ^{27}Al (n, α), ^{65}Cu(n, 2n) and ^{56}Fe(n,p) reactions.

Activation of hardened HSS (5 % cobalt), mild steel, brass, as well as aluminium, was successfully carried out using the 2 MeV Van de Graaf accelerator at IIT Kanpur. A 8 Ci tritium target obtained from BARC was used with a

bombarding deutron energy of (1.00 ± 0.01)MeV. The workpieces were mounted ~ 6 cm from the target, and a deutron current of ~ 20 μA was employed giving a total 14 MeV neutron yield of ~10^9 sec^{-1} [14]. Plates 3.1, 3.2 give views of the accelerator beam tube, target and workpiece samples mounted for irradiation.

Durations for irradiation were ~ 6 hours for steel and ~ 24 hours for brass and aluminium, so that the generated activities of ^{56}Mn, ^{64}Cu and ^{24}Na were close to saturation. The radiotracer activity, in each case, was quite adequate for carrying out loading studies using the extrapolation method for normalisation (Sec. 2.3.2).

Fig. 3.7, 3.8(a) and 3.8(b) show the NaI spectra of Van de Graaf irradiated work specimens of aluminium steel and brass, respectively. The decay of activity of the irradiated samples was studied. For the aluminium and steel specimens, the respective radiotracer half-lives of 15 hrs. (^{24}Na) and 2.6 hrs (^{56}Mn) were confirmed. In the case of brass, however, with counting of the 0.51 MeV photopeak being carried out (Fig. 3.8(b)), the activity was found to decay rapidly at first and then (after 1-2 hours) according to the expected half-life of 12.8 hrs (^{64}Cu). This was due to the fact that ^{62}Cu ($T_{\frac{1}{2}}$ ~ 9.8 mins.) and ^{63}Zn ($T_{\frac{1}{2}}$ ~ 38 mins.) are also generated by 14 MeV neutron

irradiation of brass, and both these isotopes, like ^{64}Cu, emit 0.51 MeV γ-rays (Table 3.1). In order to avoid any ambiguity in the decay corrections applied during the counting of the loaded grinding wheel, etc., the loading experiments with the 14 MeV neutron activated brass samples were conducted ~ 2 hours after the irradiation, by which time the short-lived ^{62}Cu and ^{63}Zn activities had almost completely decayed.
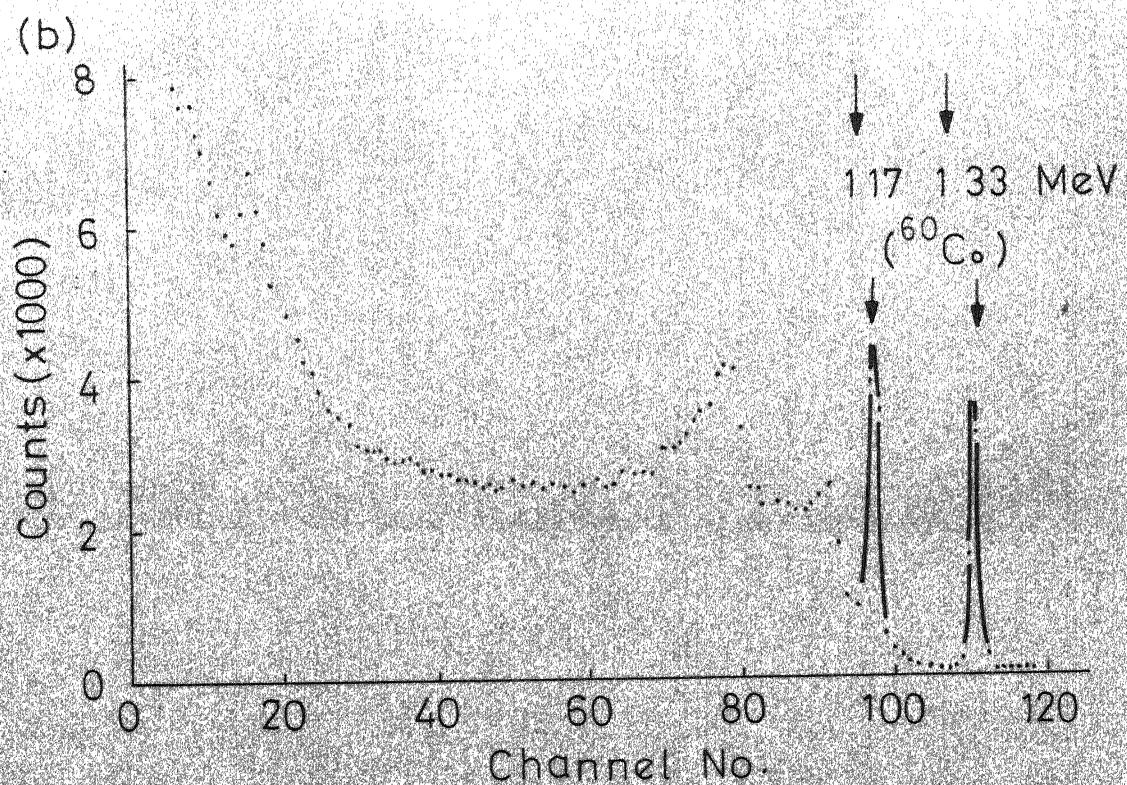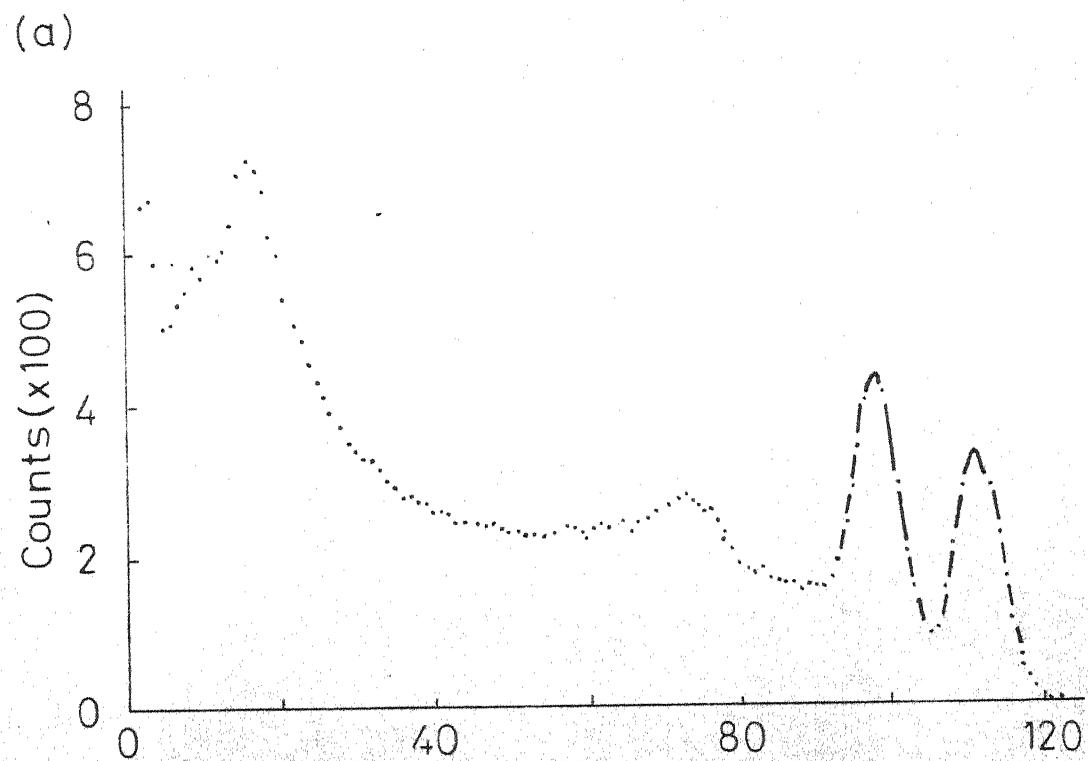
(a)

(b)

Fig.3·1 (a) NaI,(b) Ge(Li) Spectra Of
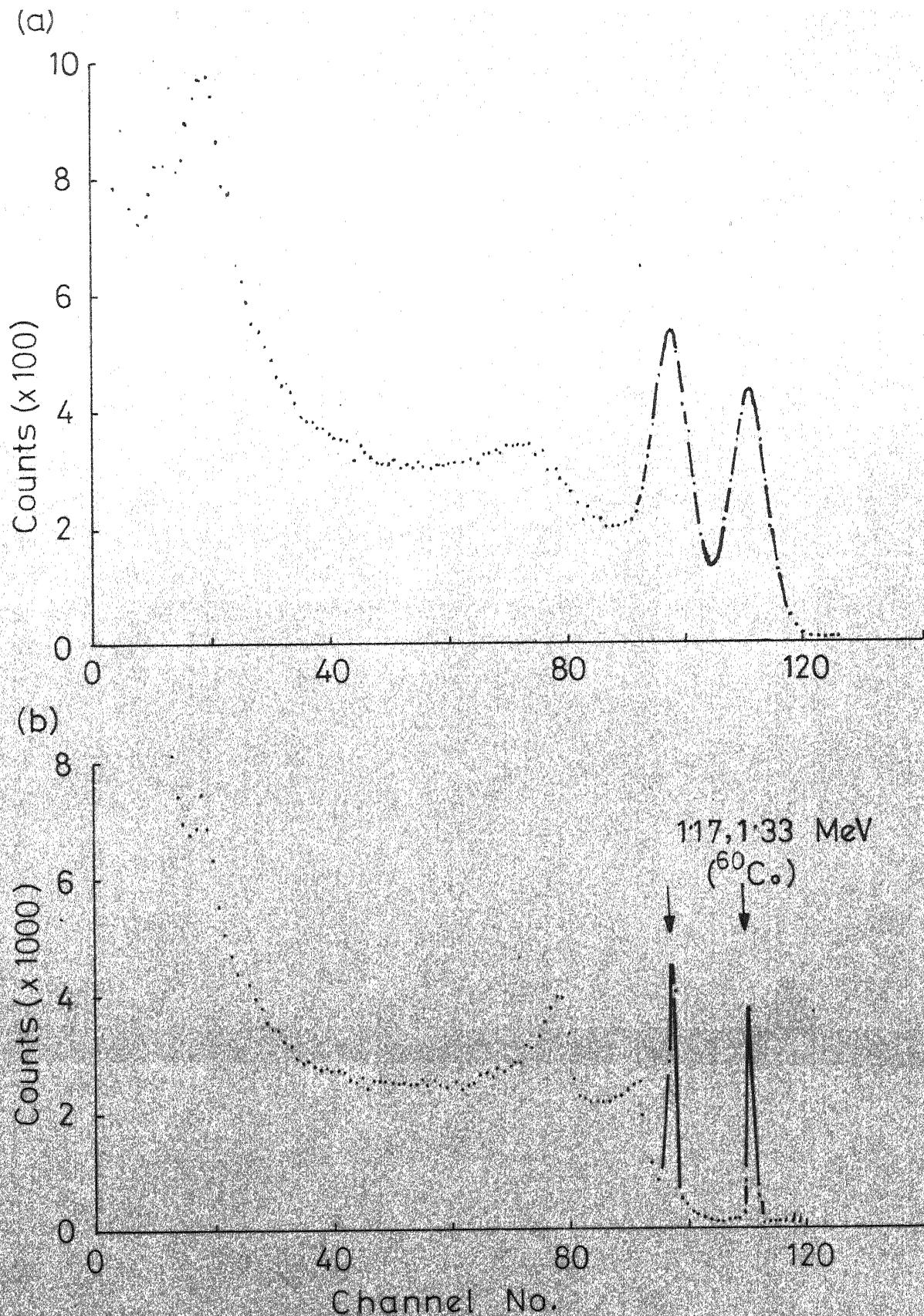BARC Irradiated Annealed
HSS Sample After~16 Months

Fig.3.2 (a) Na I (b) Ge (Li) Spectra Of BARC Irradiated Mild Steel Sample After ~16 Months
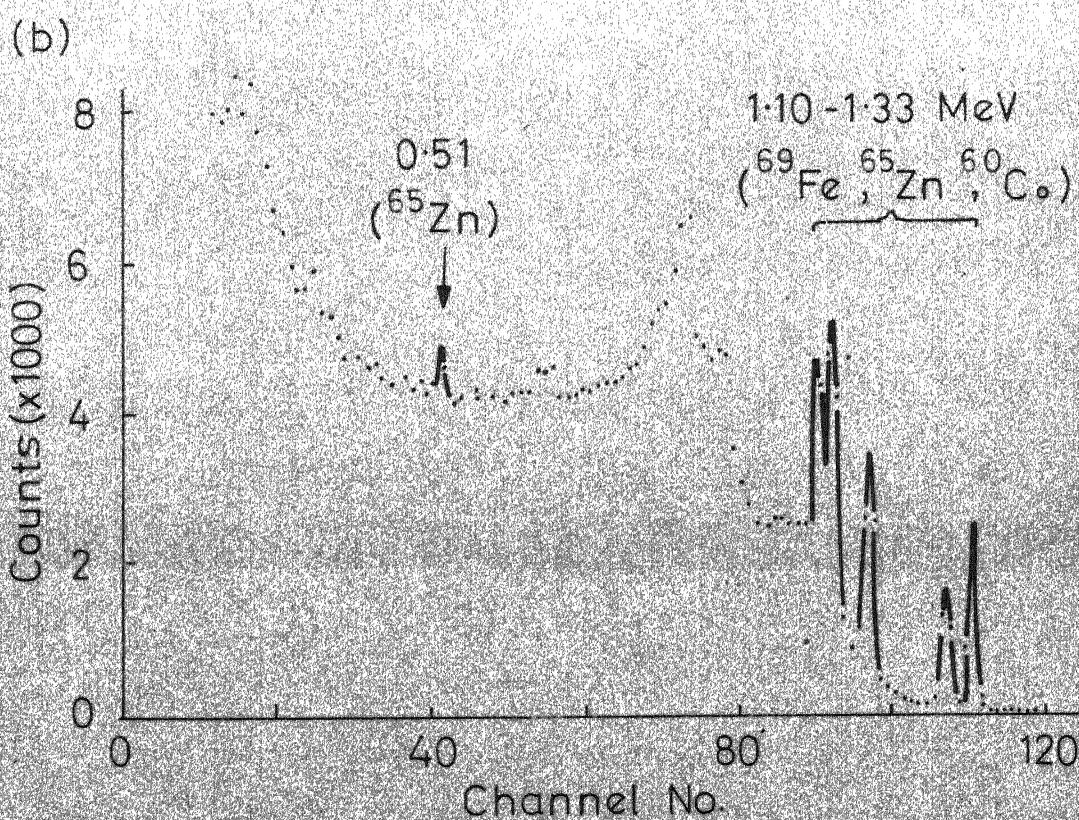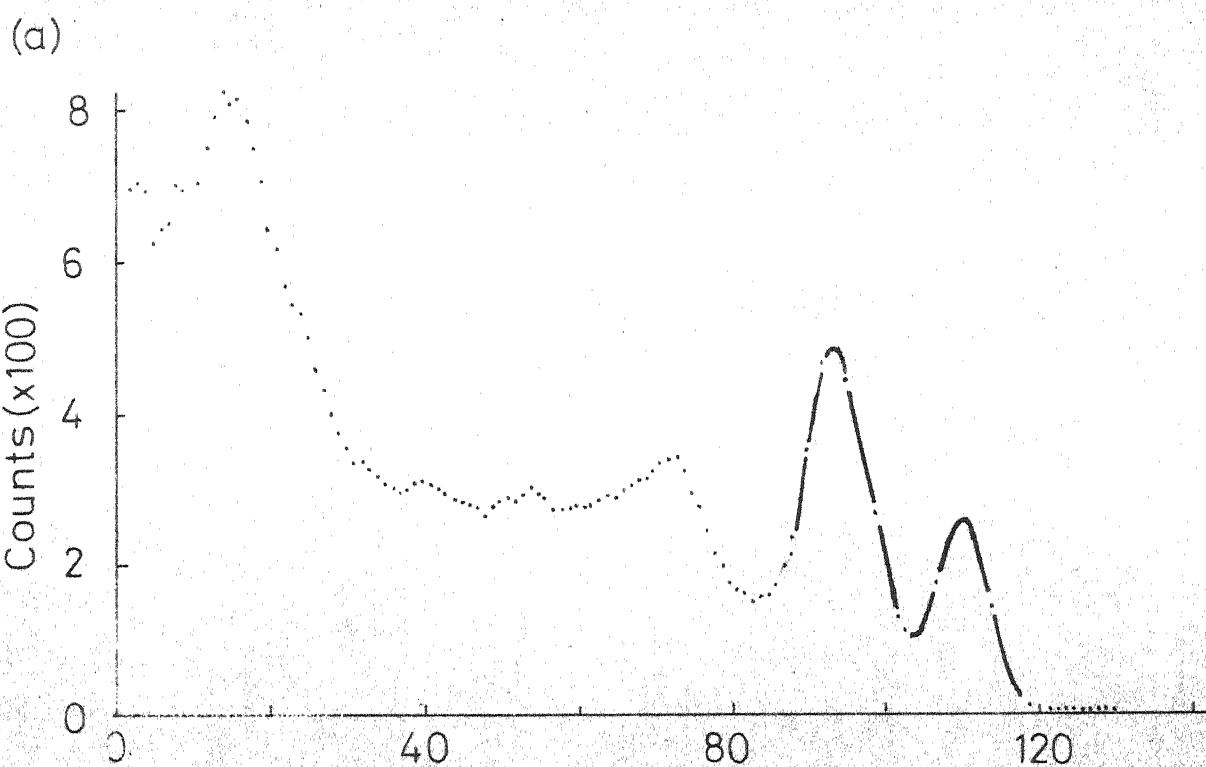
Fig.3·3 (a) Na I (b) Ge (Li) Spectra Of BARC
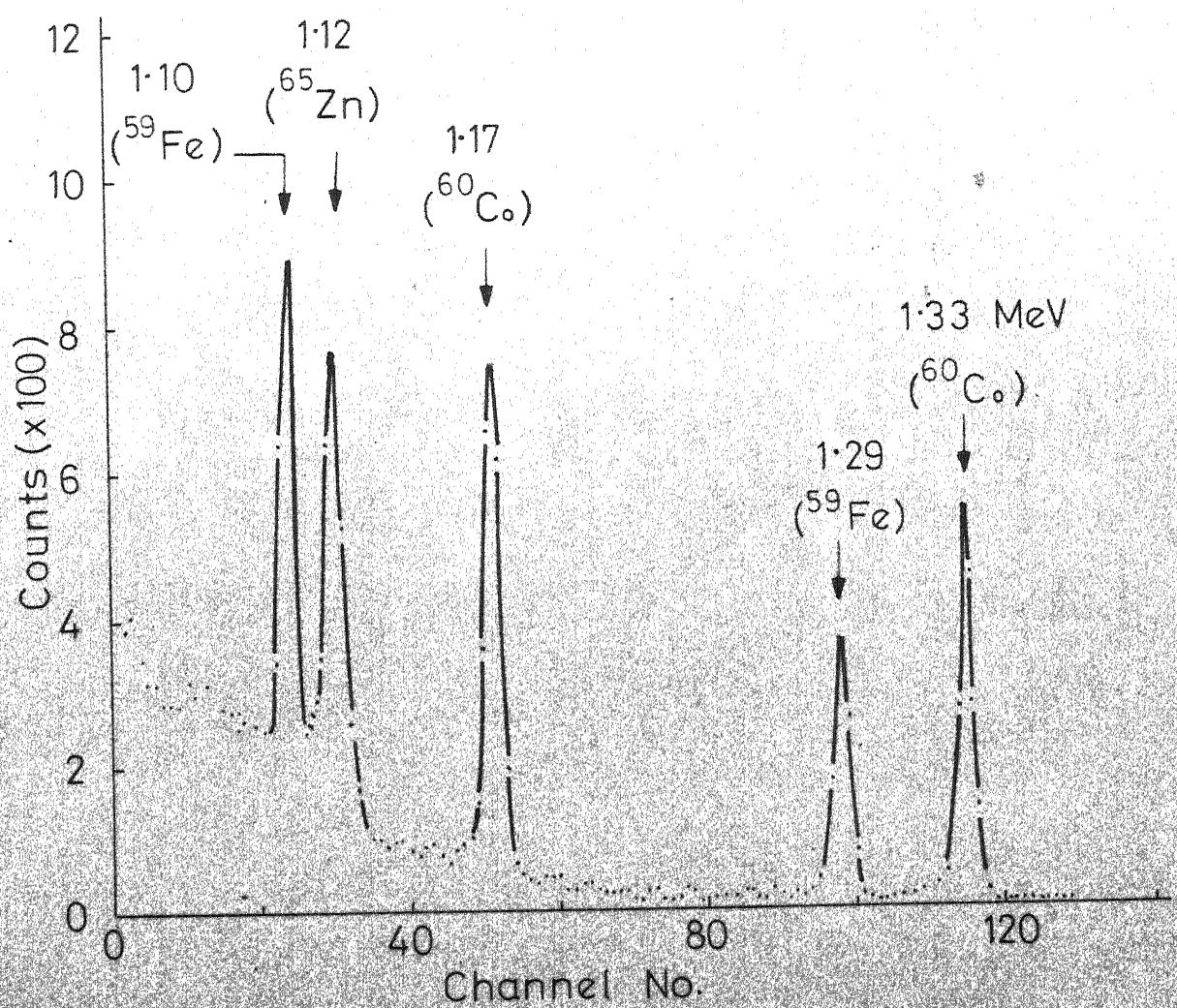Irradiated Aluminium Sample After
∼6 Months

Fig. 3·4 Bias Amplifier Ge (Li) Spectrum Of BARC Irradiated Aluminium Sample After ∼6 Months

(a)

Counts(x100)

8

6

4

2

0

0   40   80   120

Counts(x1000)

8

6

4

2

0

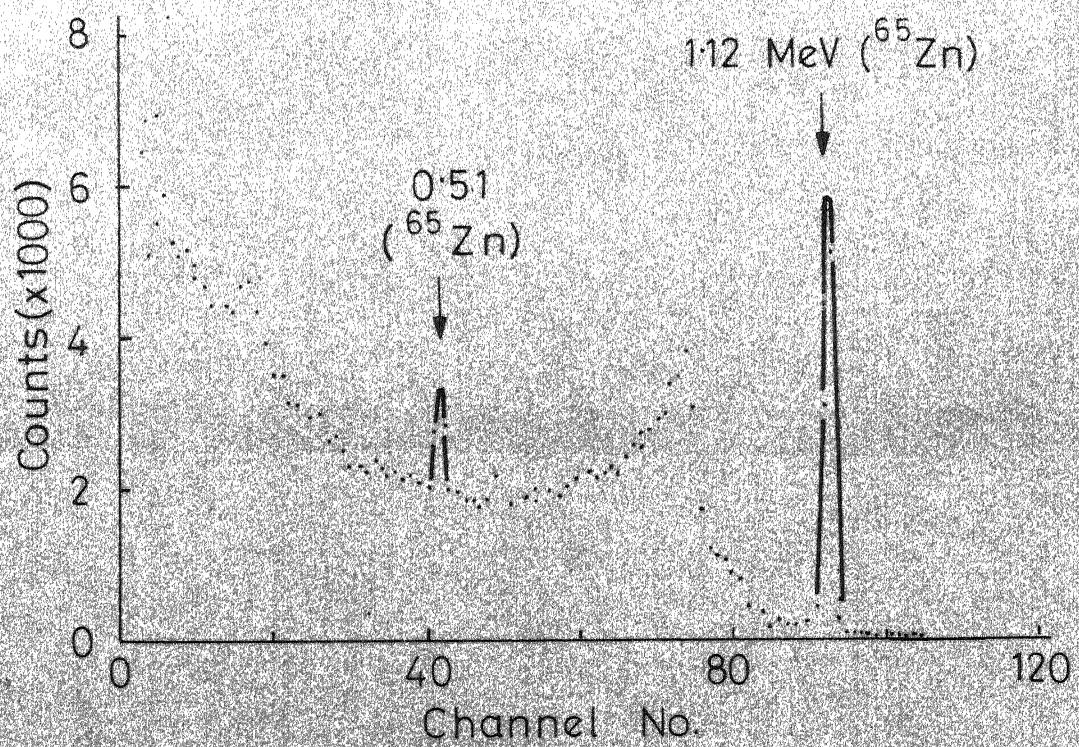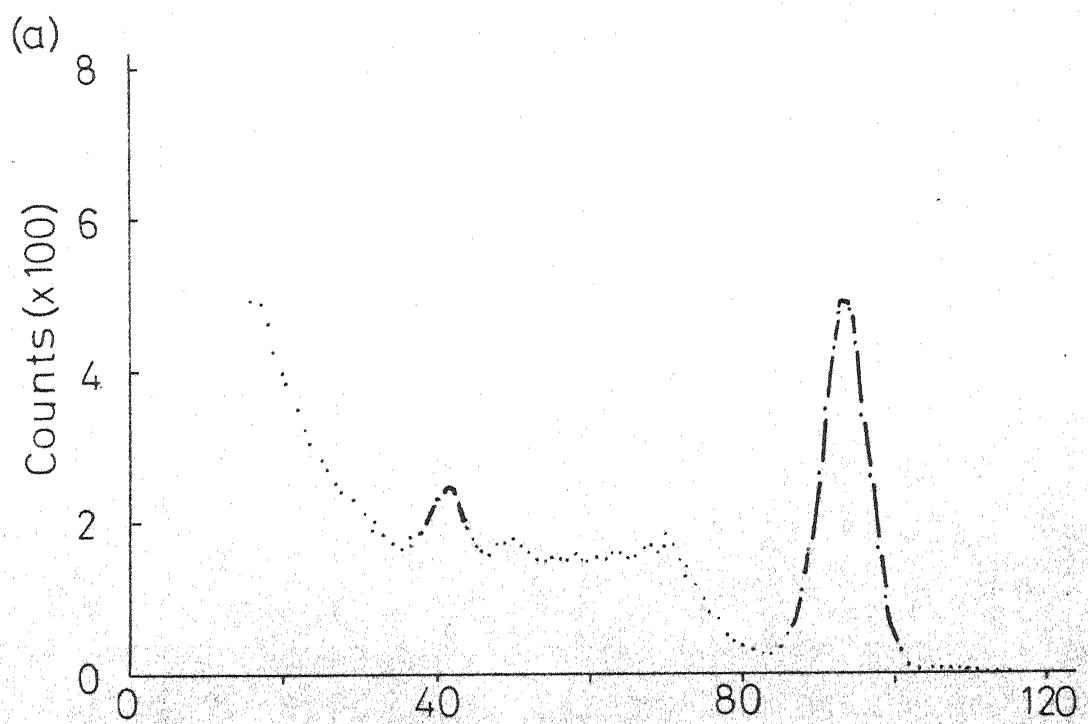1·12 MeV (^{65}Zn)

0·51
(^{65}Zn)

0   40   80   120

Channel No.

Fig. 3·5 (a) Na I; (b) Ge (Li) Spectra Of
BARC Irradiated Brass Sample
After ~ 6 Months
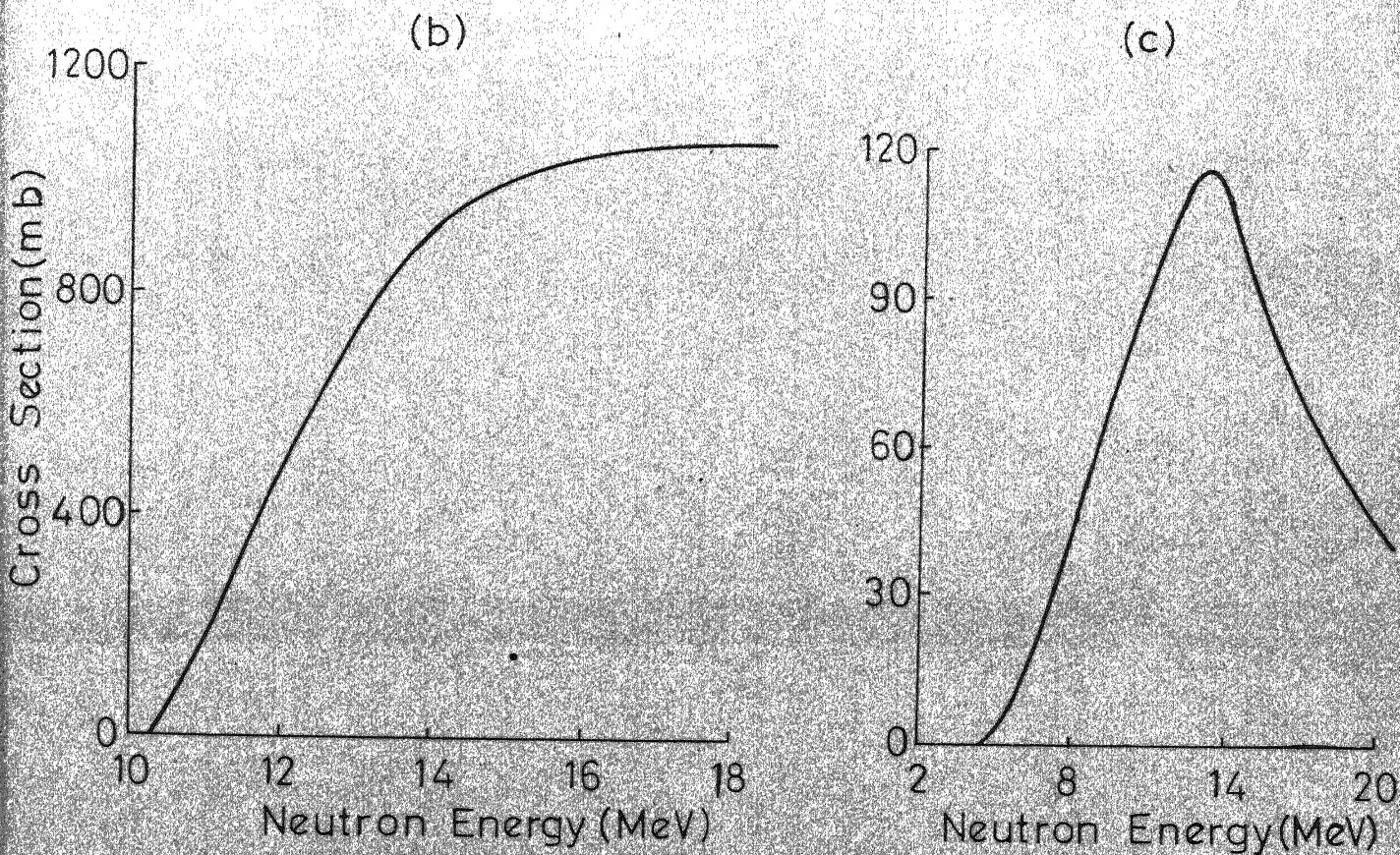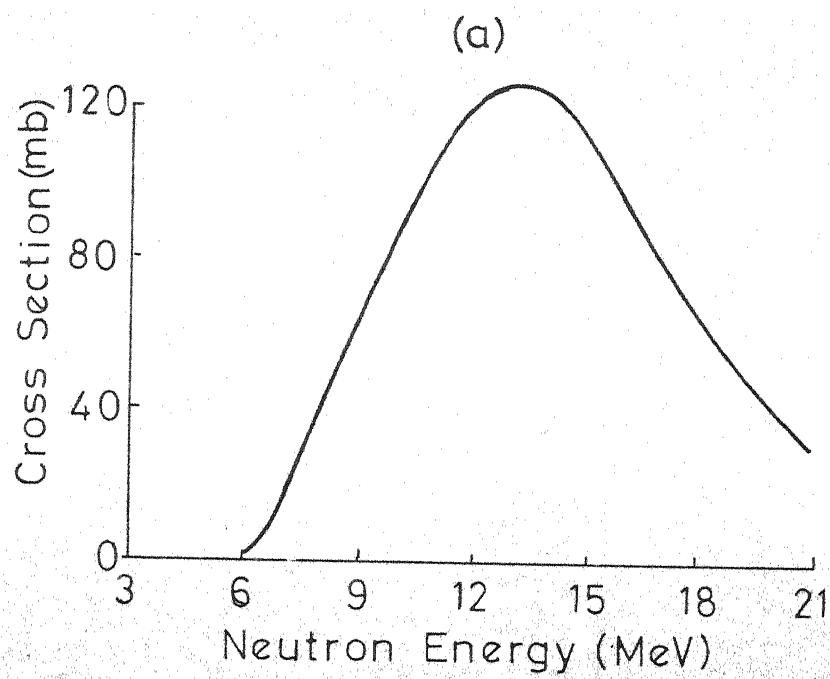
Fig. 3·6   Neutron Cross Sections For (a) ^{27}Al(n, α)
(a) ^{65}Cu(n,2n) (c) ^{56}Fe(n, p) Reactions

1·37 MeV Photopeak

1·73 MeV (Double Escape)

2·24 MeV (Single Escape)

2·75 MeV Photopeak

Counts (x 100)

Channel No.

Fig.3·7 NaI Spectrum Of Van de Graaf Irradiated Aluminium Sample

Fig.3·8 NaI Spectrum Of Van de Graaf Irradiated
(a) Steel (b) Brass Samples

Fig.3.9 Ge (Li) Spectrum Of Van de Graaf Irradiated Brass Sample

3.1 General View of the Van de Graaf Beam Room.

3.2 A Close-up View of the Samples Mounted for
14 MeV Neutron Irradiation.

CHAPTER IV

WHEEL LOADING RESULTS AND THEIR DISCUSSION
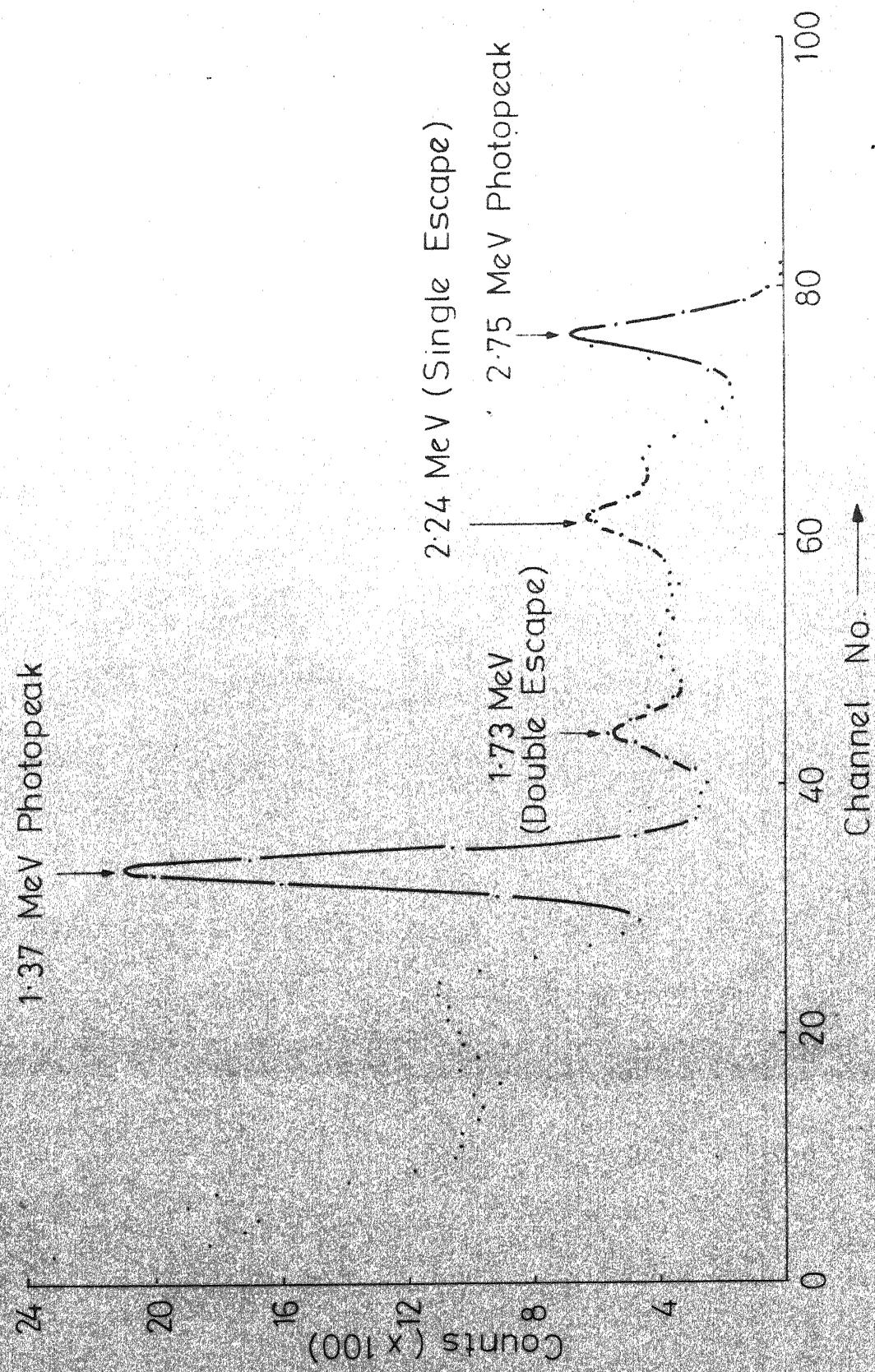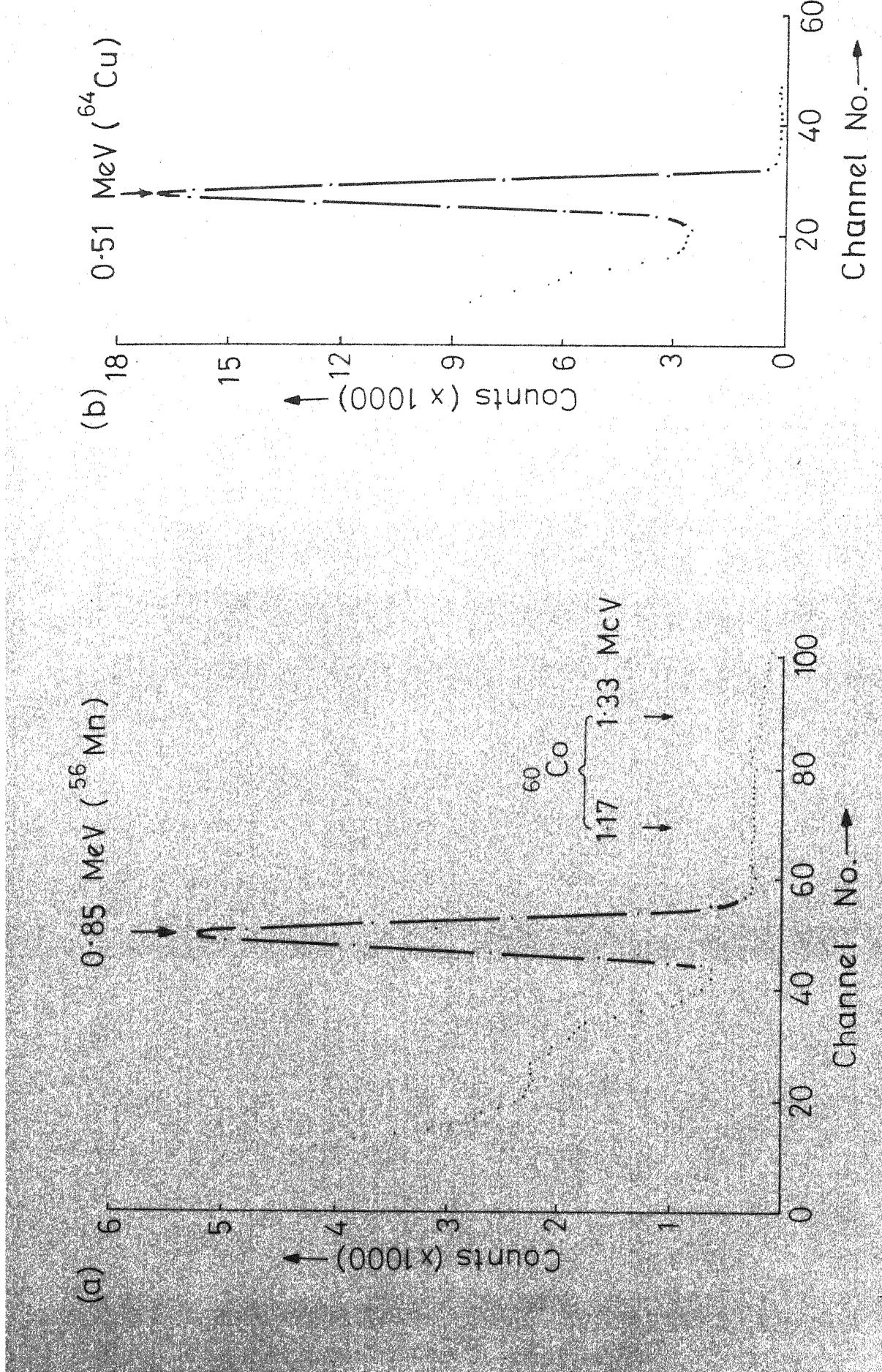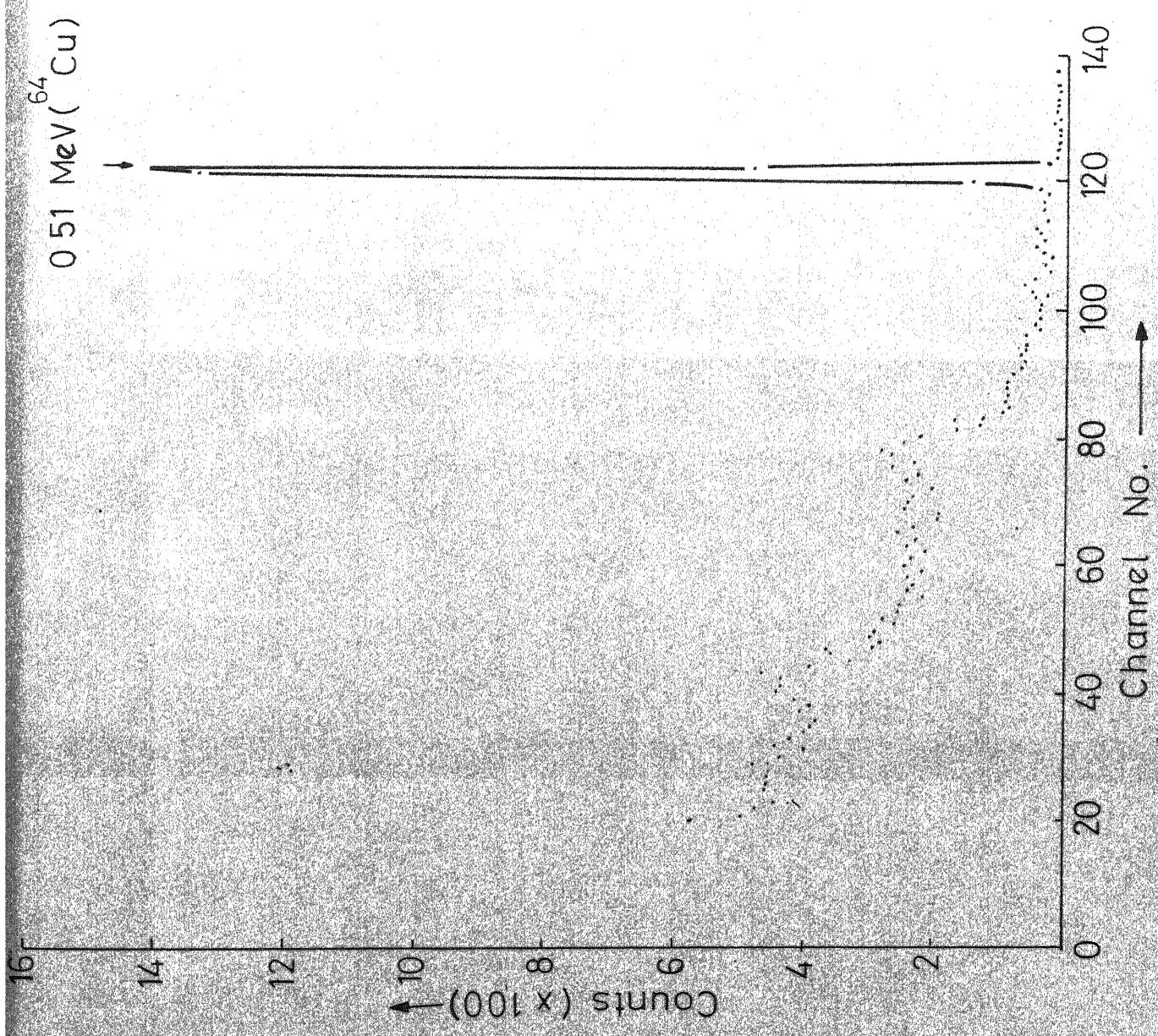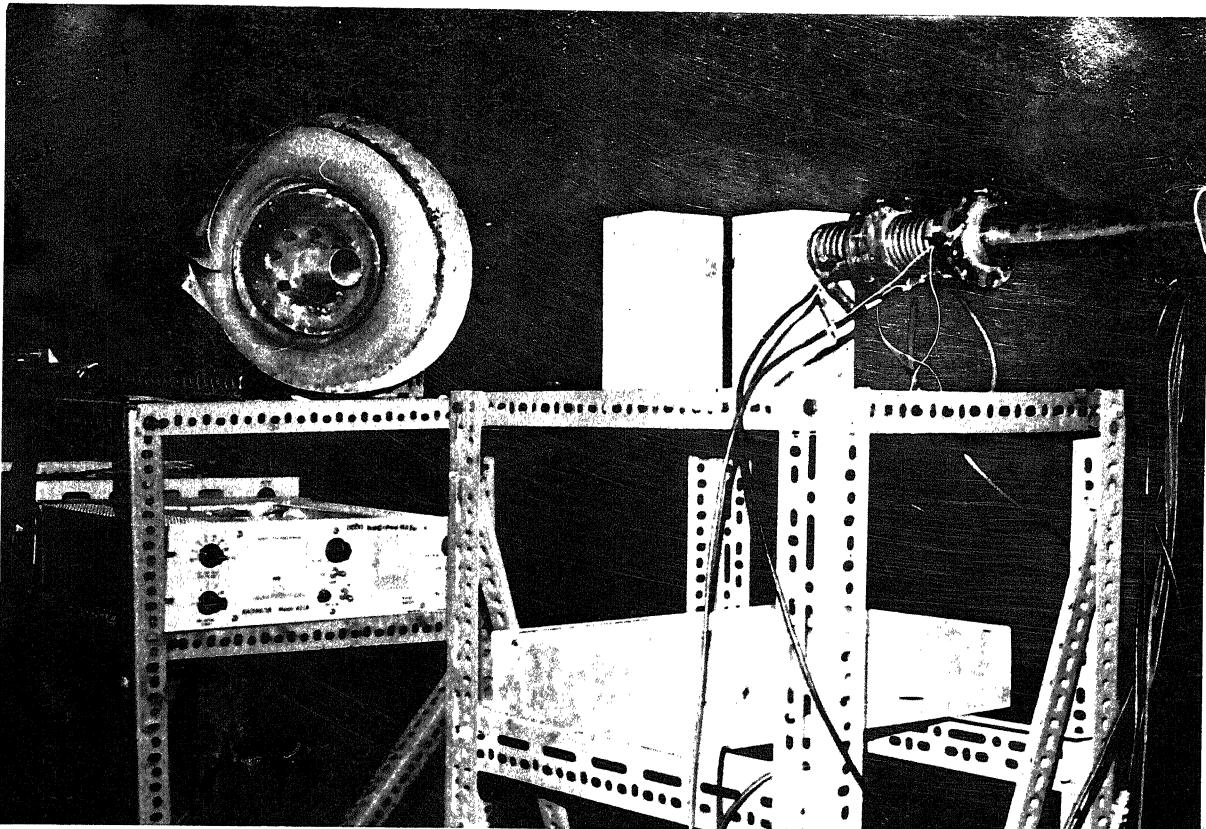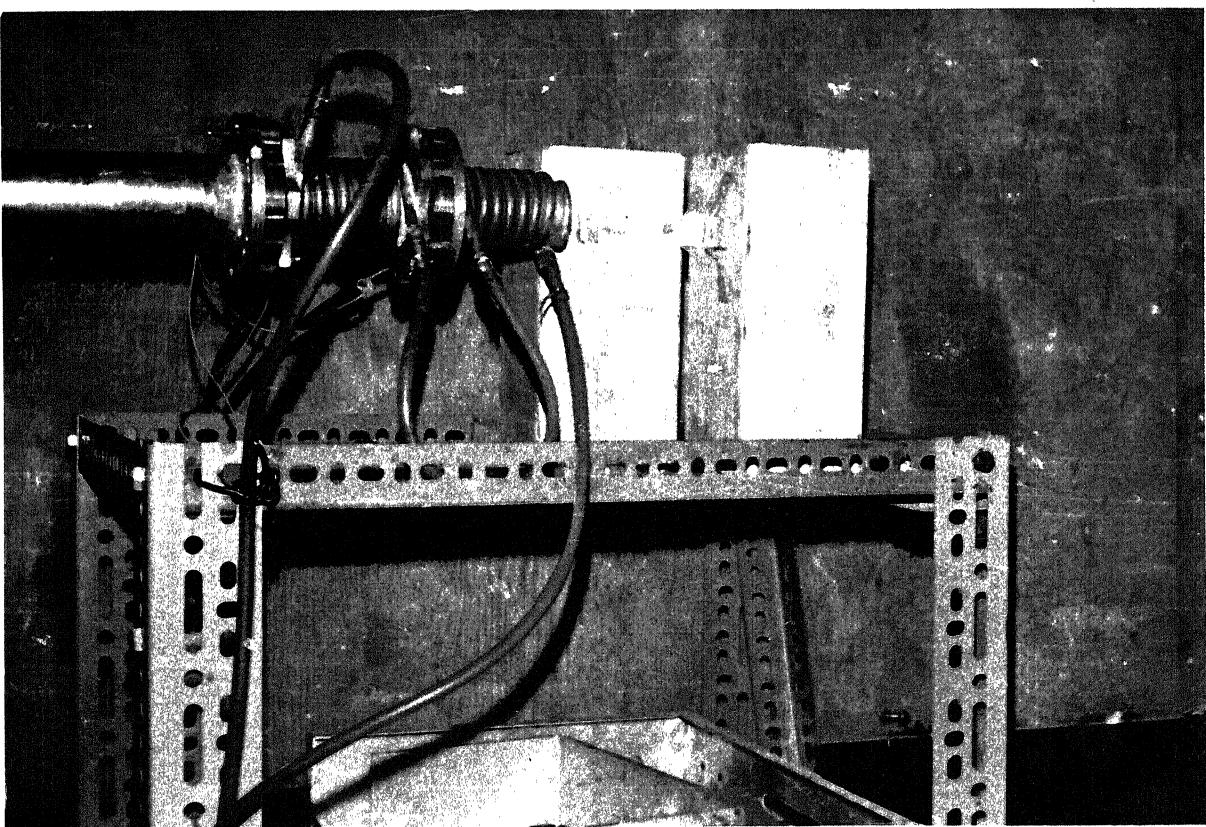
This chapter deals with the various experiments carried out to study characteristics of the wheel loading phenomenon in grinding. Loading curves were obtained for annealed HSS, mild steel, brass and aluminium under dry, plunge-cut conditions over a range of table speeds (v) and depths of cut (d).

For most of the experiments, thermal-neutron irradiated workpieces, i.e. irradiated at BARC (Sec. 3.2), were used. With ^{60}Co as the radiotracer (ann. HSS, mild steel), the 1.17, 1.33 MeV photopeaks were counted (Figs. 3.1(a), 3.2(a)). For ^{65}Zn (brass), the 1.12 MeV photopeak was counted (Fig.3.5(a)), while for ^{59}Fe radiotracer (aluminium), the 1.10, 1.28 MeV photopeaks were counted (Fig. 3.3(a)).

A few experiments were, however, carried out with 14 MeV neutron-activated work samples of hardened HSS, mild steel, brass and aluminium, in order to establish the use of alternative radiotracers for these materials (Sec. 3.3), Here, the portion of the γ-spectra counted were the 0.85 MeV photopeak for ^{56}Mn (steel samples, Fig. 3.8(a)) and the 0.51 MeV photopeak for ^{64}Cu (brass, Fig. 3.8(b)). For ^{24}Na, i.e. in

the case of aluminium, integral counting above 1.3 MeV was employed (Fig. 3.7).

The wheel loading experiments were carried out as per the experimental procedure outlined earlier (Sec. 2.3.2). The extrapolation method (Sec. 2.5.2) was used throughout, for obtaining the loaded amount absolutely from observed count rates of the wheel surface.

During the experiments, measurement of normal (F_n) and tangential (F_t) forces was carried out by feeding output voltages from the two-component, strain-gauge dynamometer to an 'Encardio-rite' recorder (Sec. 2.3.1). The dynamometer was calibrated upto 12 kgf for both F_n and F_t, using dead weights. The calibration was checked frequently for drift. Both vertical and horizontal responses were linear, and there was negligible interaction between the two.

4.1 <u>Nature of the Loading Curves</u>:

4.1.1 <u>Experiments with Annealed HSS</u>:

As a direct extension of Gohad's work, wheel loading experiments were performed for the same annealed HSS workpieces as used by him, i.e. containing ~ 0.1% cobalt and of BHN ~ 240 [9]. The wheel used, however, was different, viz. 38 A 60 K 5 VBE instead of 38A 46 J8 VBE.

At first, a series of short experiments, upto a volume removed (V_r) value of ~ 80 mm^3, was conducted to check the validity of the $V_{\ell 55}$ criterion used by Gohad [9] for this work/wheel combination. Table 4.1 gives the grinding conditions for these experiments, while Fig. 4.1 shows some of the loading curves obtained. These results are further discussed in Sec. 4.2.

Table 4.1: Grinding Conditions for $V_{\ell 55}$ Experiments with Annealed HSS

Experiment No.	1	2	3	4	5	6	7	8	9
Depths of Cut, d(mm)	.00975	.0043	.0065	.00975	.013	.01625	.0195	.00975	.013
Table speed, v(m/min)	3.3	5	5	5	5	5	5	6.7	6.7

One of the interpretations made by Gohad of his experimental results was that the loaded amount reached a steady-state, <u>constant</u> volume corresponding to dynamic equilibrium between fresh material being loaded and loaded material being removed due to wheel wear, etc. In order to check this, it was felt that the loading experiments should be conducted for a much longer time than considered by Gohad. When this

was done, it was found that the loaded volume ˉdoes
increase more rapidly at first than later, but the rate of
increase in stage II [9] is certainly not insignificant.

Fig. 4.2 shows the results from one of Gohad's experi-
ments for which a V_r-value of ~120 mm^3 was achieved, as
compared to ~60 mm^3 for the majority of his experiments.
Here, it can be seen that, after 'dynamic equilibrium' had
been attained, the amount of loaded material did increase
further. However, this was interpretated by Gohad as being
caused by the appearance of small burrs on the sides of the
workpiece, as a consequence of which some fresh cutting
surface of the wheel would be exposed to the workpiece
and would result in a second, higher 'plateau'. In order to
check the validity of this explanation, a few experiments
were conducted with and without the removal of burrs that
appeared during the grinding. Fig. 4.3 shows typical results
for a pair of such experiments, conducted upto V_r ~800 mm^3.
It was found that, while there was some finite (~5%) contri-
bution of burrs to the wheel loading, the nature of the load-
ing curve essentially remained unaffected, viz. that the
initial stage of loading was followed by a slower, but
steady, increase in loaded volume. A reinterpretation
of Gohad's data is shown by the dotted line in Fig. 4.2.

4.1.2 Experiments with Mild Steel and Brass:

Wheel loading studies for mild steel and brass were conducted for table speeds in the range 3-8 m/min. and depths of cut between .0065 - .0195 mm.

The nature of the loading curve for mild steel specimens with alumina (38A) wheels is exemplified by Fig. 4.4, which compares the loading results for two different grain sizes (46 and 60) upto $V_r \sim 300$ mm^3, the cutting conditions being v = 5 m /min, d = .0065 mm. Though the initial increase of loaded volume was higher for 46 grain size, the finally loaded volume was more for 60 grain size.

Fig. 4.5 illustrates the nature of the loading curves for brass with two different types of alumina wheels (38A 60K5 VBE and A60 P5 V99), for the same grinding conditions as above, viz. v = 5m/min, d = .0065 mm. Fig. 4.6 shows brass loading curves with a SiC wheel (39C 60L5 VK) for v = 5m/min and d - values of .013 and .0195 mm. It is seen that the A60 P5 V99 wheel had the greatest tendency to load.

In all the above experiments, for both mild steel and brass, the basic nature of the loading curves is seen to be similar, viz. a newly dressed wheel loads rapidly in the initial stages, and this is followed by a steady increase in the loading at a slower rate (Sec. 4.1.1). The initial

and partly to the greatly reduced wheel wear which would result in a much smaller number of loaded particles being removed from the wheel surface.

The above described approach to saturation loading in the case of aluminium, with work material tending to fill pores on the cutting surface completely was accompanied by a marked reduction in volume removal rate. (The corresponding portion of the loading curve is shown dotted). Forces increased, and further grinding resulted in a reduction of the loaded volume due to rubbing between the wheel and work surfaces.

Aluminium loading studies were conducted with a SiC wheel (39C 60H5 VK) for table speeds between 2-6 m/min. and d-valves between .00325 - .00975 mm, upto $V_r \sim$ 100 mm^3 for each experiment. Fig. 4.8 shows the loading curves obtained, the basic nature of these being similar to that for the alumina wheel discussed above.

4.2 Selection of Loading Criteria:

Values of the loaded volume, V_{L55} (corresponding to volume - removal of 55 mm^3), obtained from the series of short experiments performed with annealed HSS with alumina (38A 60K5 VBE) wheel (Sec. 4.1.1, Table 4.1) are shown plotted

in Fig. 4.9 against table speed (v), depth of cut (d), volume removal rate (α v.d) and chip thickness (α $v^{\frac{1}{2}}$ $d^{1/4}$) It is seen that this particular loading criterion [9] fails to bring out any systematic trend in the variation of loading with grinding conditions, as would be expected from empirical considerations.

For the studies conducted for the other work materials, viz. mild steel, brass and aluminum, it was felt that loading criteria should be chosen with the following conditions satisfied:

(a)   The criterion should be at a point on the loading curve well away from   the initial transient loading region

(b)   Forces should be steady at this point, and

(c)   Volume removal rate should be unaffected.

Three different types of criteria have been tried out, viz.

(i)   the loaded volume, V_l , corresponding to a fixed volume removed.

(ii) V_l corresponding to a fixed number of passes.

(iii) V_l corresponding to a constant grinding time.

From consideration of the loading curves for mild steel and brass for alumina (38A 60K5 VBE) and SiC(39C 60L5 VK wheels (Figs. 4.4 to 4.6) the loading criteria, or parameters, selected were:

(i) $V_{\ell\ 150\ mm^3}$ - loaded volume corresponding to volume

removal of 150 mm^3.

(ii) $V_{\ell 150 P}$ - loaded volume corresponding to 150   grinding

passes.

(iii) $V_{\ell 15\ sec}$ - loaded volume corresponding to grinding

time of 15 seconds.

Similarly, for the aluminium workpiece, with a series

of experiments having been conducted with SiC(39C 60L5 VK)

wheel (Fig. 4.8), the parameters chosen were $V_{\ell 40\ mm^3}$, $V_{\ell 40\ P}$

and $V_{\ell 4\ sec}$. Forces were not near-constant at these points,

in the case of aluminium, but the more important consideration

was that the points should lie before the approach-to-satura-

tion region of the loading curve where the volume removal

rate gets significantly affected.

For clear graphical representation of the various data

obtained, symbols have been standardised for the different

experiments (v, d combinations) carried out, and these are

shown in Fig. 4.10. Variation of the loading parameters

with v, d, volume removal rate, chip thickness, etc. are

presented and discussed in the next section.

4.3   Effects of Grinding Conditions on Loading Parameters:

A series of experiments were conducted with both

SiC(39C 60L5 VK) and alumina (38A 60K5 VBE) wheels in the

case of brass, and with alumina wheel only in the case of mild steel. Table speeds of 3, 5 and 8 m/min. and depths of cut of .0065, .013 and .0195 mm were considered for these two materials. In the case of aluminium, the SiC wheel was used for v-values of 2, 4 and 6 m/min. and d-values of .00325, .0065 and .00975 mm.

For each experiment, the wheel loading was measured only at the three points corresponding to the three different criteria discussed in Sec. 4.2. A statistical accuracy of typically ± 4%, was obtained for each measurement. However, the overall accuracy of the results was limited by random effects in the grinding process, which caused the repeatability of the experiments to be only within ~ 10%.

4.3.1 Variation with Table Speed and Depth of Cut:

Figs. 4.11 and 4.12 show the variation of loading parameters for with v and d, respectively, for the work/wheel combination of brass/SiC. It is seen that $V_{\ell 150 \, mm^3}$ fails to show up any specific trend of variation, while $V_{\ell 15 \, sec}$ increases consistently with both v and d.

Fig. 4.13 gives the variation for brass/alumina. $V_{\ell 15 \, sec}$ and $V_{\ell 150P}$ are seen to increase continuously with d, but only upto a certain value with v. $V_{\ell 150 \, mm^3}$, on the other hand decreases continuously with both v and d.

For mild steel/alumina (Fig. 4.14), one again sees that $V_{L15\ sec}$ and V_{L150P} show more consistent trends than $V_{L150\ mm^3}$.

Results for aluminium/SiC are shown in Fig. 4.15, the loading parameters considered being $V_{L40\ mm^3}$, V_{L40P} and $V_{L4\ sec}$ in this case. The sensitivity of loading to v, d values is seen to be greater for aluminium than brass or mild steel.

From the $V_{L15\ sec}$ results with alumina wheel, it is seen that loading is greater, as would be expected, for brass than for mild steel. A comparison of the $V_{L15\ sec}$ obtained with SiC and alumina wheel in the case of brass, shows that, while at low d-values the alumina wheel loads more than the SiC, this trend is reversed at a higher depth of cut. This may be explained by the greater wheel wear rate that would be expected with the alumina wheel for large v, d values, which would result in a higher 'falling off' rate for the loaded particles. The same argument may be used to explain the decrease in $V_{L15\ sec}$ with both v and d (at higher values of v and d), in the case of mild steel/alumina (Fig. 4.14).

4.3.2 Variation with Material Removal Rate and Chip Thickness:

From an empirical point of view, it was felt that a parameter characterising loading should depend on some

appropriate combination of cutting conditions, such as material removal rate ($\alpha\ v\ d$) or chip thickness ($\alpha\ v^{1/2}\ d^{1/4}$).

Figs. 4.16 and 4.17 show the variation of the three types of loading parameters with vd and $v^{1/2}\ d^{1/4}$, respectively, for the case of brass/SiC. It is seen that, while there is not any significant variation for $V_{l150\ mm3}$, both $V_{l150\ P}$ and $V_{l15\ sec}$ show increasing trends with both combinations of v and d. One would, of course, expect the variation to be well defined for only one, if any, of the two combinations. Consideration of the scatter in the data indicates that the smoothest variation is for the $V_{l15\ sec}$ - vs - chip thick plot.

The data for brass/alumina (Fig. 4.18) is less comprehensive. Here, a decreasing trend is observed for $V_{l150\ mm3}$, while results for the constant-time criterion ($V_{l15\ sec}$) are the most consistent.

Figs. 4.19 and 4.20 are the plots for mild steel/ alumina where again, $V_{l150\ mm3}$ is seen to show little variation. The $V_{l150\ P}$ data has considerable scatter, while for $V_{l15\ sec}$ the variation appears smoother with material removal rate than with chip thickness, except for the datum for the highest v and d values. If one considers

particles at the higher v, d values for the alumina wheel (sec. 4.3.1) both plots of $V_{\lambda 15\ sec}$ appear more consistent.

The data for aluminium/SiC is shown plotted in Fig. 4.21, with the constant time parameter of $V_{\lambda\ 4\ sec}$ showing the least scatter in the two plots.

Again, one would not expect any empirically determined variation to be equally well defined with respect to both v d and $v^{1/2}\ d^{1/4}$, but the present data, though limited, does indicate more consistent trends when the loading parameter considered is one based on constant grinding time, rather than on fixed V_r or fixed number of passes.

4.3.3 Variation with Forces:

Figs. 4.22 - 4.25 show the variation of normal and tangential forces with v and d, in the case of brass/SiC, brass/alumina, mild steel/alumina and aluminium/SiC, respectively. Unidirectional, increasing trends are seen in each case. From Figs. 4.23, 4.24, it is seen that for the alumina wheel, F_t is considerably higher in the grinding of mild steel than in the case of brass, while F_n values are similar. Comparison of Figs. 4.22, 4.23 shows that the forces are similar for the SiC and alumina wheels, in the case of brass.

The variation of loading parameters with F_t and F_n
are shown in Figs. 4.26 and 4.27 for brass/SiC, in Fig.4.28
for brass/alumina, in Fig. 4.29 for mild steel/alumina and
in Fig. 4.30 for aluminum/SiC. Scatter in the plots is least
for those of constant-time loading criteria which indicate
increasing trends of loading with both F_n and F_t. Thus, one
might conclude that the factors which cause increased grinding
forces also induce higher wheel loading.

The variation of the loading with grinding coefficient,
(F_t/F_n), is plotted in Figs. 4.31 - 4.34 for brass/SiC, brass/
alumina, mild steel/alumina and aluminium/SiC, respectively.
No consistent trends are observable, except for the $V_{l_4 \text{ sec}}$
criterion in the case of aluminium, for which a consistent
decrease in the grinding coefficient with increase in loading
is apparent. This may be explained by the fact that, it is
only in the case of aluminium that wheel loading would have a
much more dominating effect on the force pattern than other
effects such as attritious wear of the grains, etc.

4.3.4 Effects of Grain Size:

Experiments with three different grain sizes (viz. 46,
60 and 80) of alumina wheel were carried out in the grinding
of brass and mild steel. Figs. 4.35, 4.36 show the variation of
forces, grinding coefficient and loading parameters with grain

size, for the experiments with brass and mild steel, respectively. The trends are similar for the two materials. Forces decrease with grain size, the grinding coefficient indicating a slight dip at 60 grain size. The wheel loading is seen to first increase with grain size (46 to 60) and then decrease (60 to 80). While this is consistent with the dip in grinding coefficient, the results appear ambiguous as one would expect a unidirectional variation with grain size.

4.4 Comparison of Results for BARC and Van de Graaf Irradiated Work Samples:

As mentioned earlier, in order to establish the use of alternative radiotracers for loading studies, activation of mild steel, brass, aluminium and hardened HSS was carried out using the Van de Graaf at IIT Kanpur as a source of 14 MeV neutrons. Experiments were conducted for the activated workpieces using the wheels and grinding conditions listed in Table 4.2.

Table 4.2: Grinding Conditions for Experiments with Van de Graaf Irradiated Workpieces.

Work Material	Wheel	v(m/min)	d(mm)	Wheel Speed (rpm)
Mild Steel	38A 60K5 VBE	5	.0065	3000
Hardened HSS	38A 60K5 VBE	5	.0065	3000
Brass	39C 60L5 VK	5	.0065	3000
Aluminium	38A 60K5 VBE	4	.0065	2000

The experiments were carried out as for BARC irradiated workpieces, except that appropriate decay corrections had to be applied in the γ-counting. In each experiment, a reference piece of work material, which had been irradiated along with the workpiece, was used to monitor any drift in the electronics. The decay-corrected, singles count rates from the wheel were normalised to yield absolute results using the extrapolation method (Sec. 2.3.2).

Because of the lower induced activities, statistical accuracies (typically $\pm 6\%$) were slightly poorer for these experiments, as compared to those conducted with BARC irradiated workpieces. Secondly, as the specimens had to be irradiated relatively close to the target (at ~ 6 cm distance), there was some heterogeneity of the induced activity in the direction of the incident neutrons. Finite corrections had to be applied for this effect.

Figs. 4.37-4.39 show comparisons of the loading curves obtained with Van de Graaf and BARC irradiated workpieces of mild steel, brass and aluminium, respectively. It is seen that in each case, the nature of the loading curves is consistent and that the absolute values of loaded volume agree within $\sim 10\%$, i.e. within experimental errors. This confirms the absence of any systematic errors, e.g. diffusion effects which might be suspected in the case of aluminium with ^{59}Fe radiotracer.

Fig. 4.40 gives the relative loading curve obtained
for the 14 MeV neutron activated hardened HSS workpiece
(^{56}Mn radiotracer), a normalisation to absolute results not
having been made in this case since a BARC irradiated specimen
was not available for comparison.
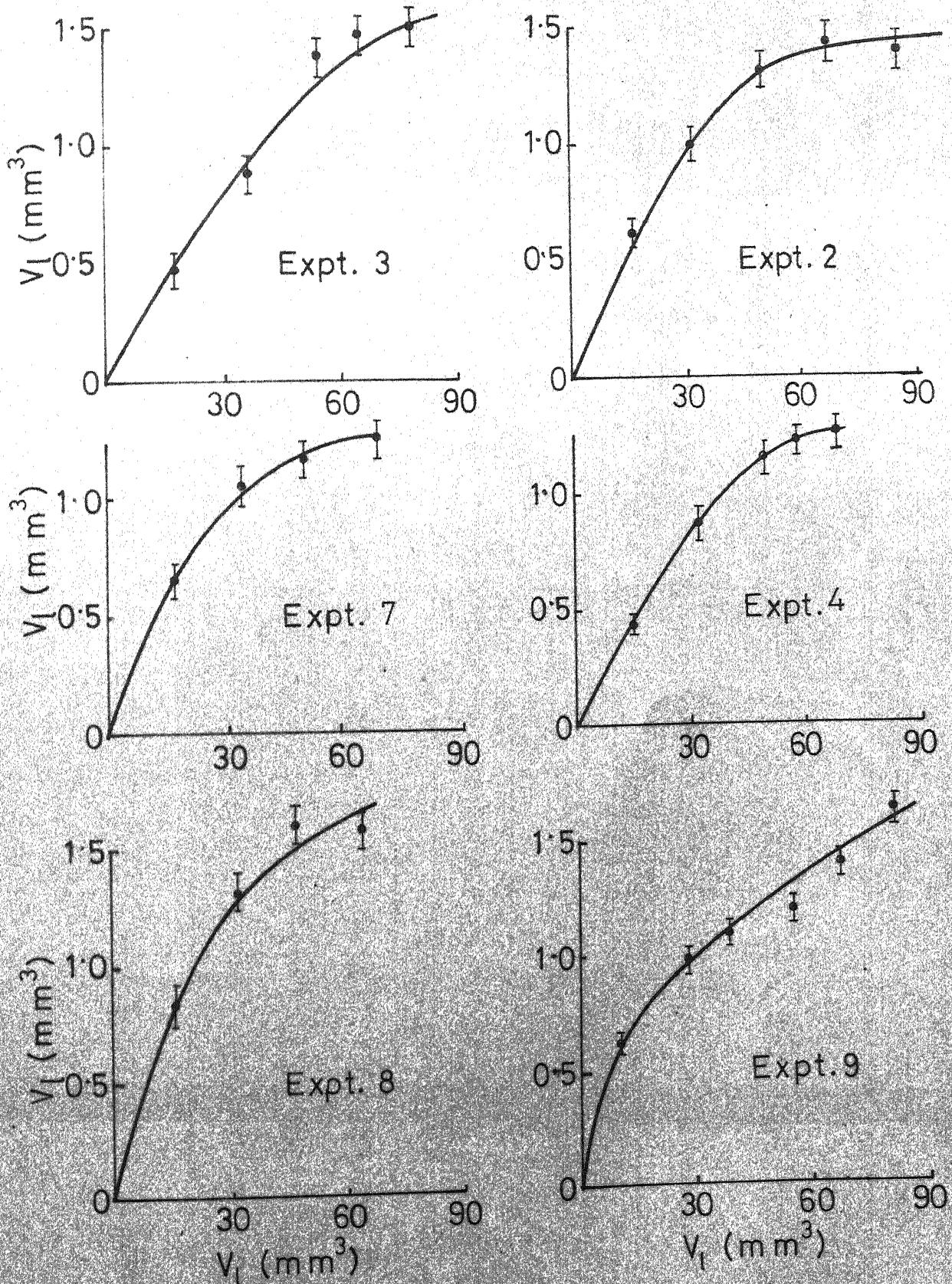
Fig. 4·1   Loading Curves For Ann. HSS
($V_{I\,55}$ Expts., Table 4.1)

Work Material: Ann. HSS
38A 46 J8 Wheel
$v = 5$ m/min
$d = \cdot 0065$ mm

——— Curve From Ref. 9
- - - - Possible Variation
         Without Burrs

$V_r (mm^3)$

$V (mm^3)$
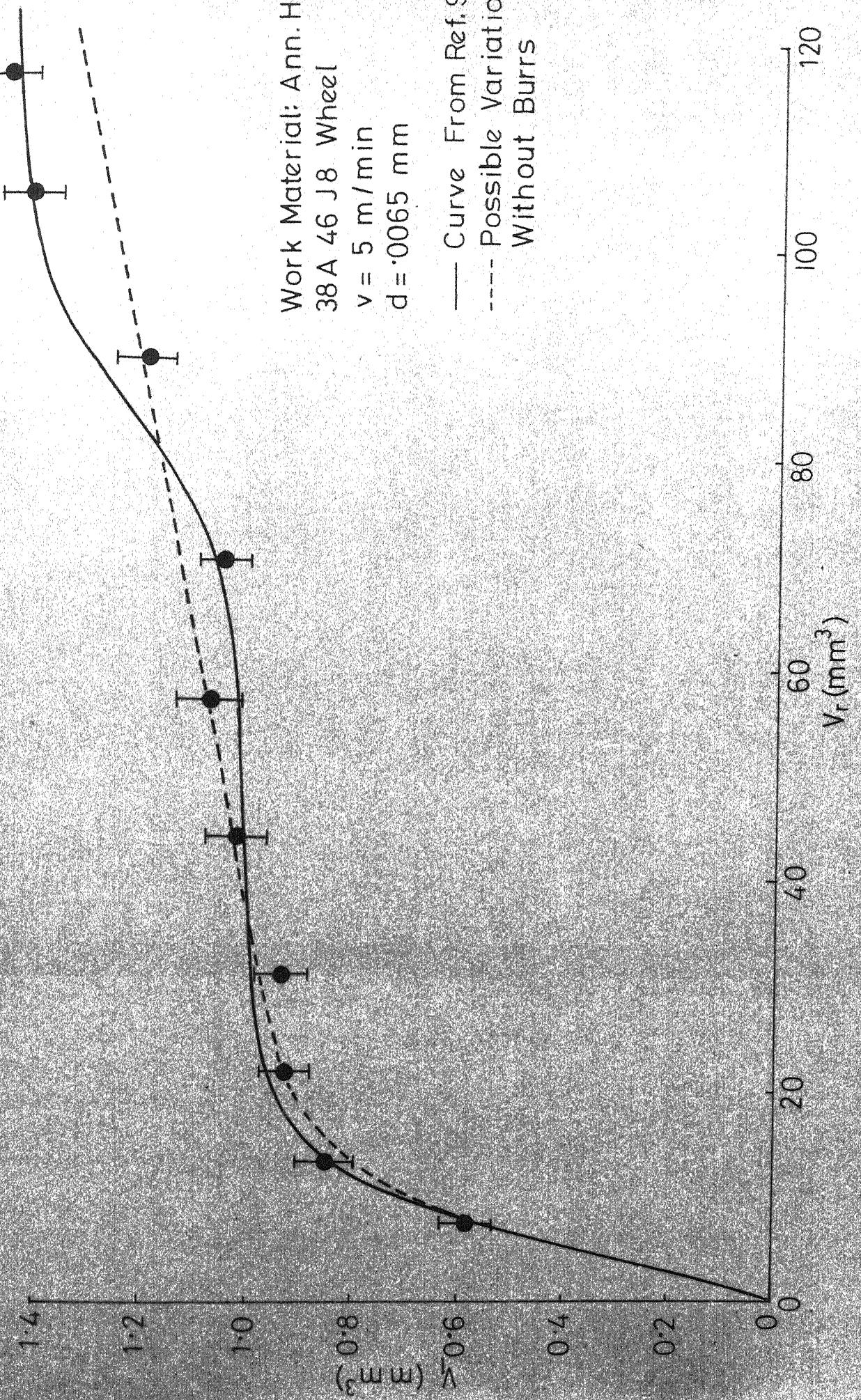
Fig. 4·2 Reinterpretation Of A Loading Curve From Ref. No.[9]

38A 60 K5 VBE
V = 5 m/min
d = 0.013 mm

F_n

F_t

Force (kgf)

V_r (mm^3)
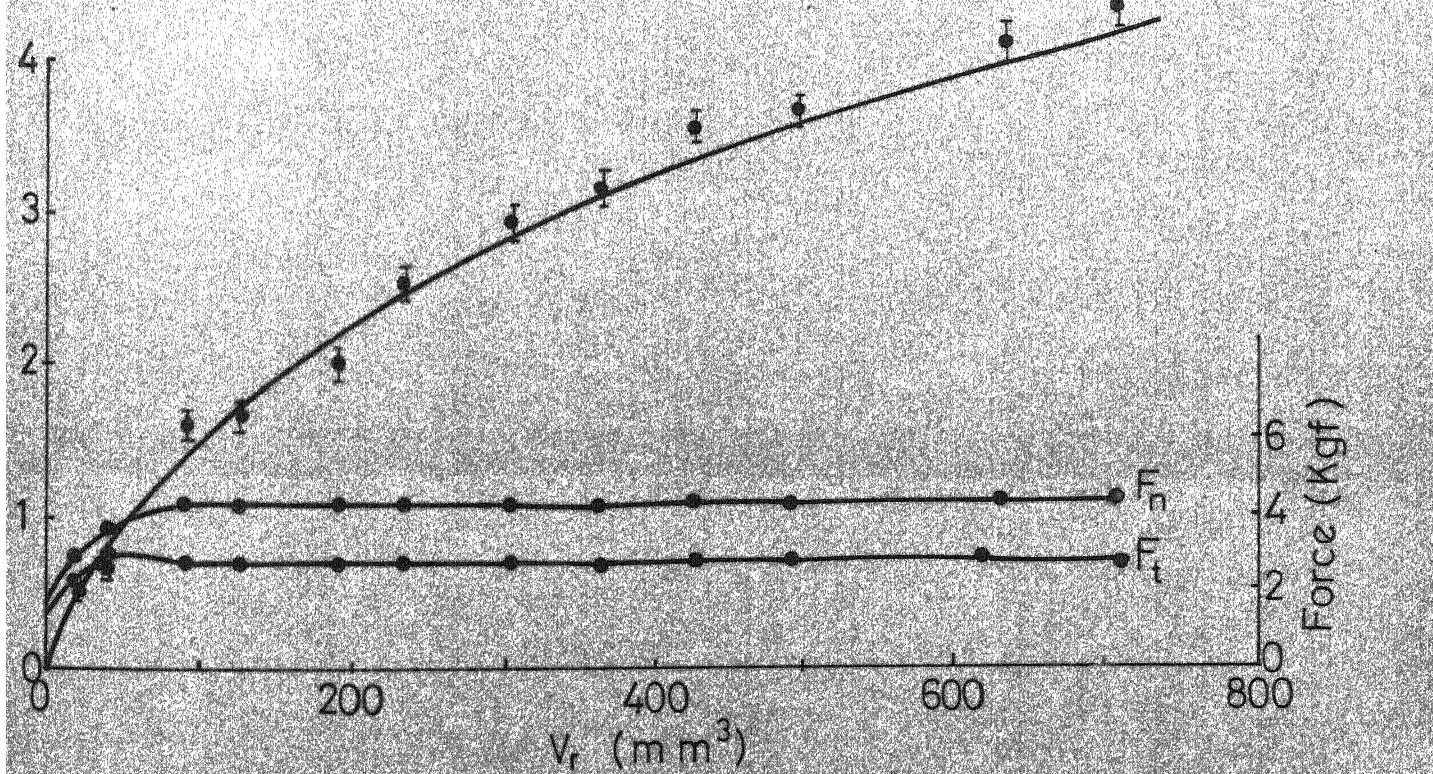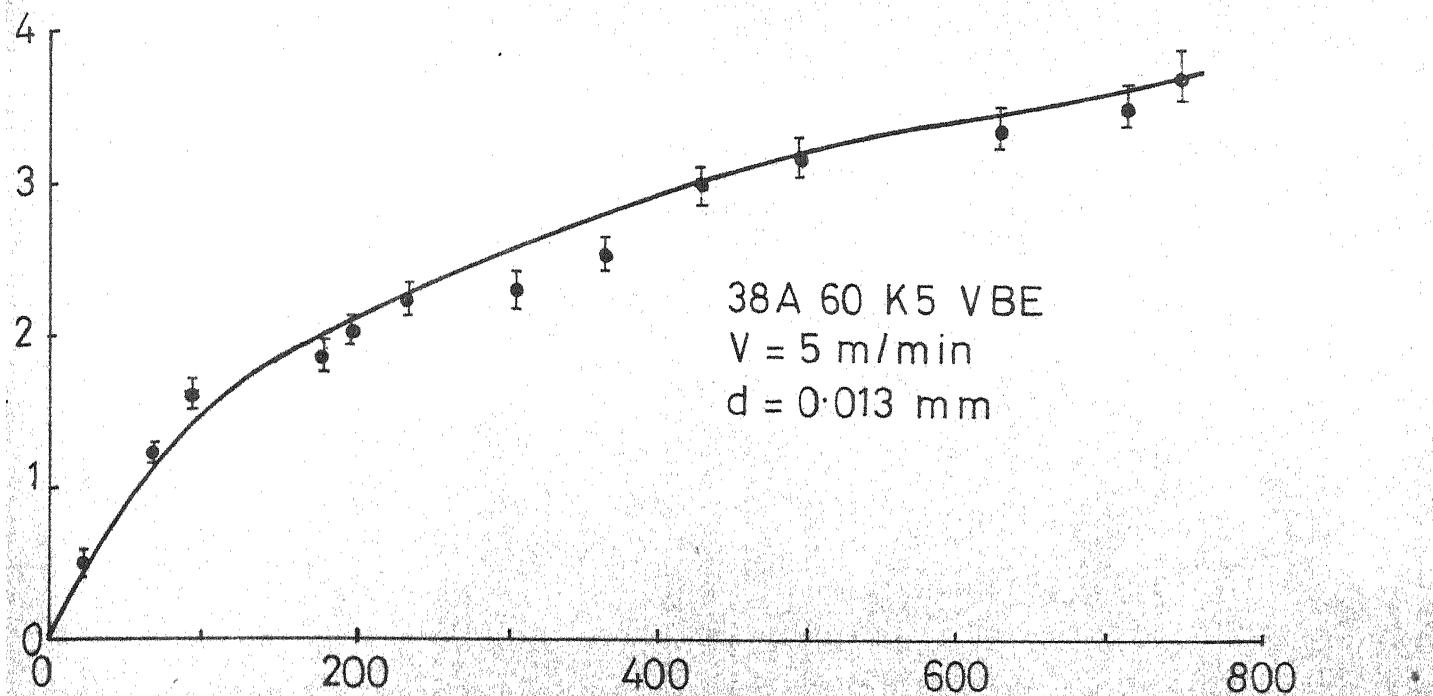
g. 4.3 Loading Curve For Ann. HSS (a) With
        Burr Removal, (b) Without Removal
        Of Burrs

Top chart labels:
V_l (mm^3) — vertical axis

38 A 46 K 5 V B E
v = 5 m/min
d = ·0065 mm

Bottom chart labels:
V_l (mm^3) — vertical axis

38 A 60 K 5 V B E
v = 5 m/min
d = ·0065 mm

V_r (mm^3) — horizontal axis
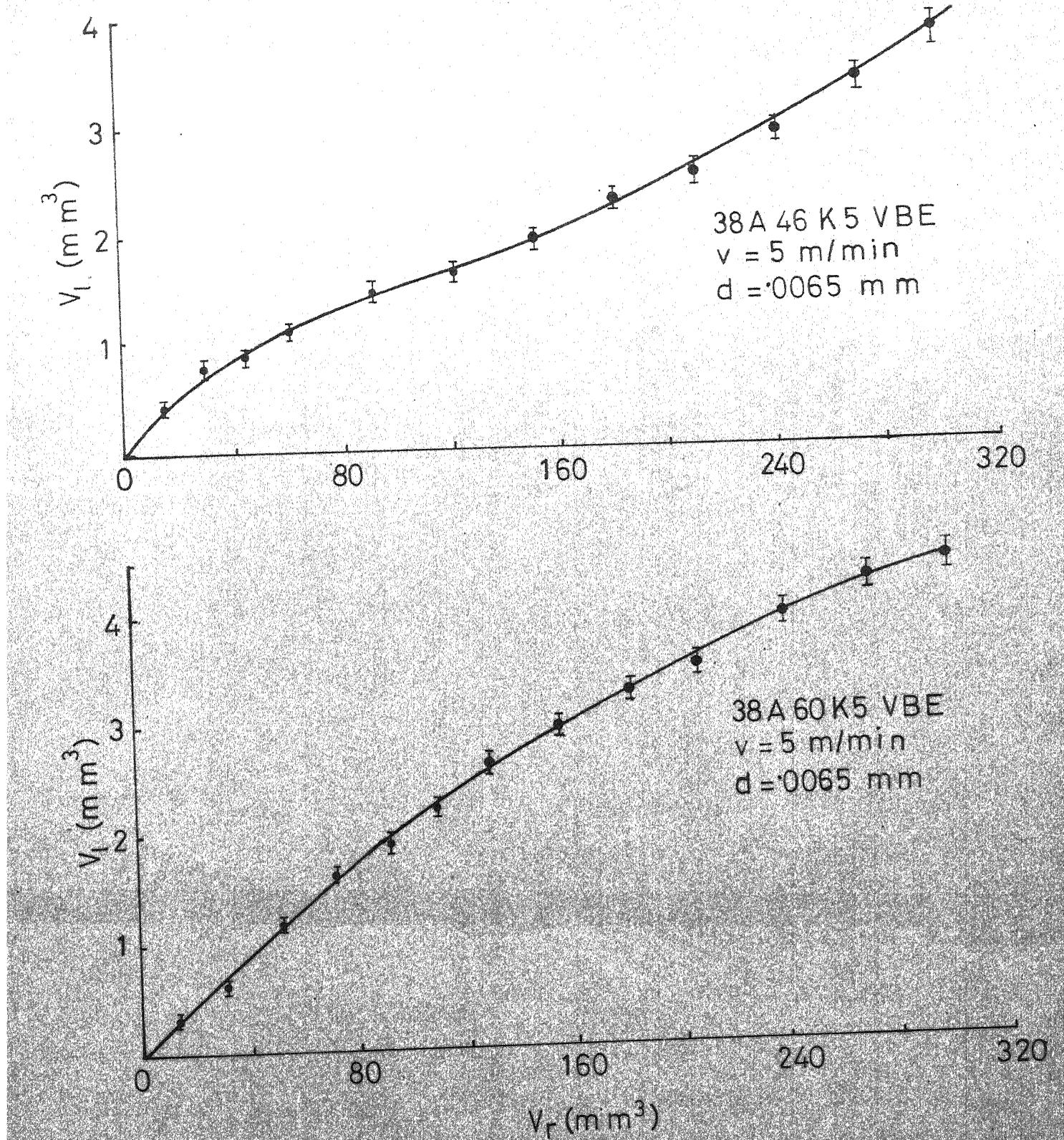
Fig. 4·4 Comparison Of Loading Curves For Mild Steel With 60 K 5 And 46 K 5 Wheels

(a)

38 A 60 K 5 V B E
V = 5 m / min
d = ·0065 mm

(b)

A 60 P 5 V 99
V = 5 m / min
d = ·0065 mm

F_n

F_t

$V_r \, (mm^3)$
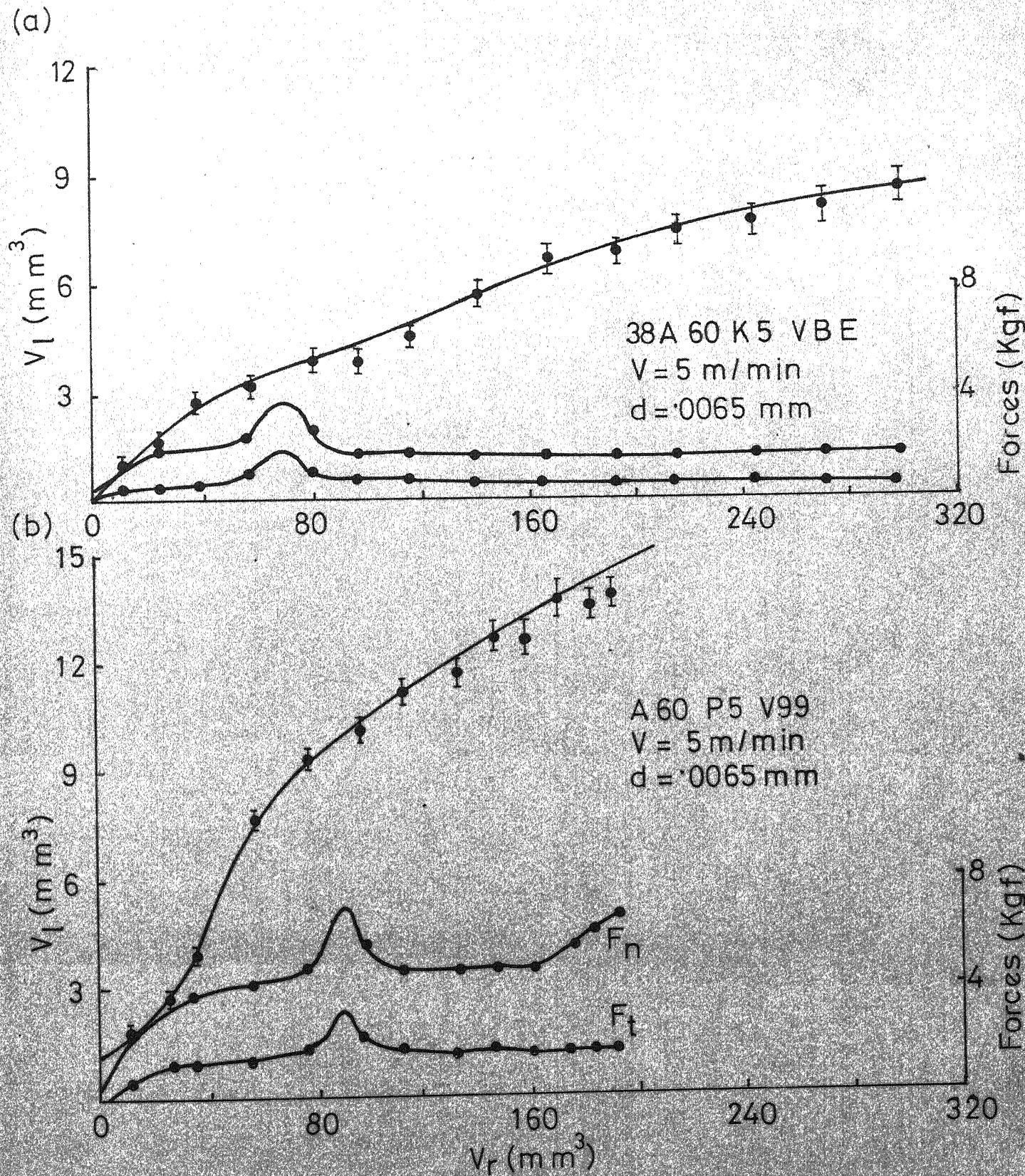
Fig. 4·5   Loading Curves For Brass For Different Wheels
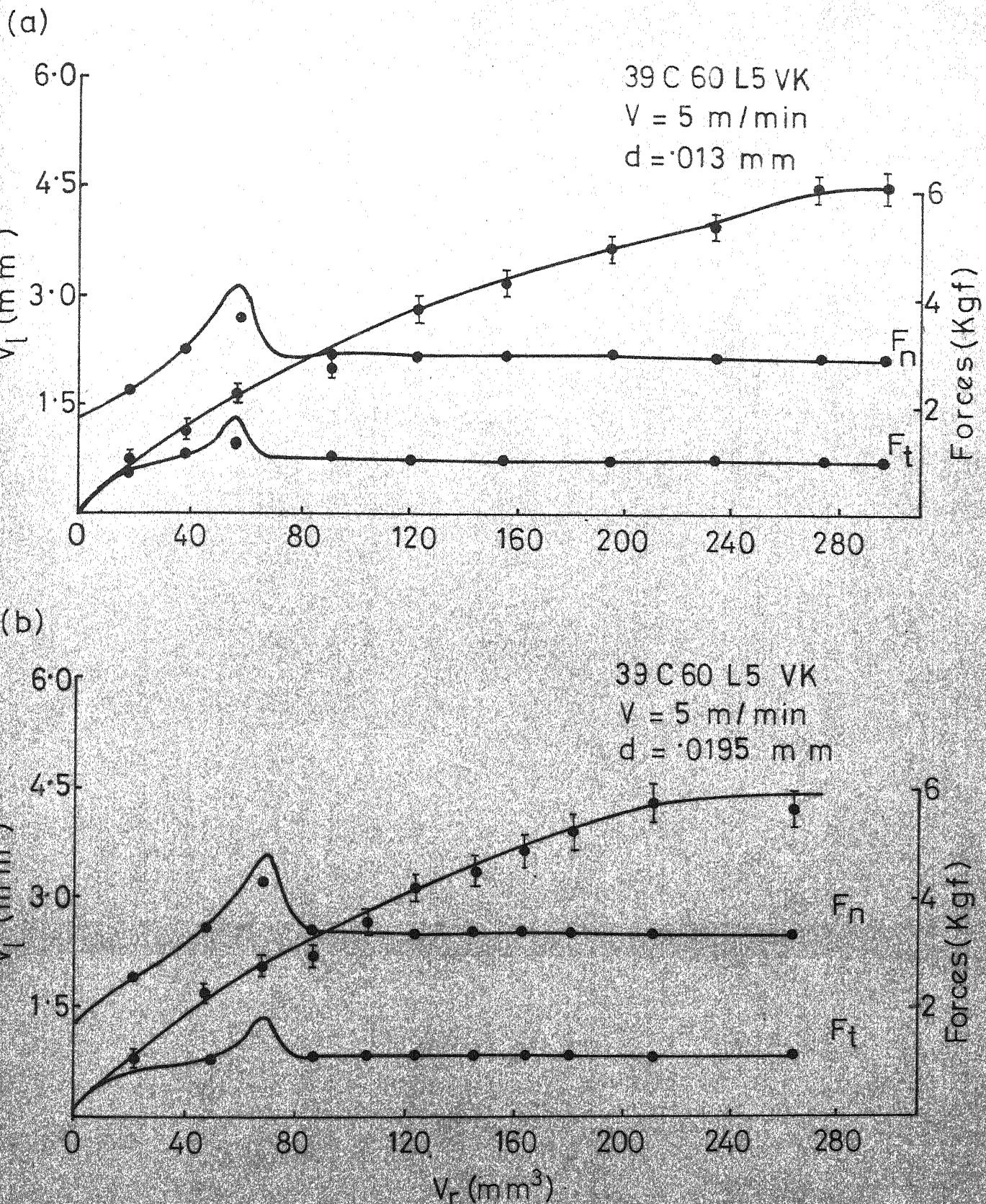
Fig. 4·6 Loading Curves For Brass For Different Down Feeds

(b) Removal Of Burrs
38A 60 K5 VBE
V = 4 m/min
d = ·0065 mm

(a) With Burrs
38A 60 K5 VBE
V = 4 m/min
d = ·0065 mm

(c)
A 60 P 5 V 99
V = 4 m/min
d = ·0065 mm
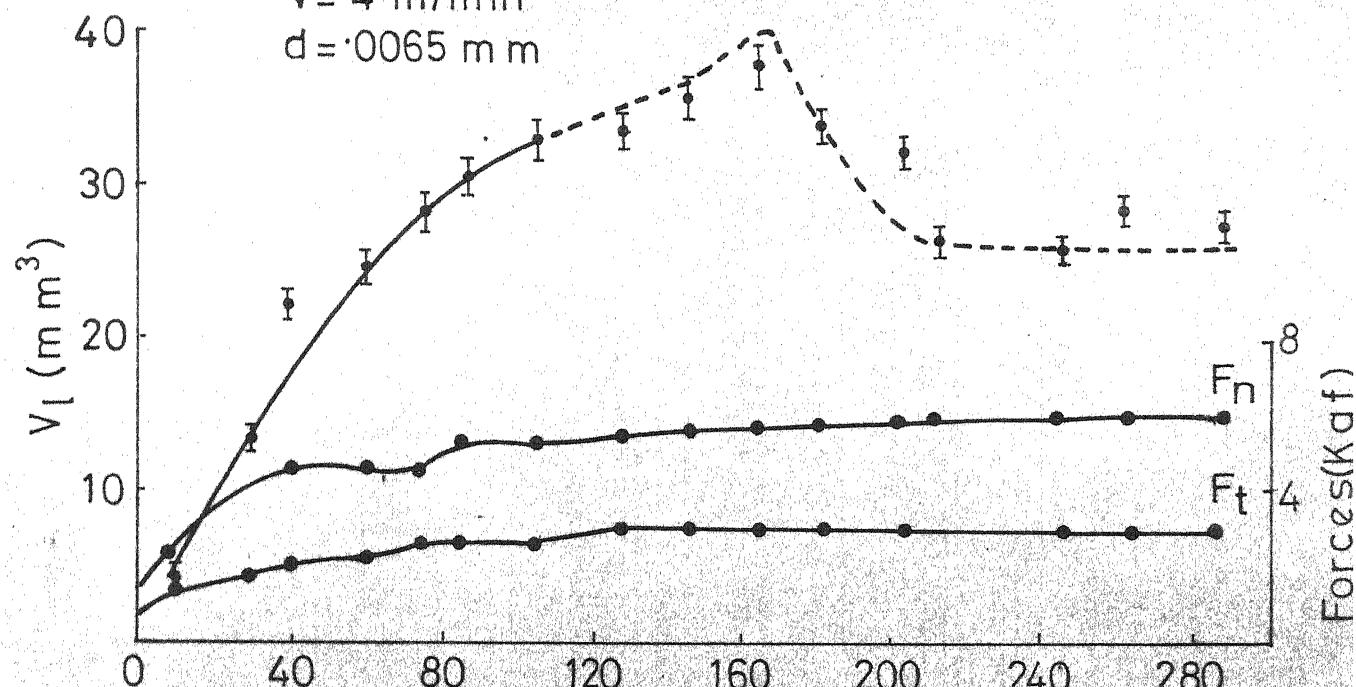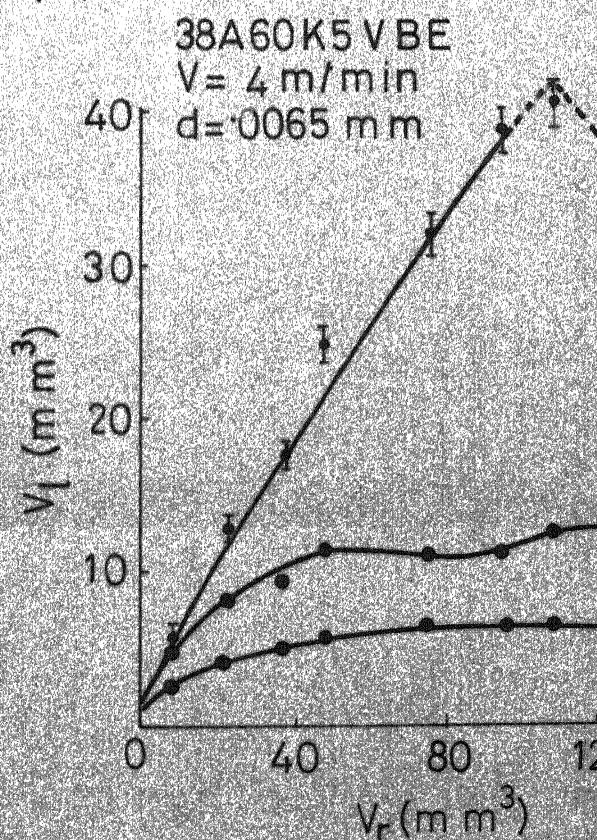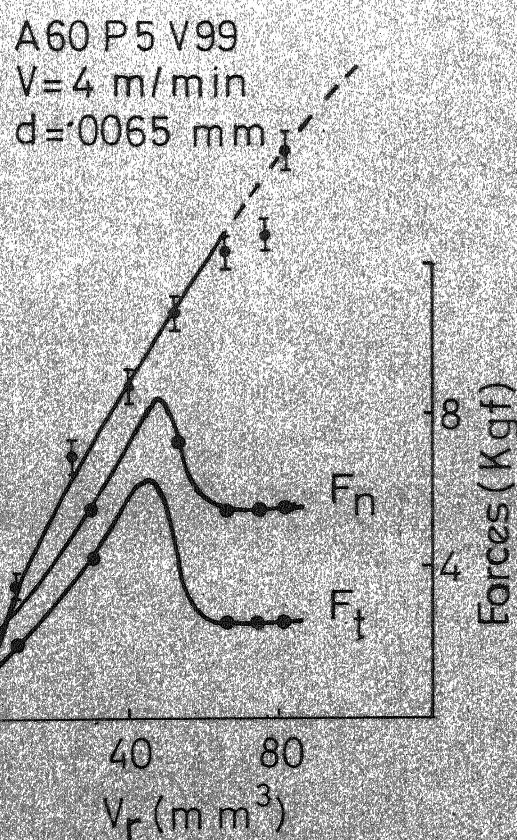
Fig. 4·7   Loading Curves For Aluminium With Different Wheels
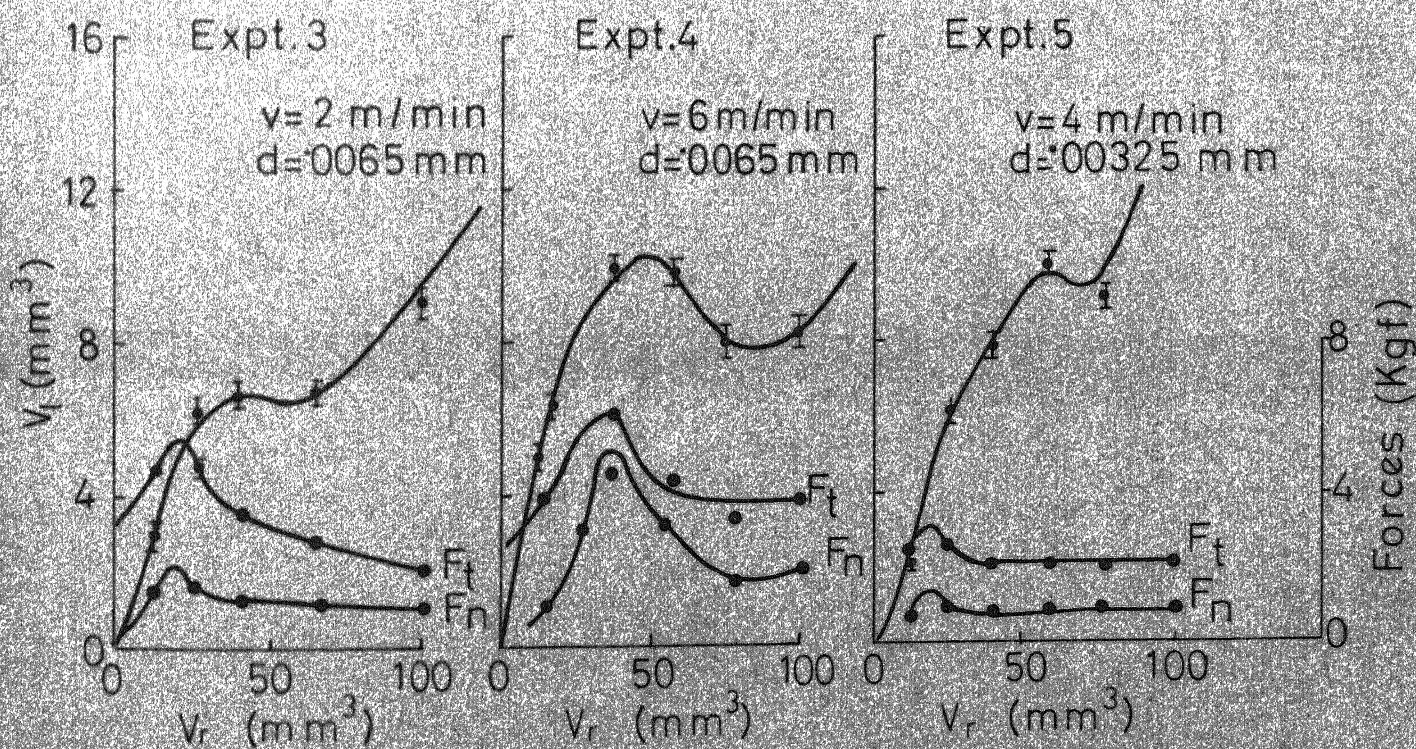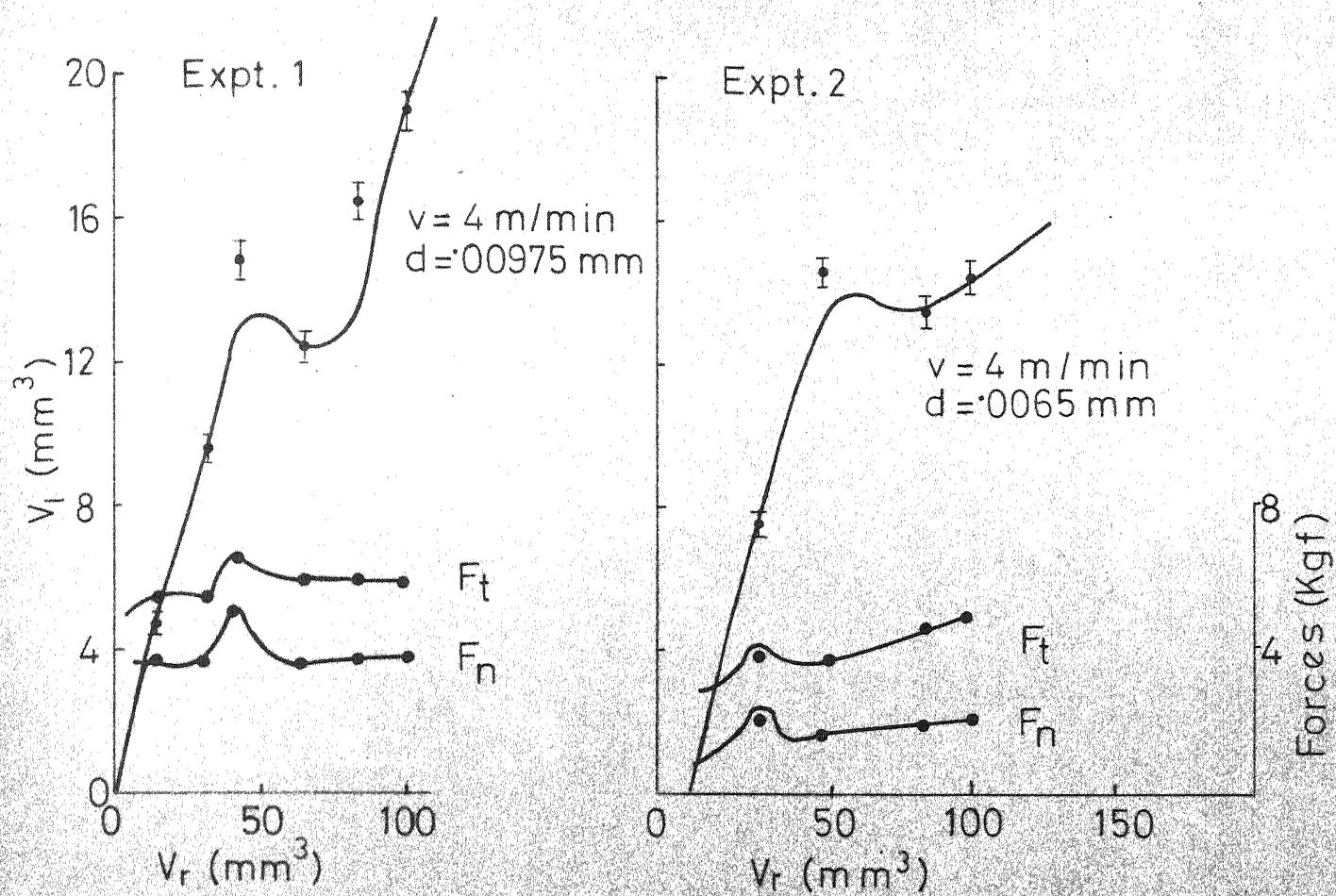
Fig. 4·8   Loading Curves For Aluminium
With 39 C 60 L 5 VK Wheel
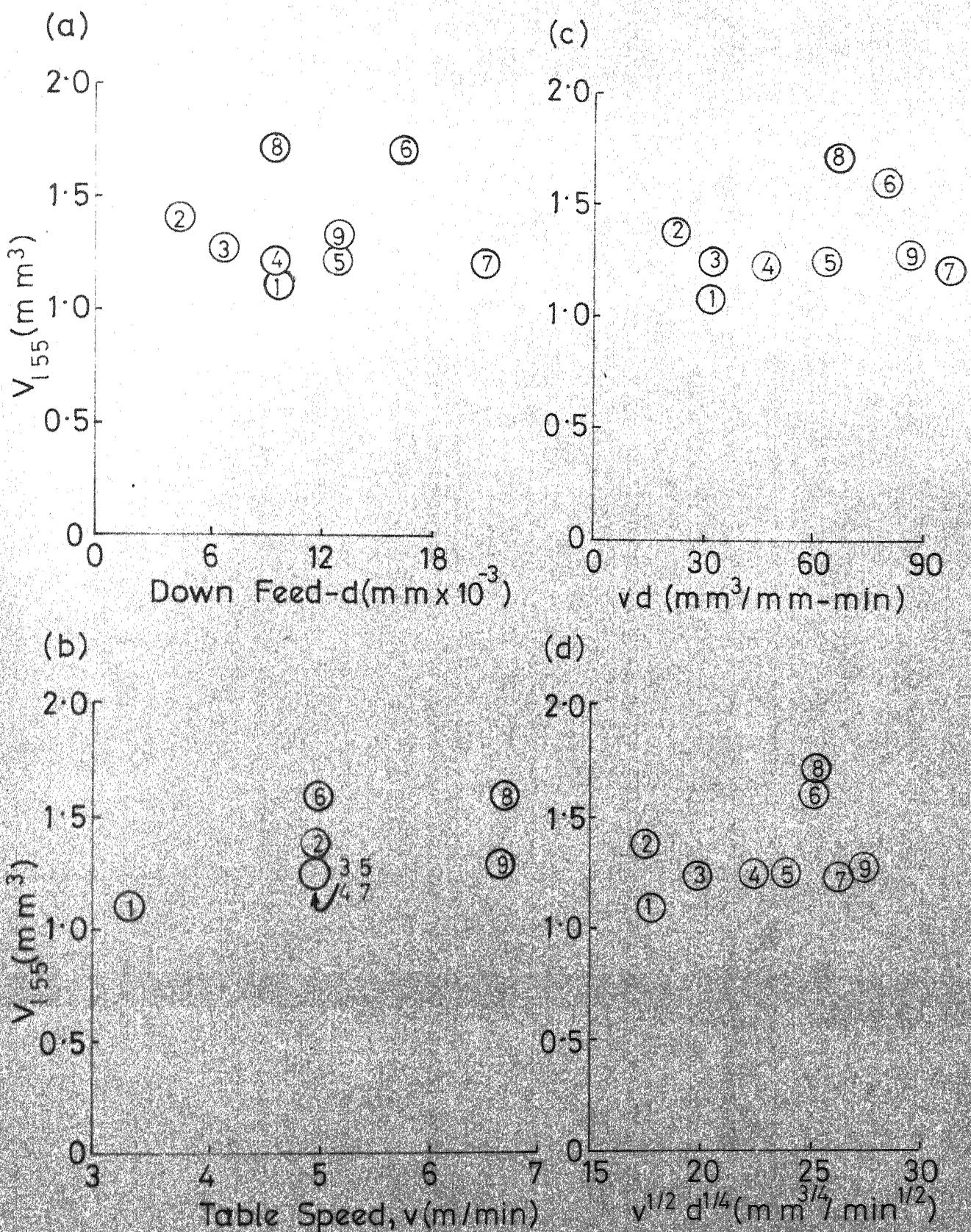
Fig. 4·9 Variation Of V_{155} With (a) Down Feed (b) Table Speed (c) MRR (d) Chip Thickness For Annealed HSS (38A 60K5VBE Wheel)

Material: Brass, Mild Steel
Wheel Speed: 3000 RPM

Notation	Table Speed (m/min)	Down Feed (mm)
○	3	·0065
◐	5	"
●	8	"
△	3	·013
◭	5	"
▲	8	"
□	3	·0195
◨	5	"
■	8	"

Material: Aluminium
Wheel Speed: 2000 RPM

Notation	Table Speed (m/min)	Down Feed (mm)
○	2	·00325
◐	4	"
●	6	"
◭	4	·0065
◨	4	·00975

Fig. 4·10 Nomenclature For Loading Parameters
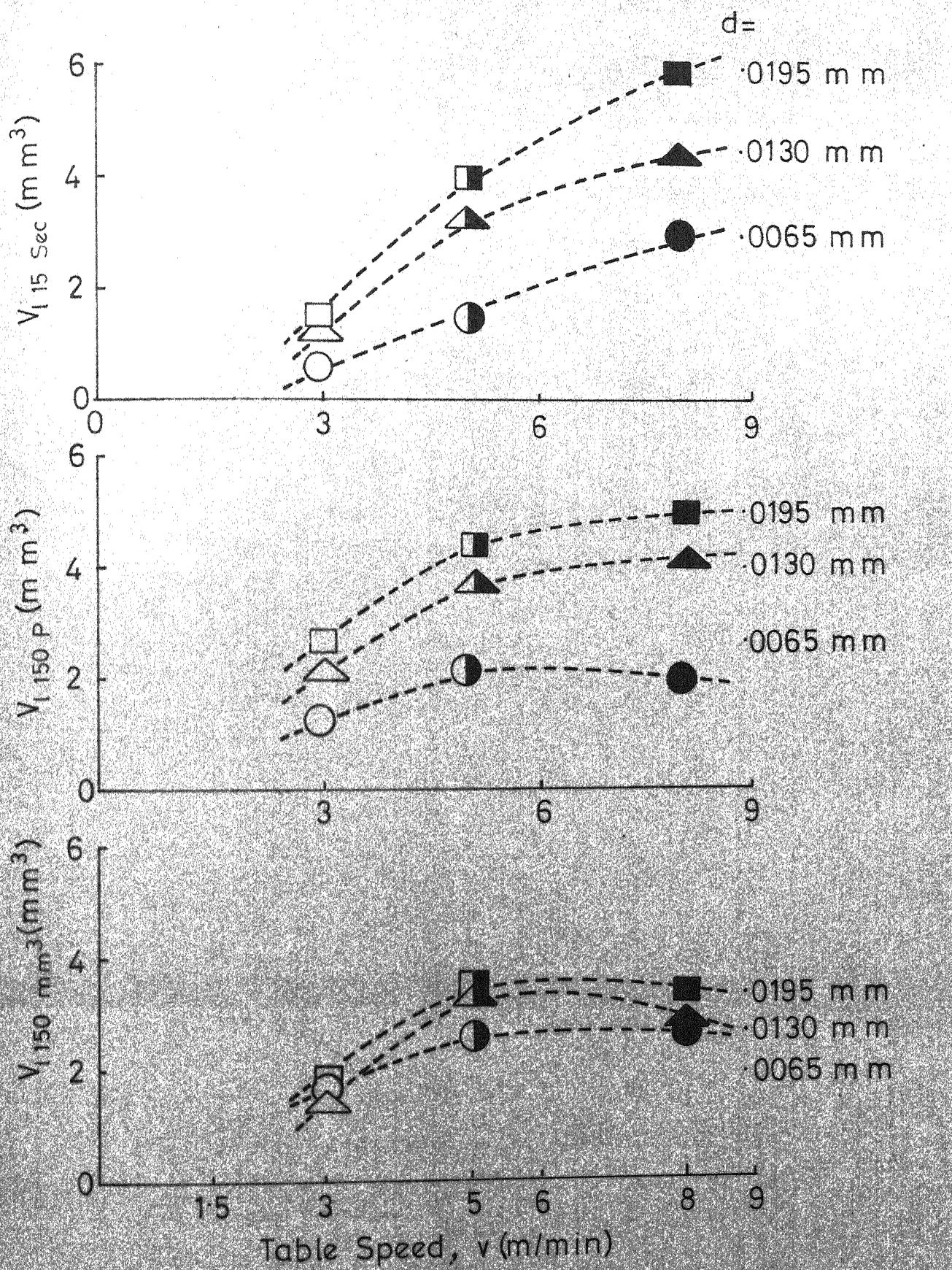
Fig. 4·11 Variation Of Loading Parameters With Table Speed For Brass (39 C 60 L 5 VK)
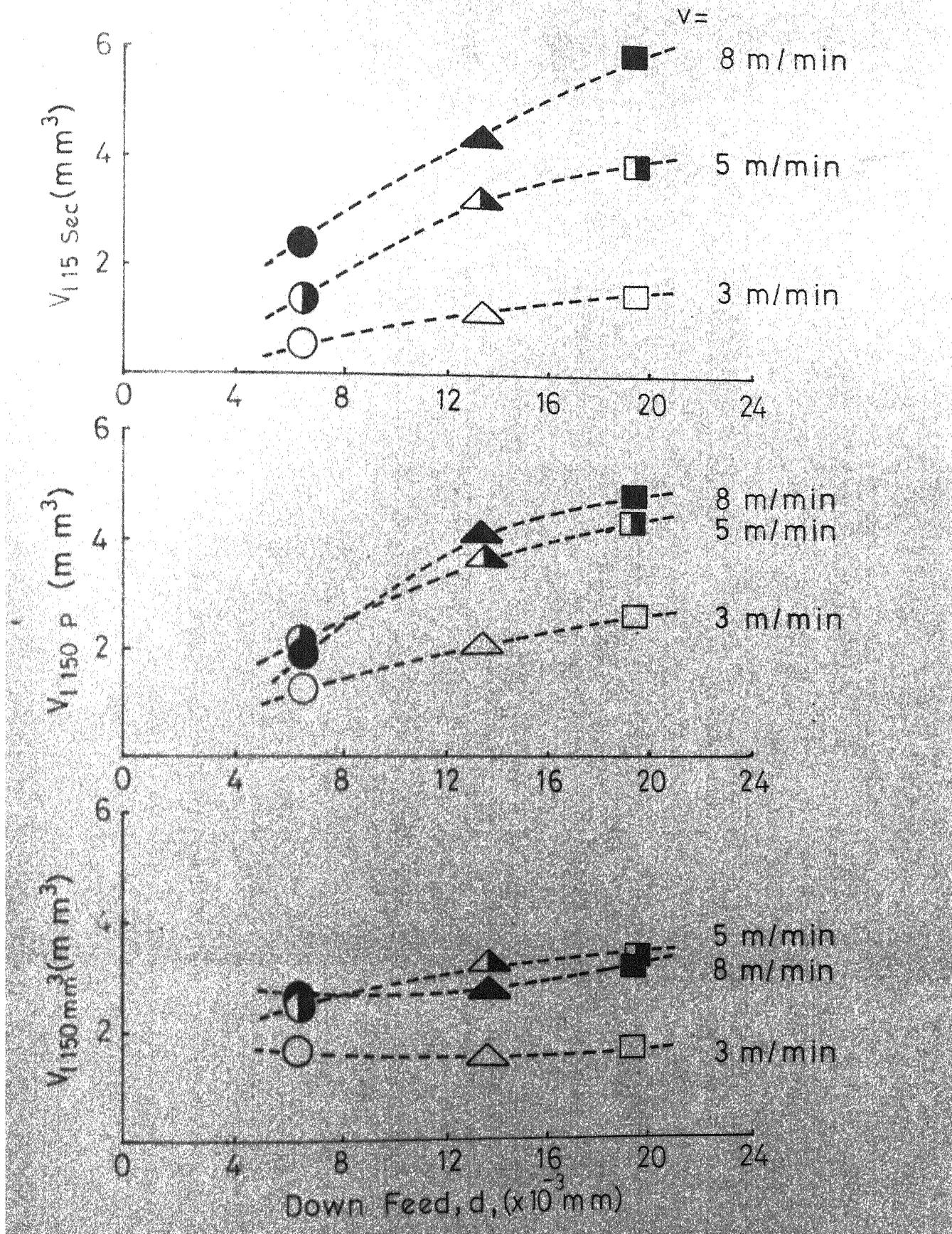
Fig. 4.12   Variation Of Loading Parameters
With Down Feed For Brass
(39 C 60 L 5 VK Wheel)
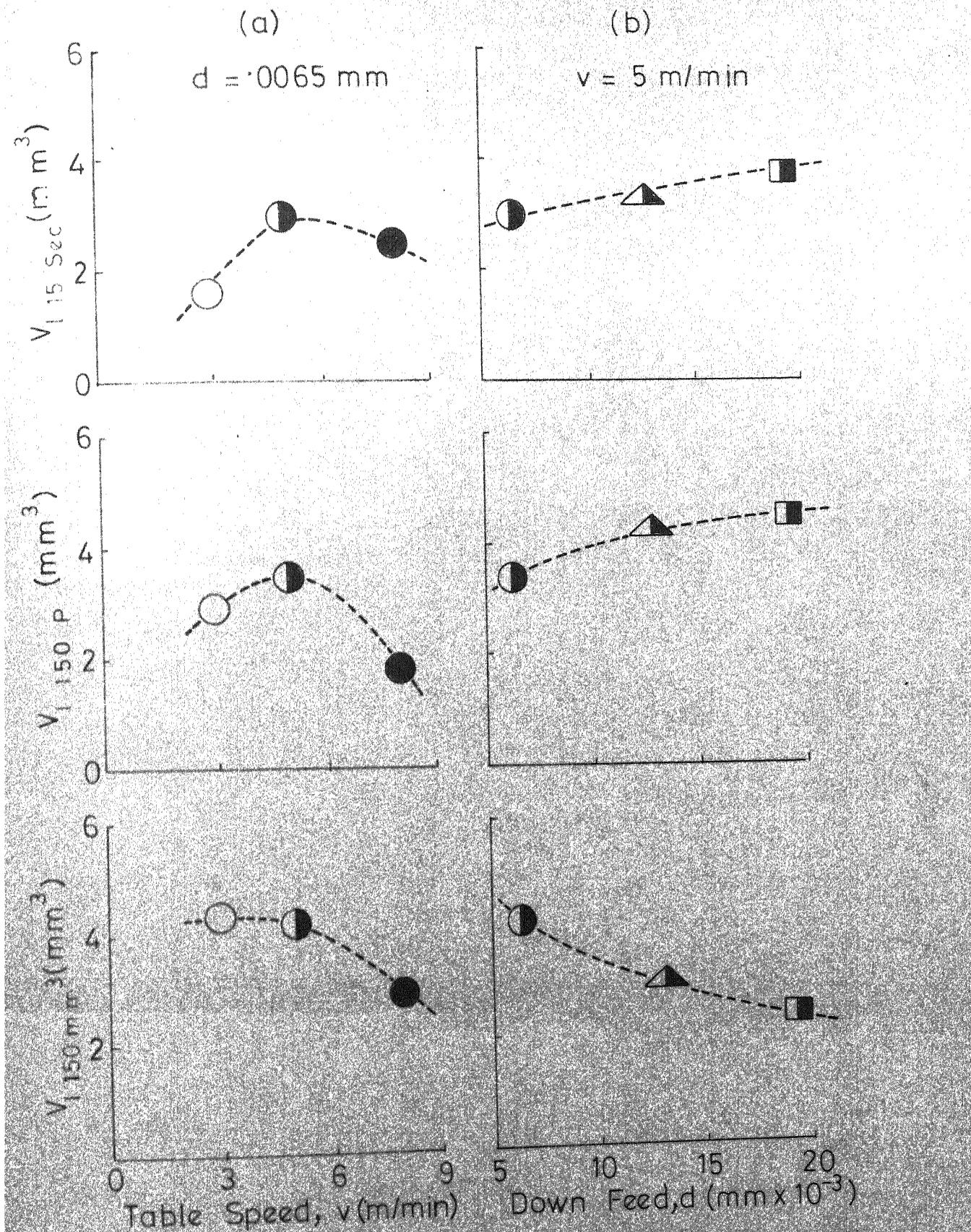
Fig.4·13 Variation Of Loading Parameters
With (a) Table Speed (b) Down Feed
For Brass (38 A 60 K 5 VBE Wheel)
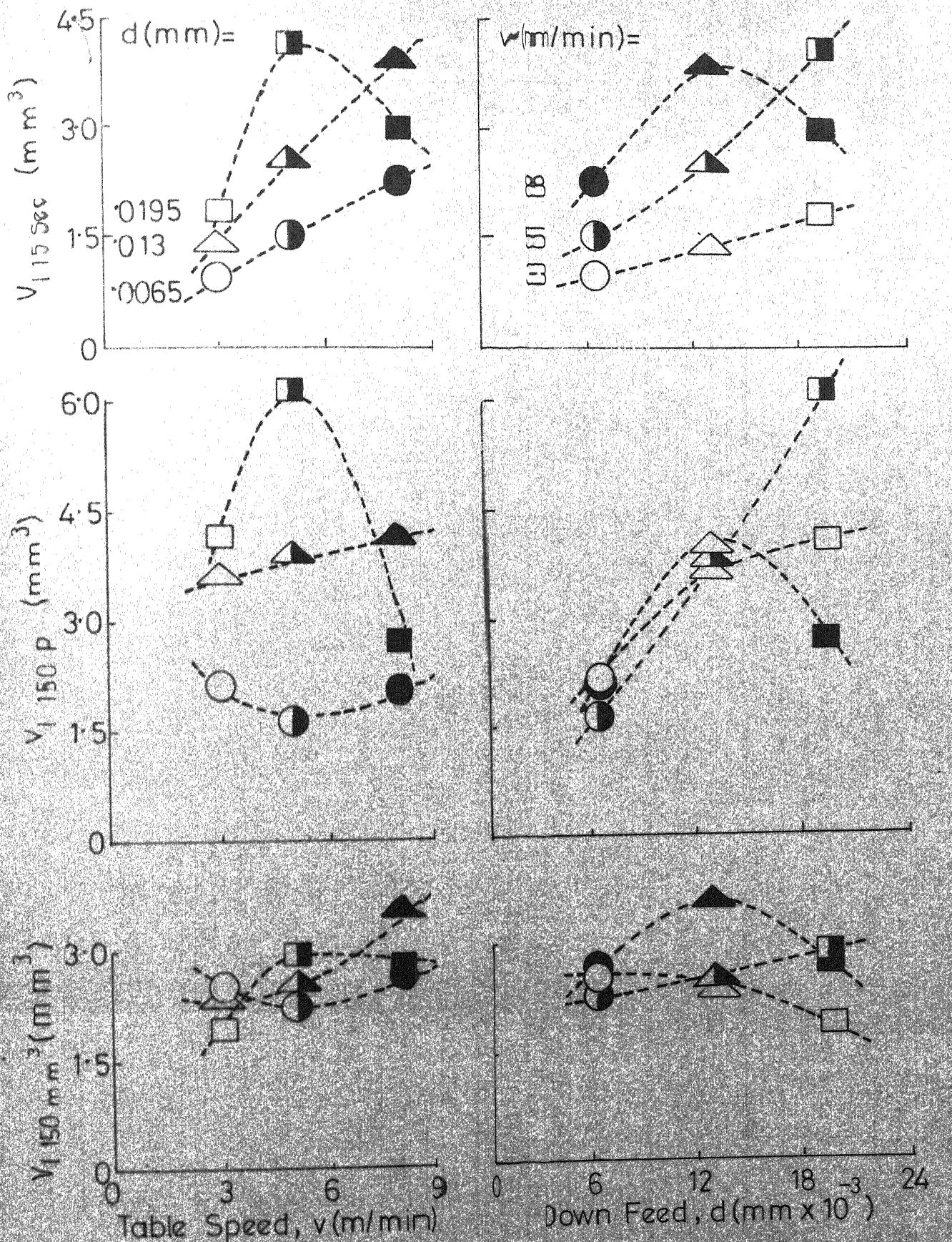
Fig.4·14 Variation Of Loading Parameters With (a) Table Speed (b) Down Feed For Mild Steel (38 A 60 K5 VBE Wheel)
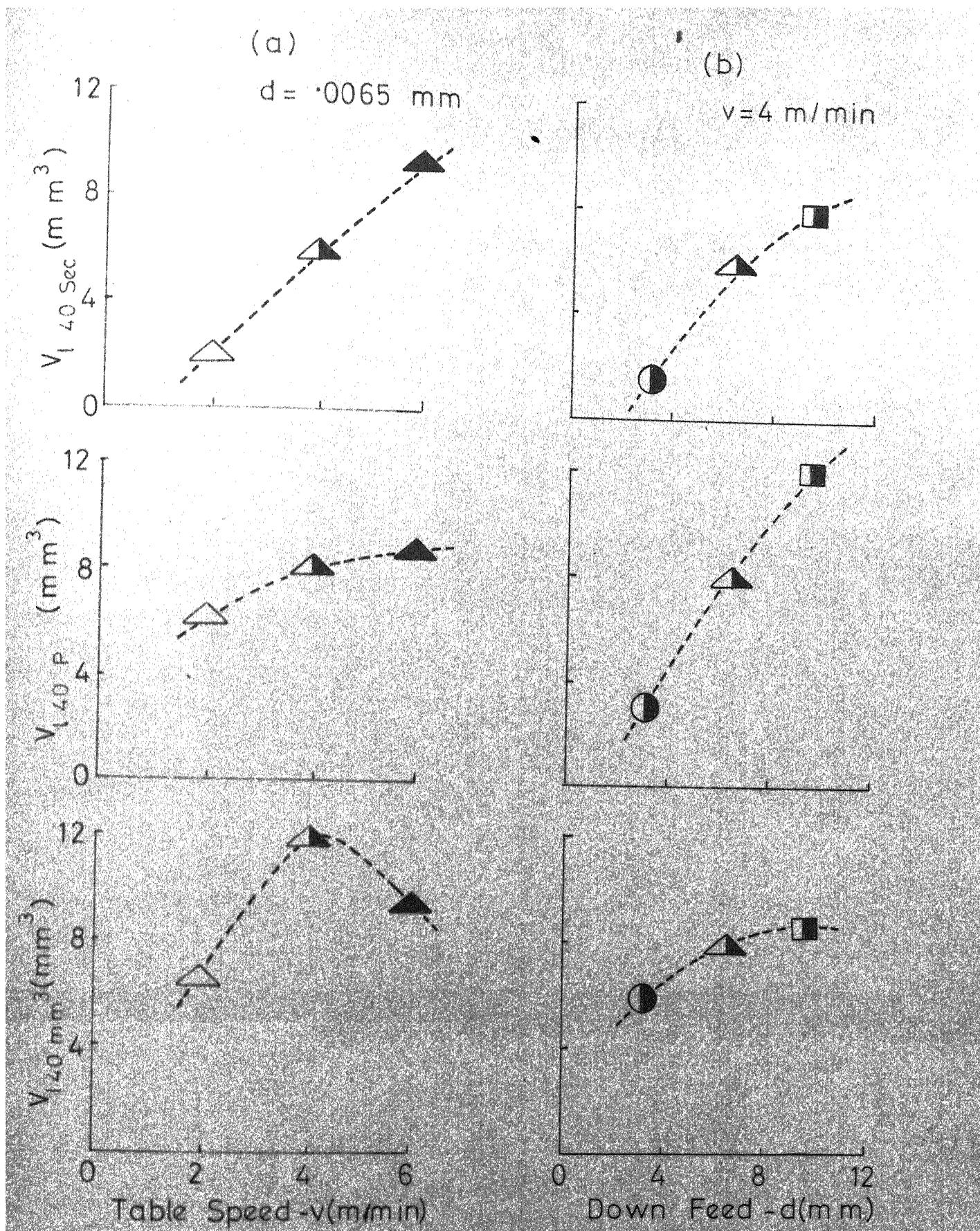
Fig. 4·15 Variation Of Loading Parameters With
(a) Table Speed (b) Down Feed
For Aluminium (39 C 60 L 5 VK Wheel)
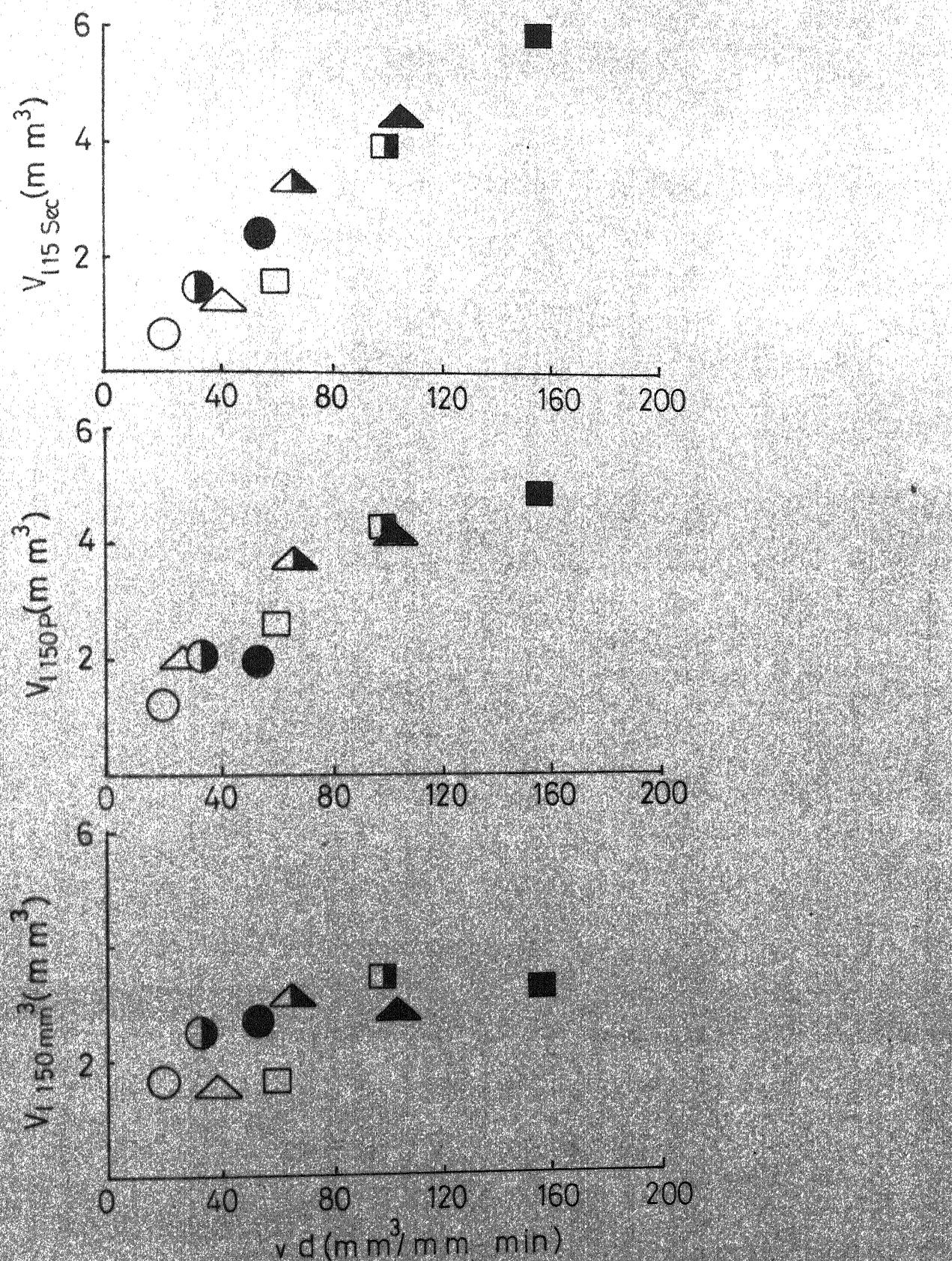
Fig. 4·16 Variation Of Loading Parameters
With Material Removal Rate
For Brass (39 C 60 L5 VK Wheel)
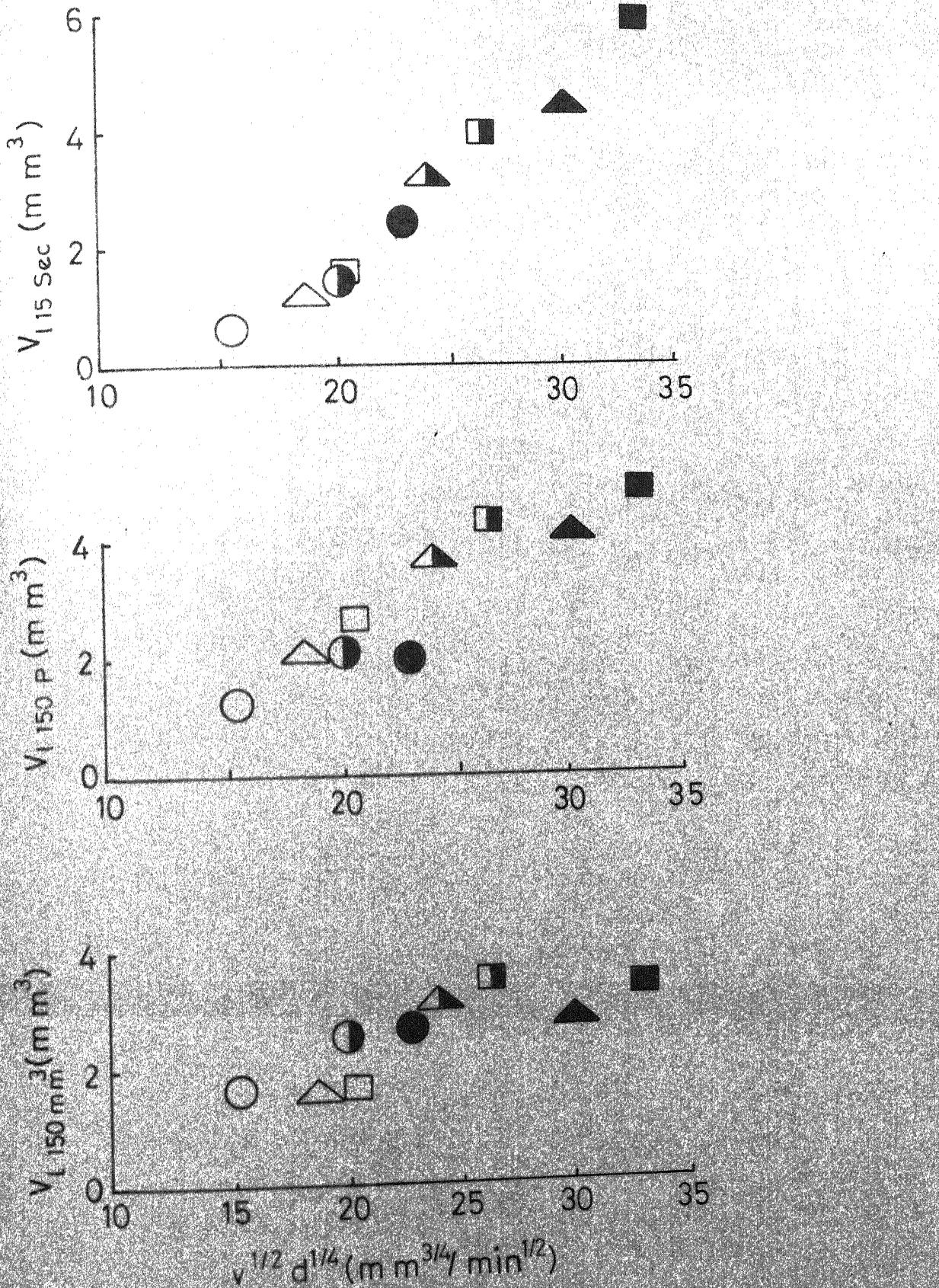
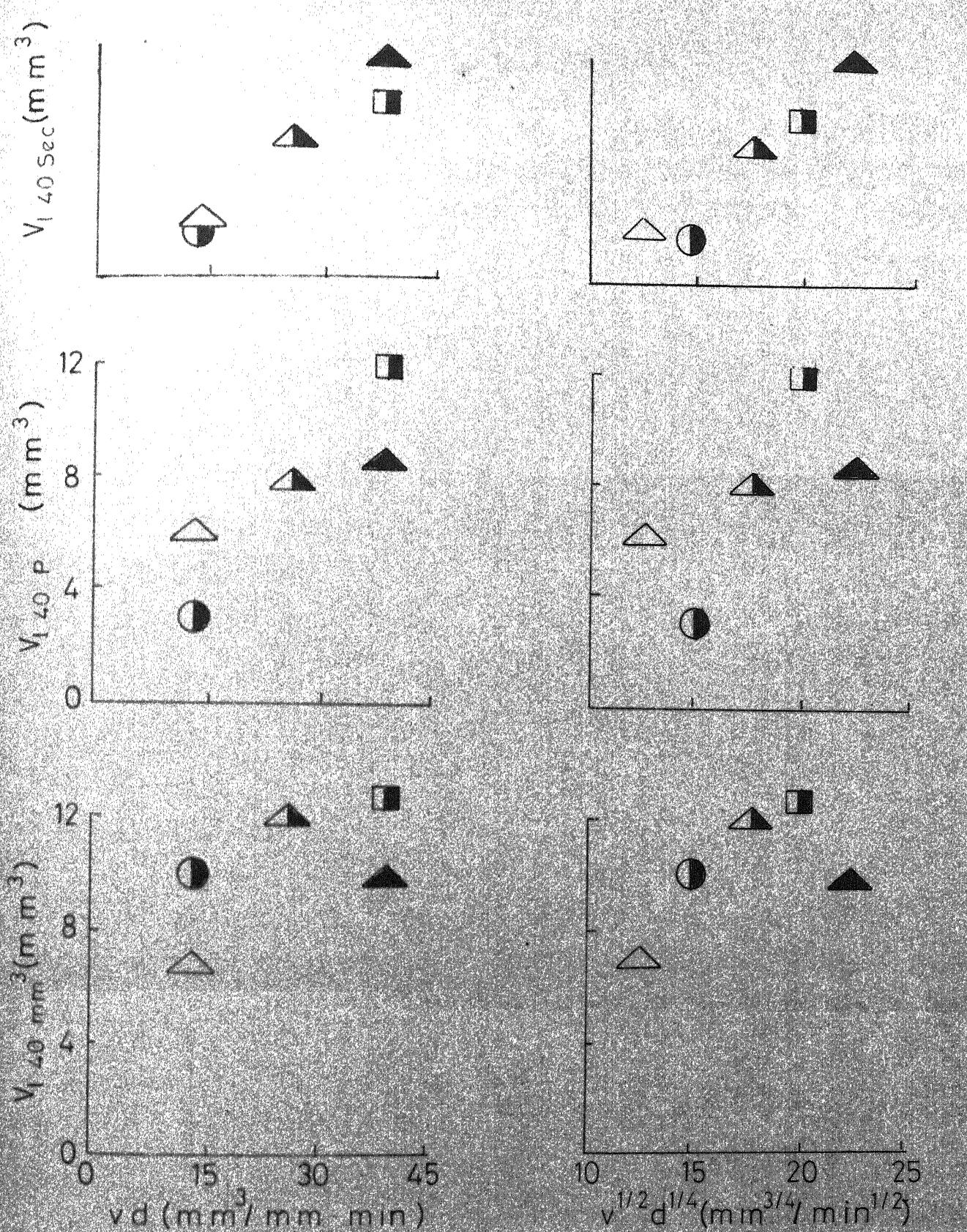Fig.417 Variation Of Loading Parameters With Chip Thickness For Brass (39 C 60 L5VK Wheel)
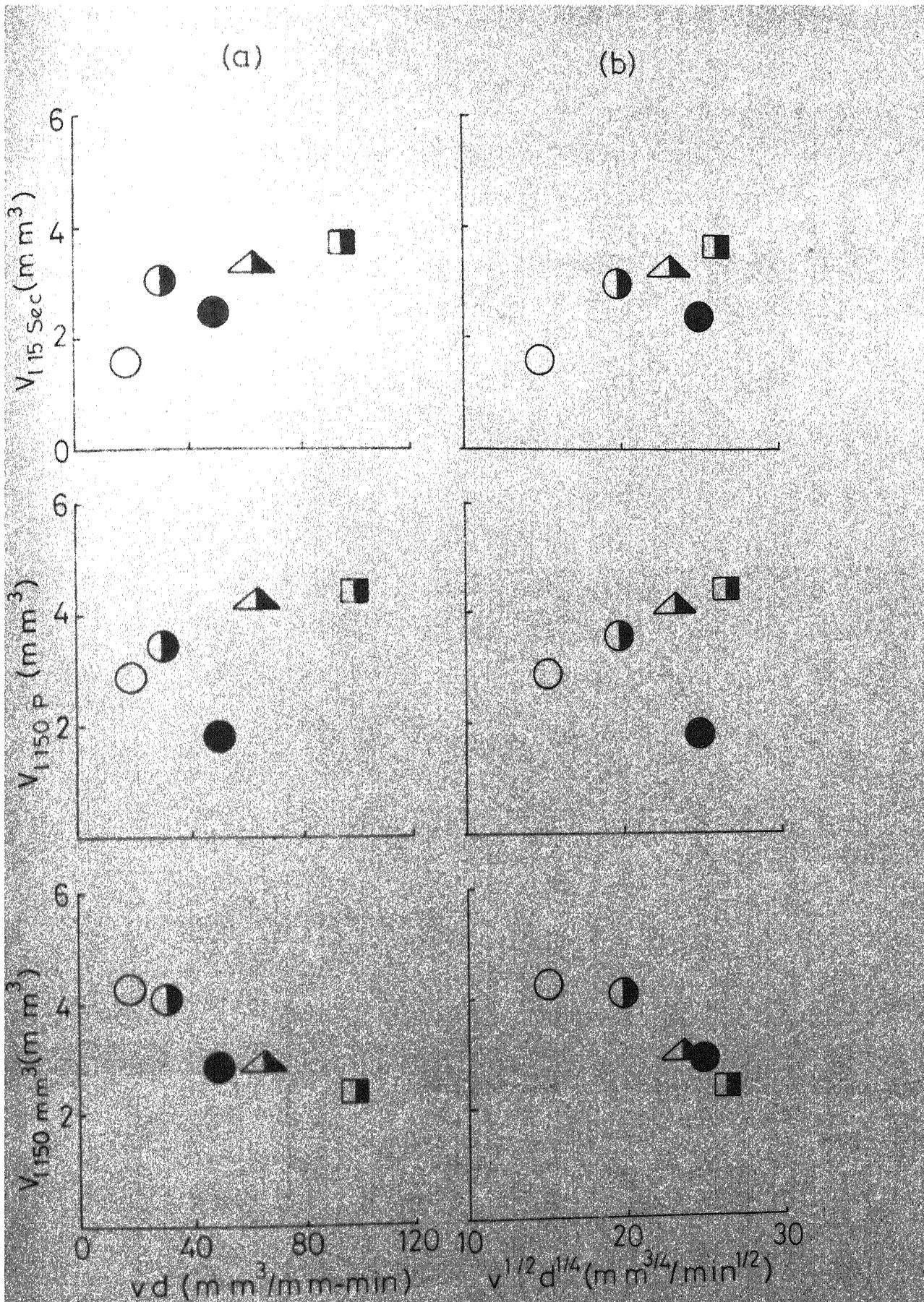
Fig. 4·18   Variation Of Loading Parameters With (a) Material Removal Rate (b) Chip Thickness For Brass (38 A 60 K 5 V BE Wheel)
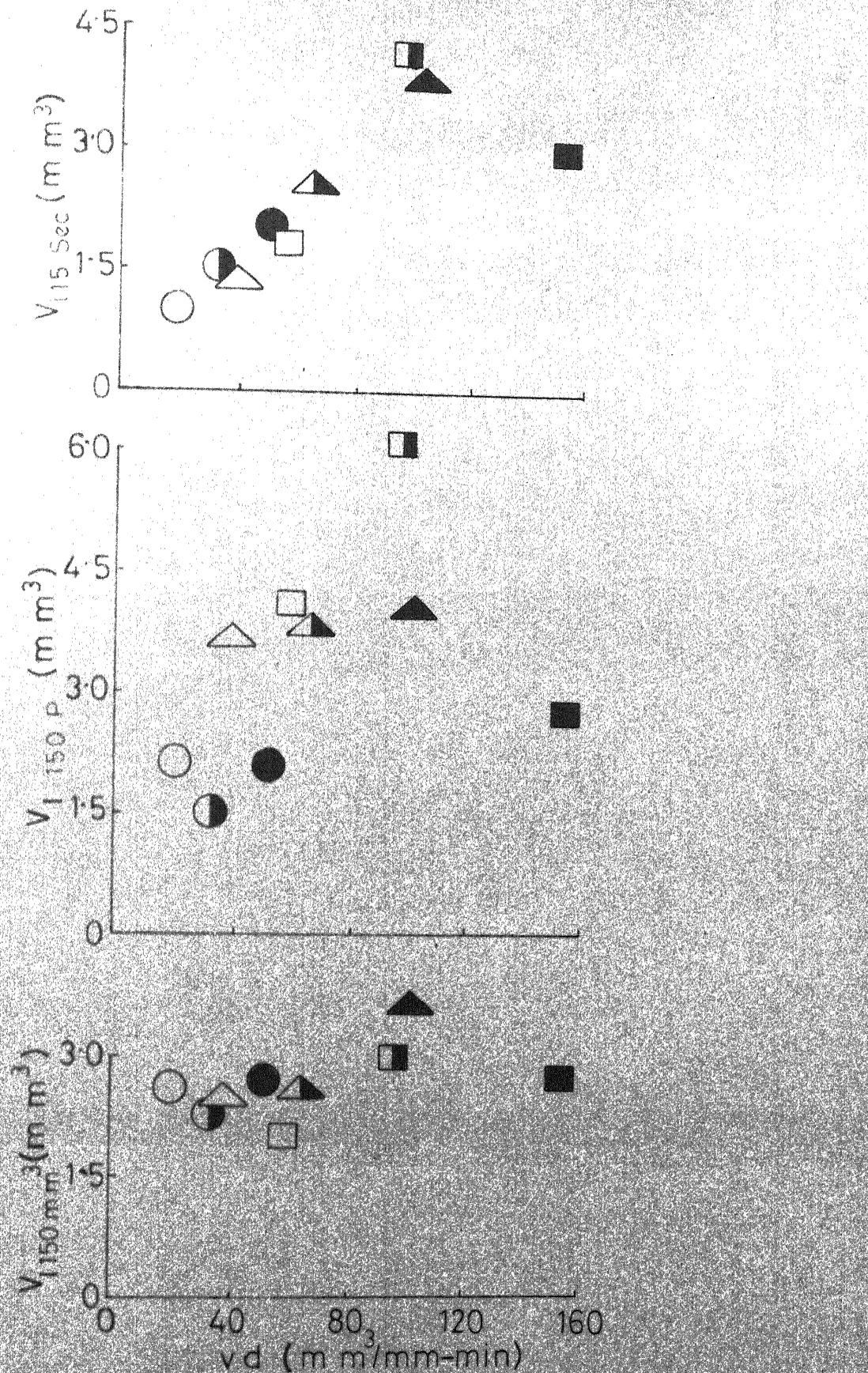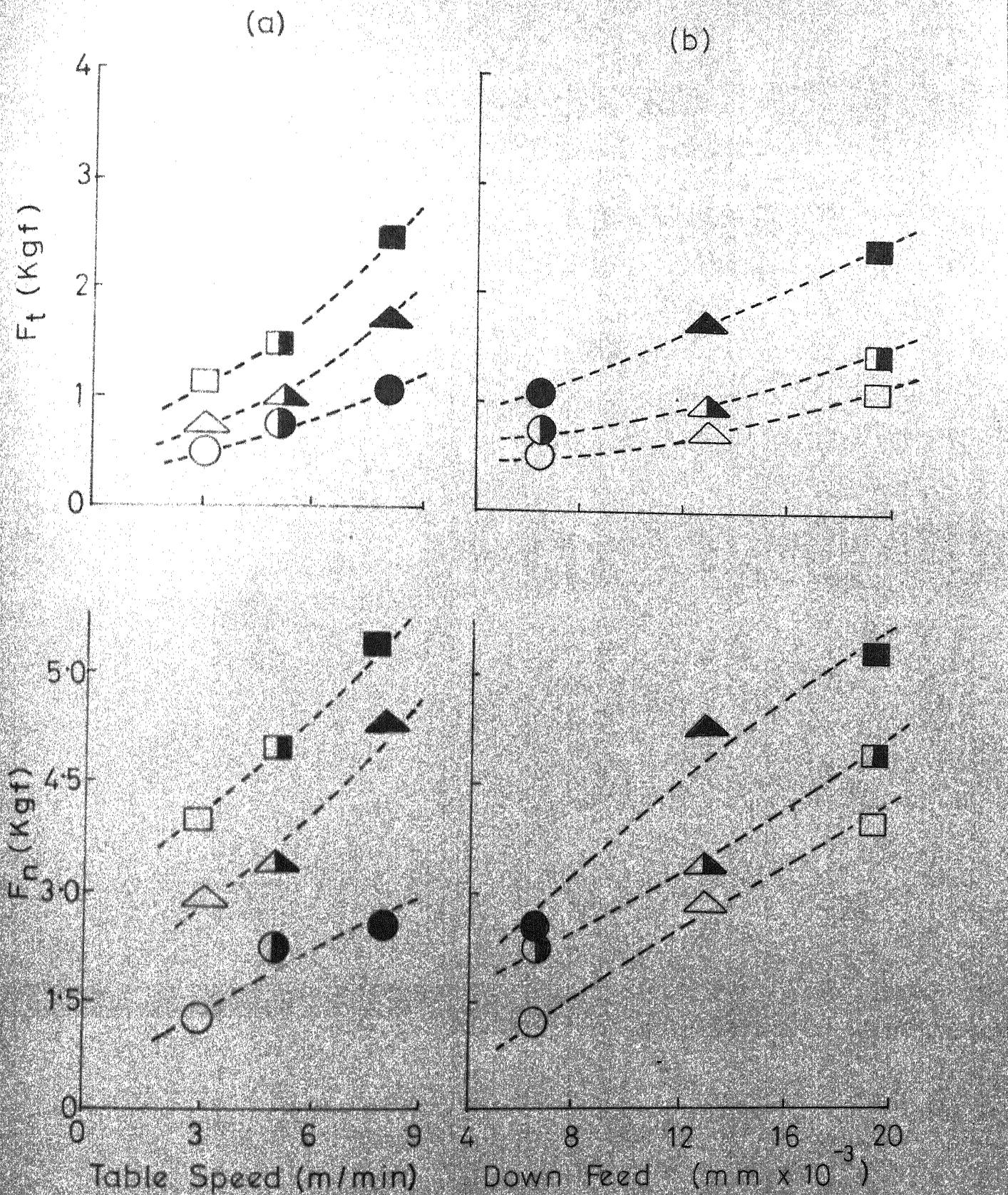
Fig.4·19 Variation Of Loading Parameters With Material Removal Rate For Mild Steel (38 A 60 K 5 V B E Wheel)
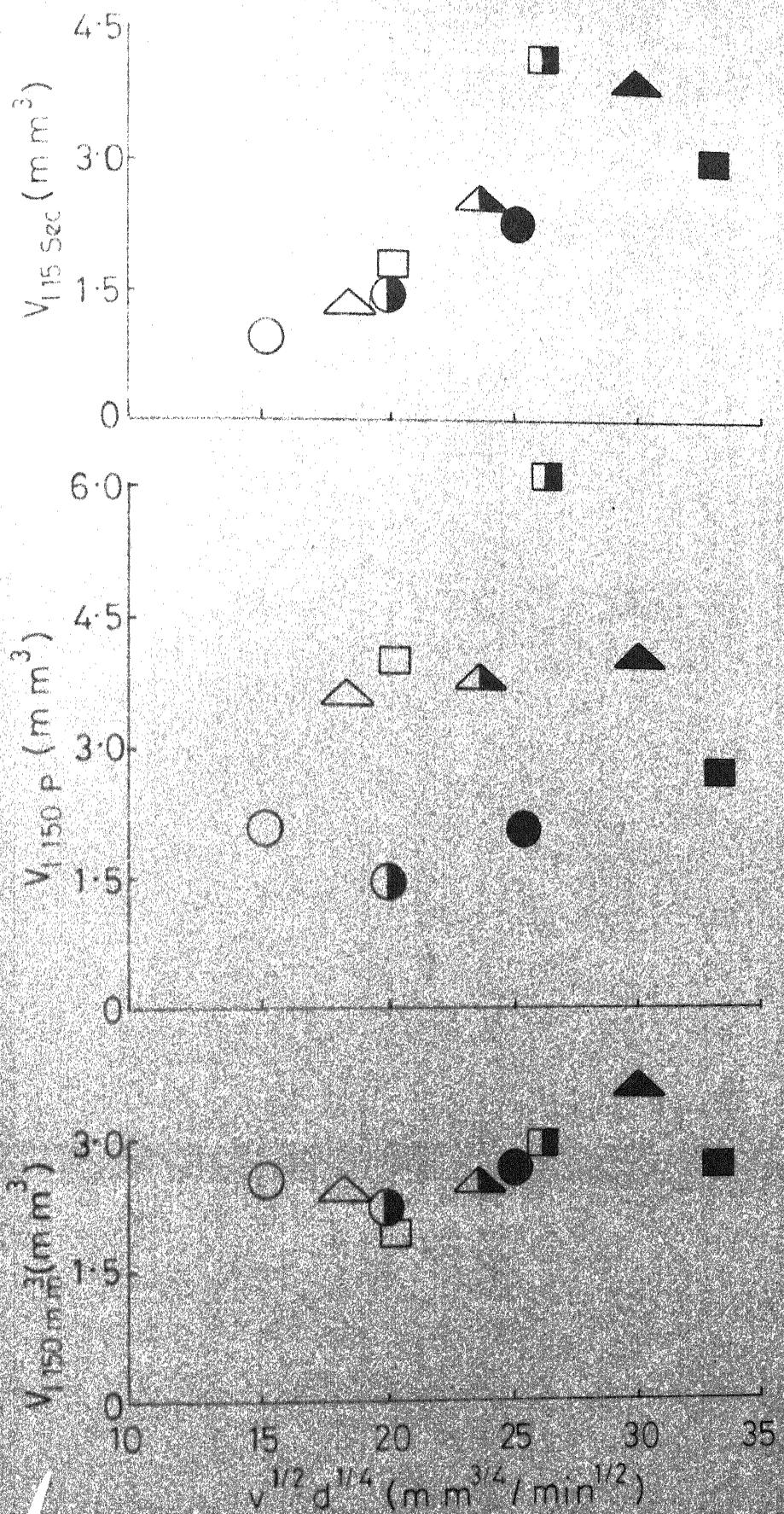
Fig. 4·20 Variation Of Loading Parameters With Chip Thickness For Mild Steel (38 A 60 K 5 VBE Wheel)

Fig. 4·21 Variation Of Loading Parameters With
(a) Material Removal Rate (b) Chip
Thickness For Aluminium (39 C 60 L 5
VK Wheel)

Fig. 4·22 Variation Of Forces With (a) Table
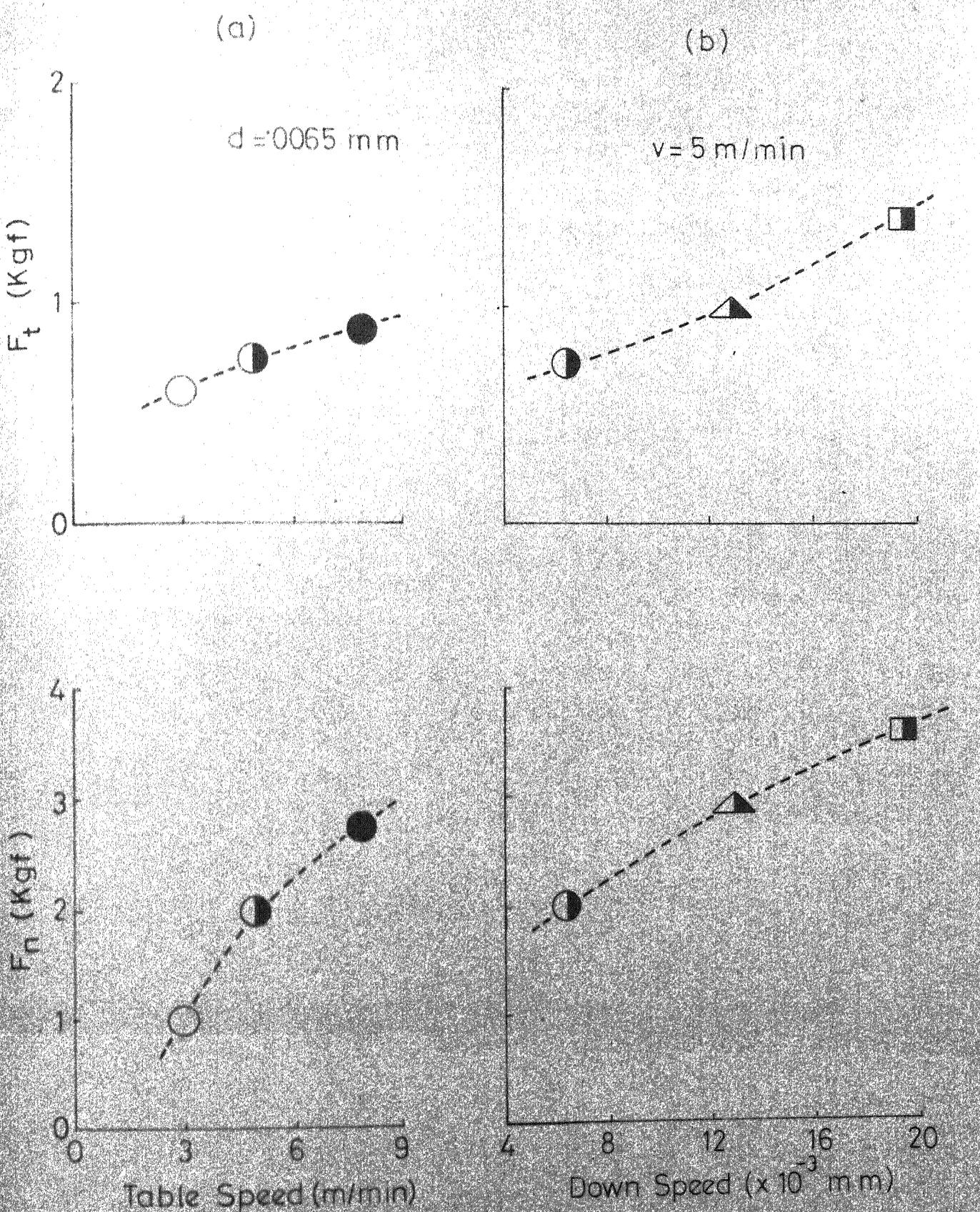Speed (b) Down Feed For Brass
(39 C 60 L 5 VK Wheel)

Fig 4·23 Variation Of Forces With (a) Table
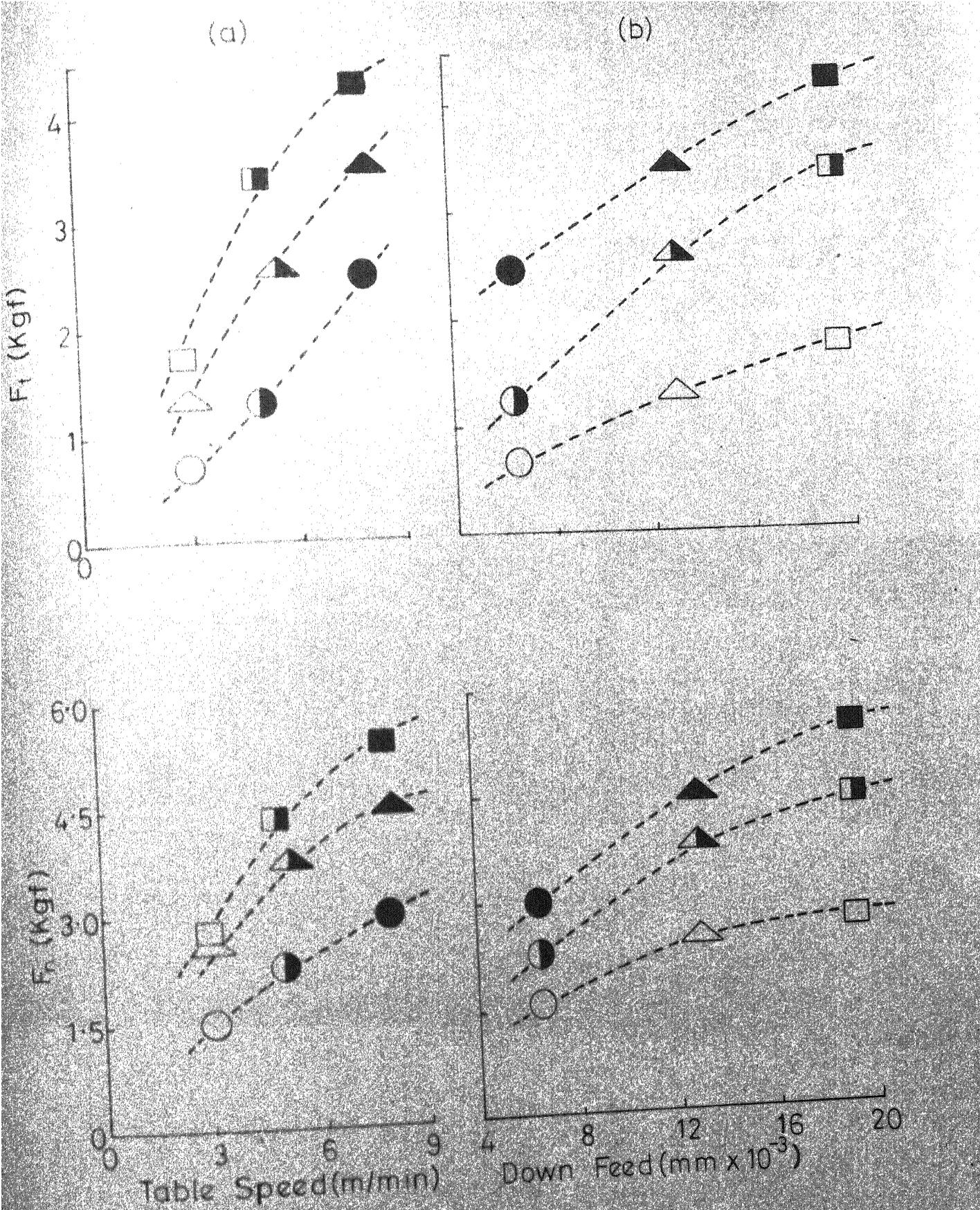Speed (b) Down Feed For Brass
(38 A 60 K 5 V B E Wheel)

Fig 4.24 Variation Of Forces With (a) Table Speed (b) Down Feed For Mild Steel (38 A 60 K 5 VBE Wheel)
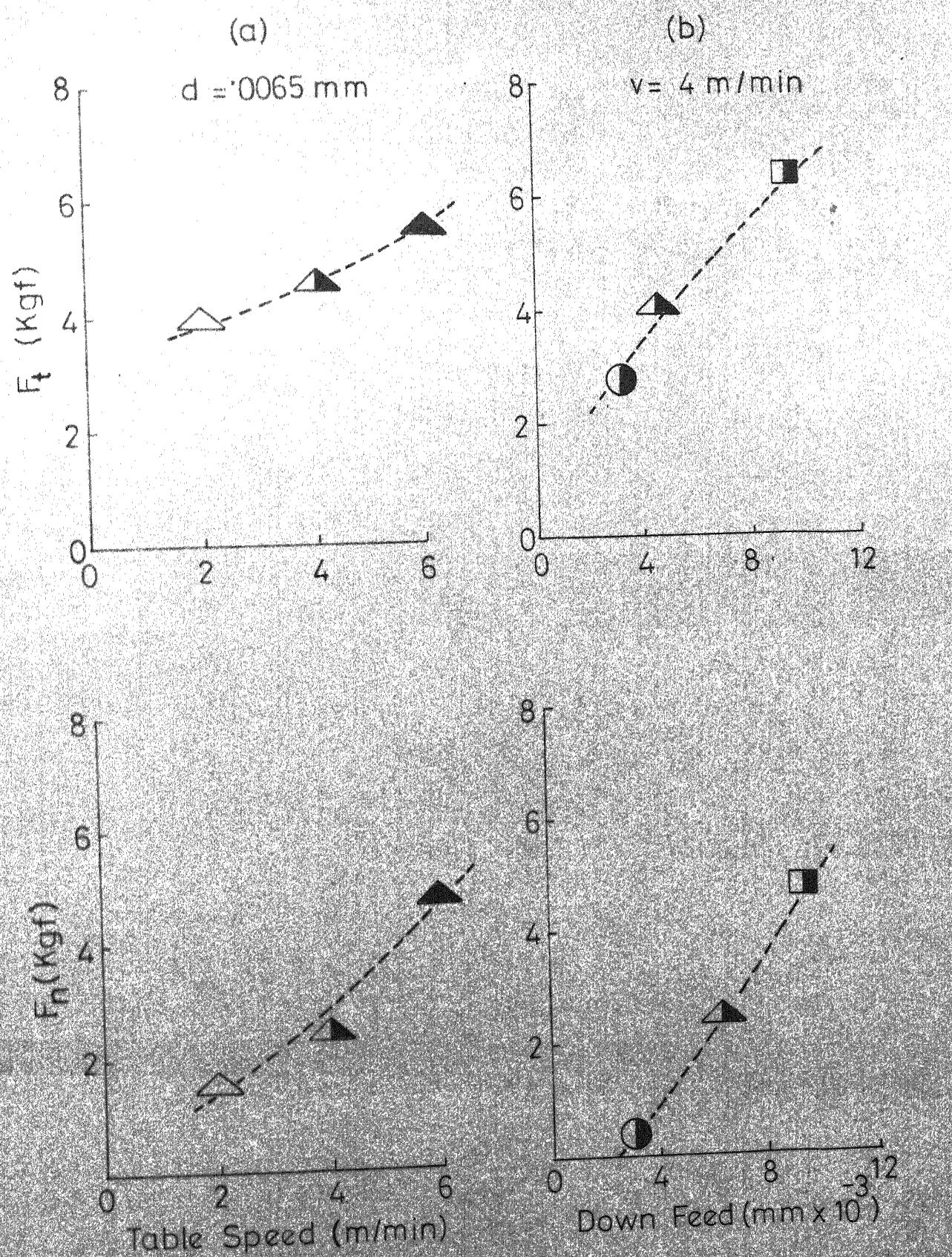
Fig. 4·25 Variation Of Forces With (a) Table Speed (b) Down Feed For Aluminium (39 C 60 L 5 VK Wheel)
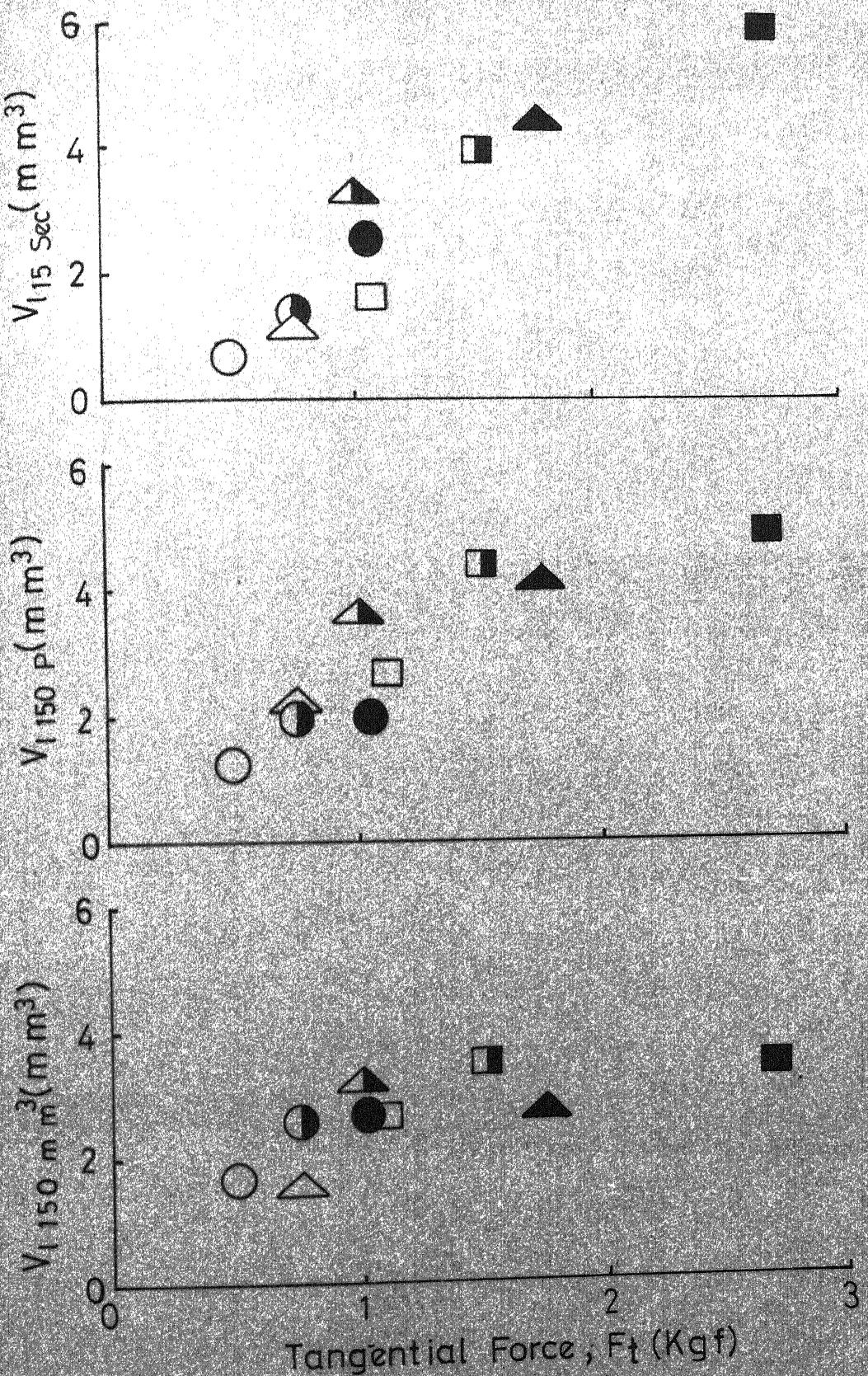
Fig. 4·26   Variation Of Loading Parameters
With Tangential Force For Brass
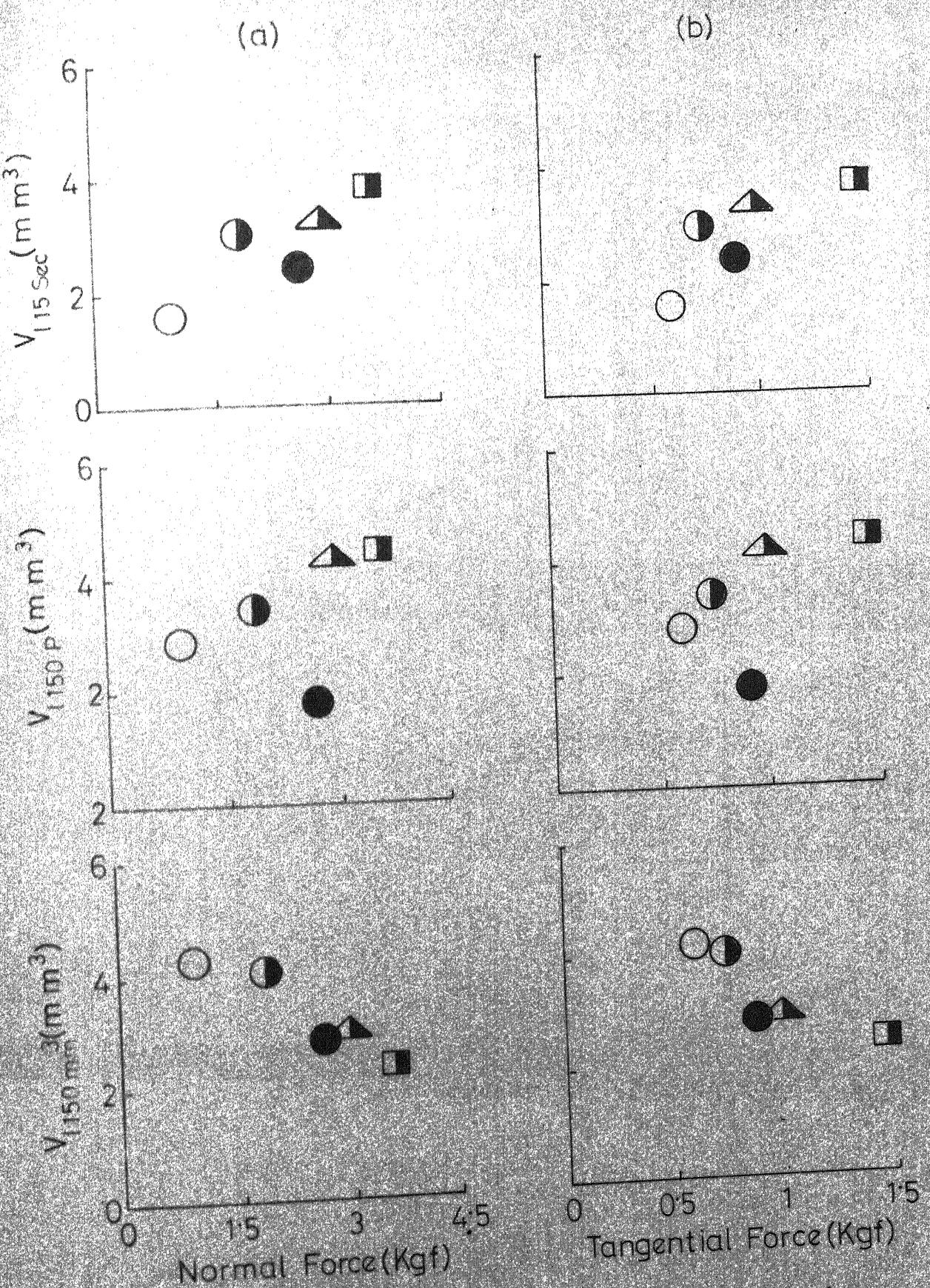(39 C 60 L5 VK Wheel)

Fig 4·28 Variation Of Loading Parameters With (a) Normal Force (b) Tangential Force For Brass (38 A 60 K 5 V B E Wheel)
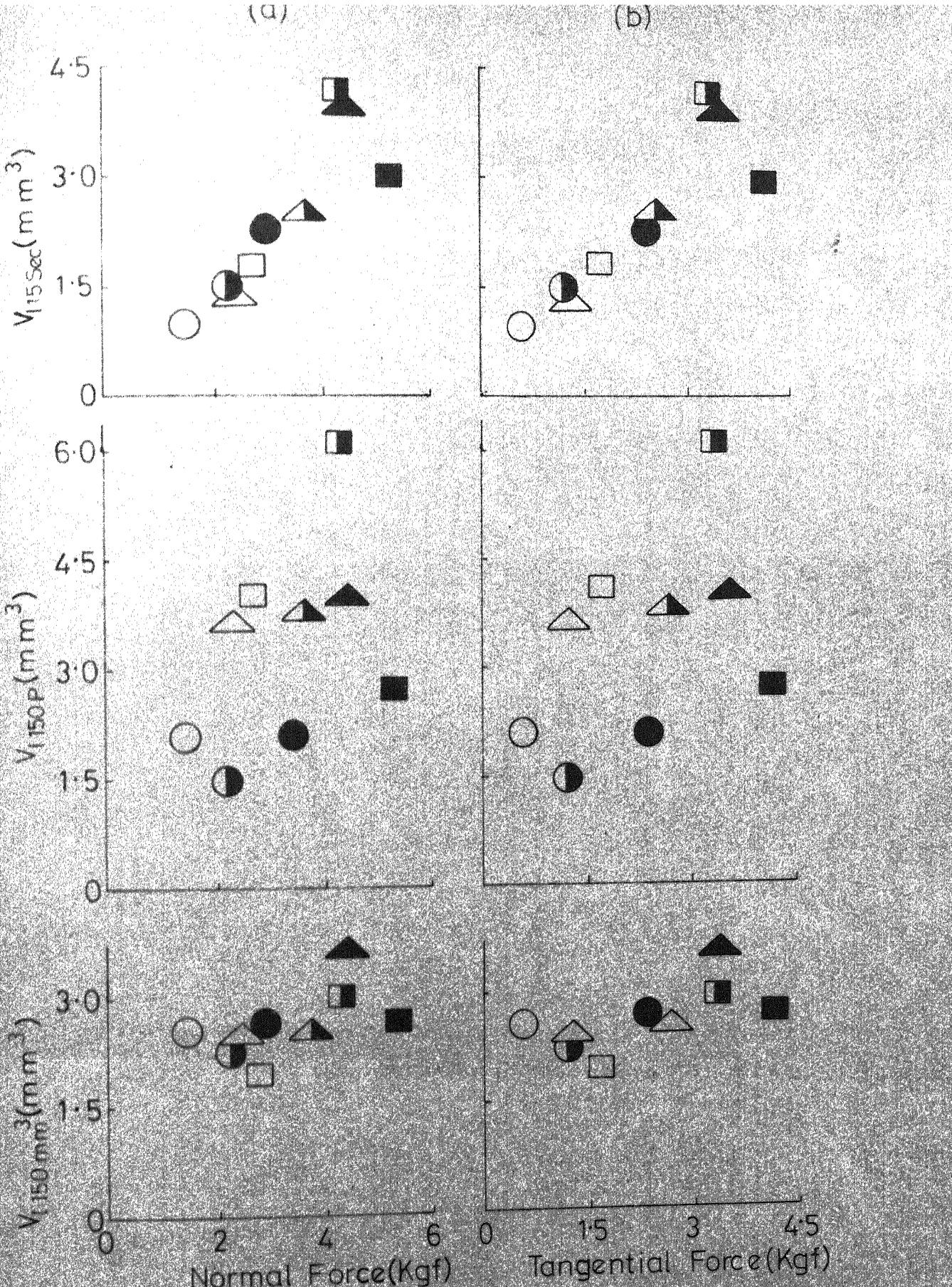
Fig. 4.29 Variation Of Loading Parameters With (a) Normal Force (b) Tangential Force For Mild Steel (38 A 60 K 5 V B E Wheel)
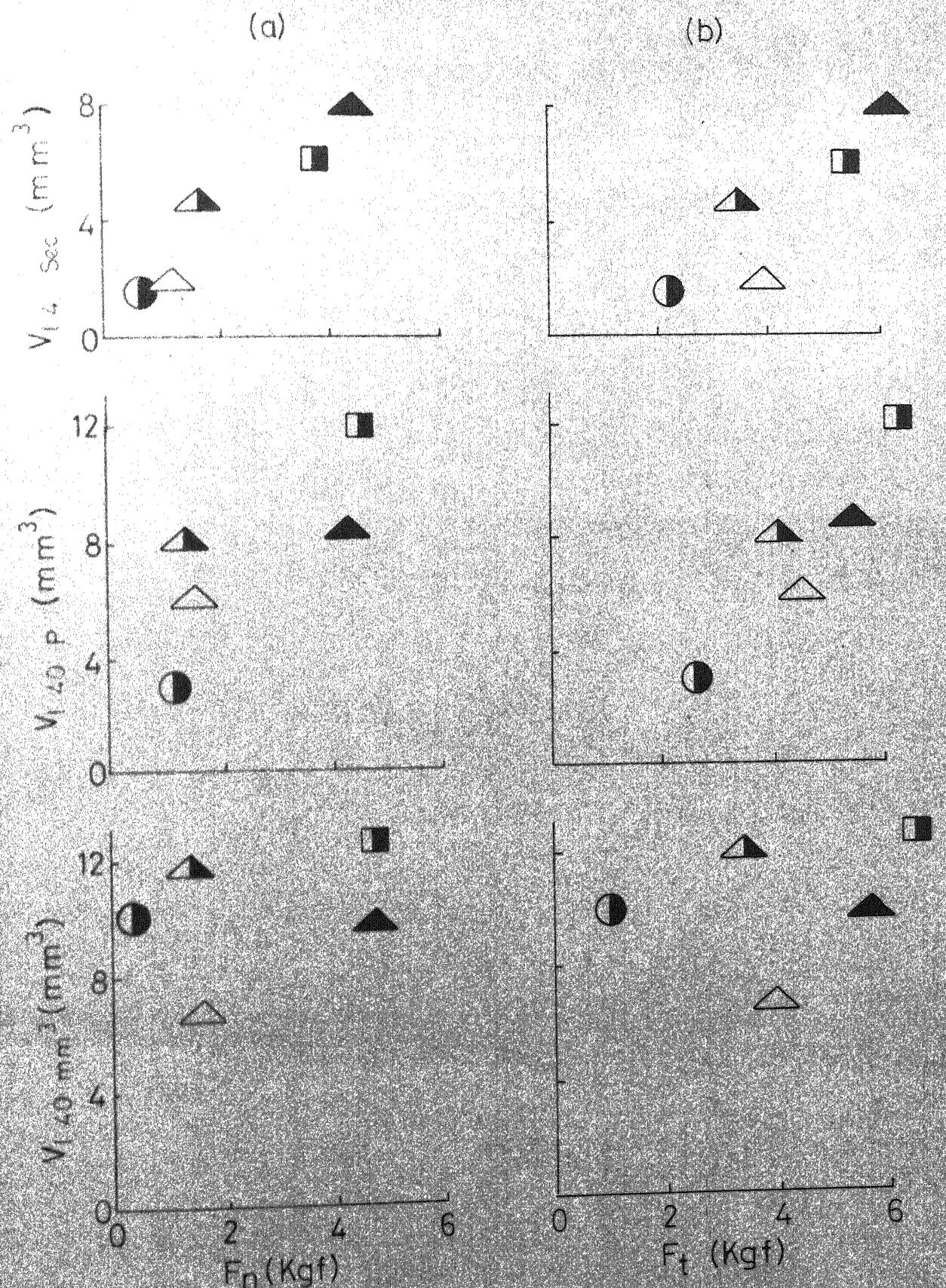
Fig. 4·30 Variation Of Loading Parameters
With (a) Normal Force (b) Tangential
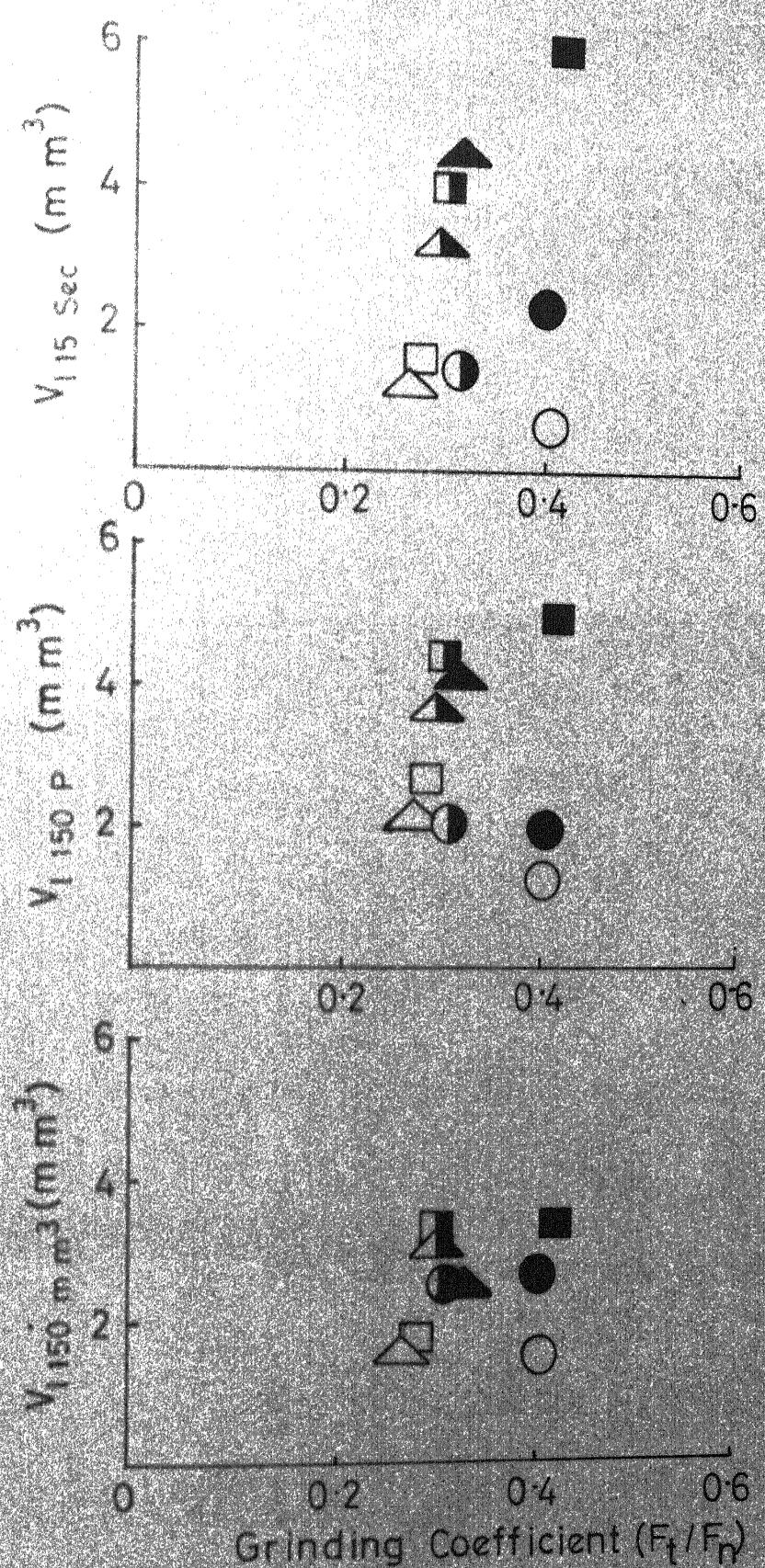Force For Aluminium (39 C 60 L 5
VK Wheel)

Fig. 4·31 Variation Of Loading Parameters With Grinding Coefficient For Brass (39 C 60 L5 VK Wheel)

Fig 4·32 Variation Of Loading Parameters
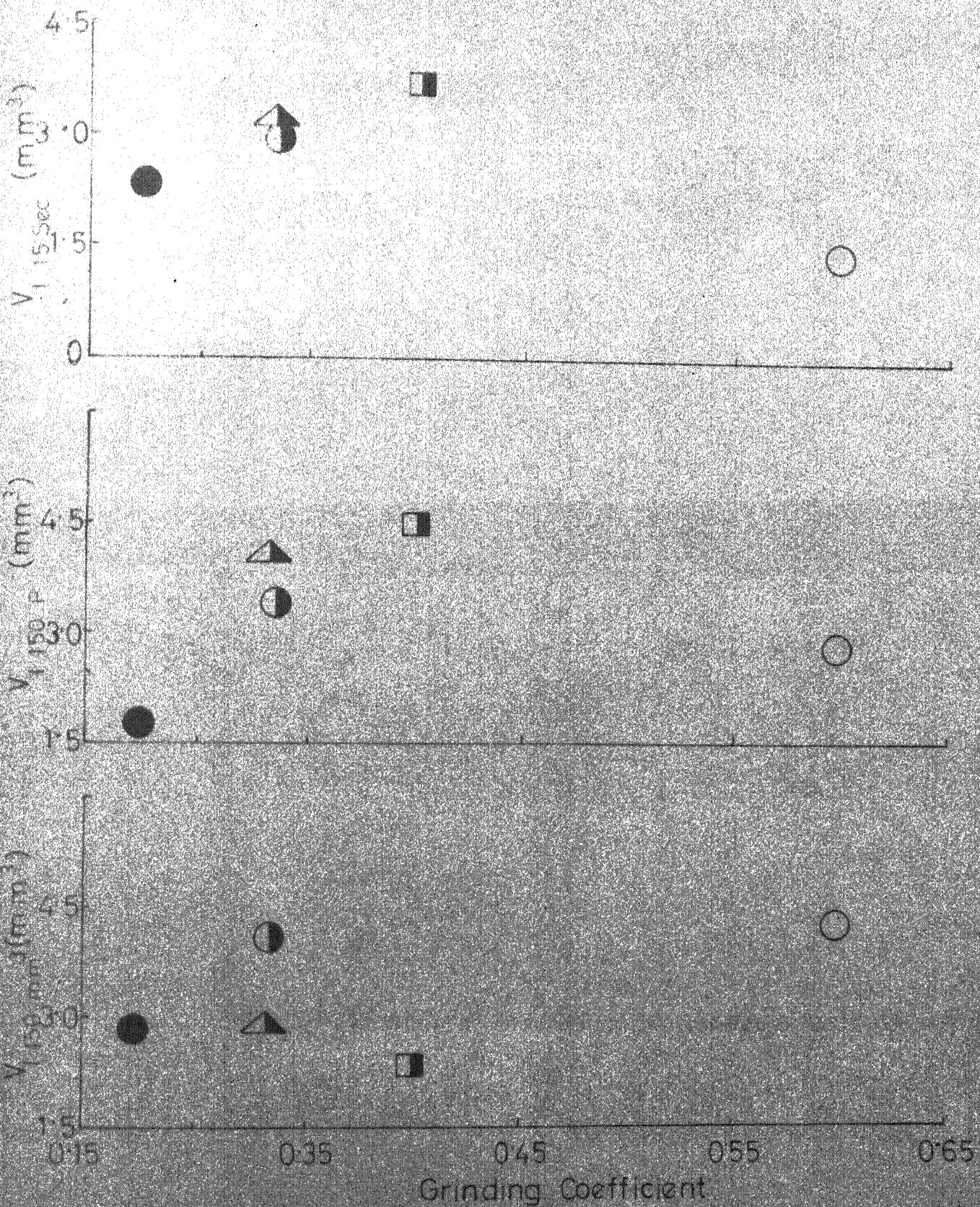With Grinding Coefficient For
Brass (38 A 60 K 5 V B E Wheel)

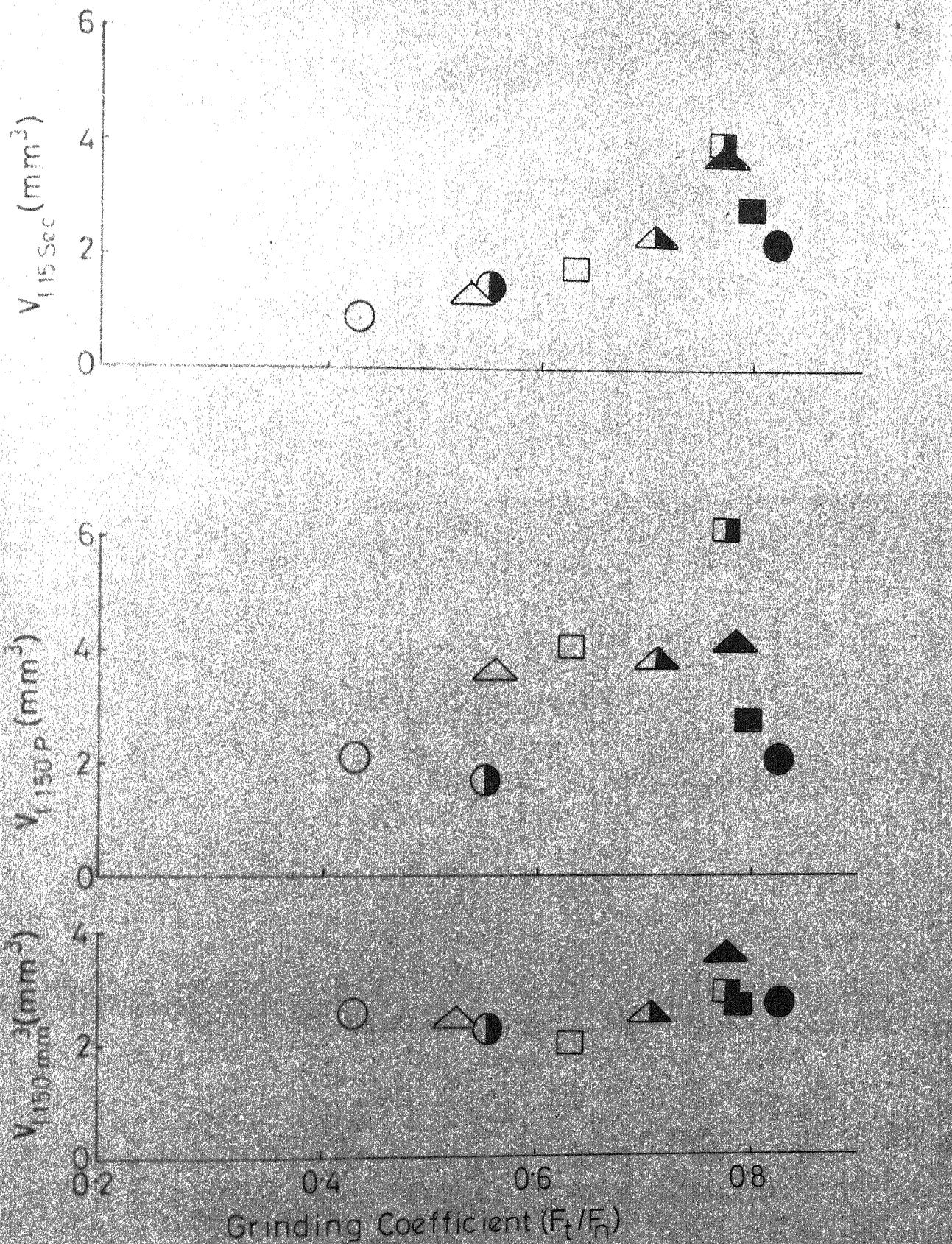Fig. 4·33 Variation Of Loading Parameters With Grinding Coefficient For Mild Steel (38 A 60 K 5 Wheel)
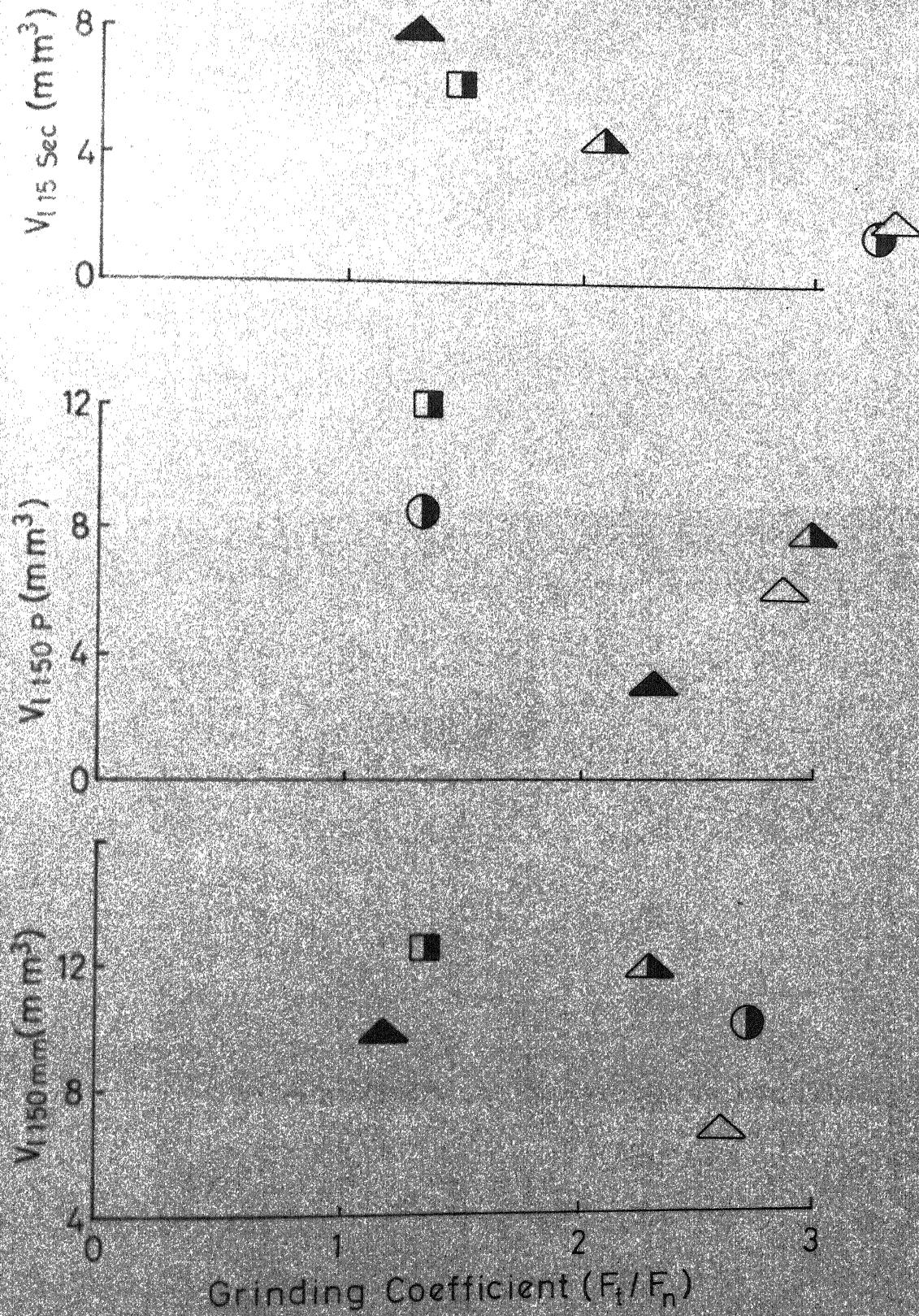
Fig.4·34 Variation Of Loading Parameters With Grinding Coefficient For Aluminium (39 C 60 L 5 VK Wheel)
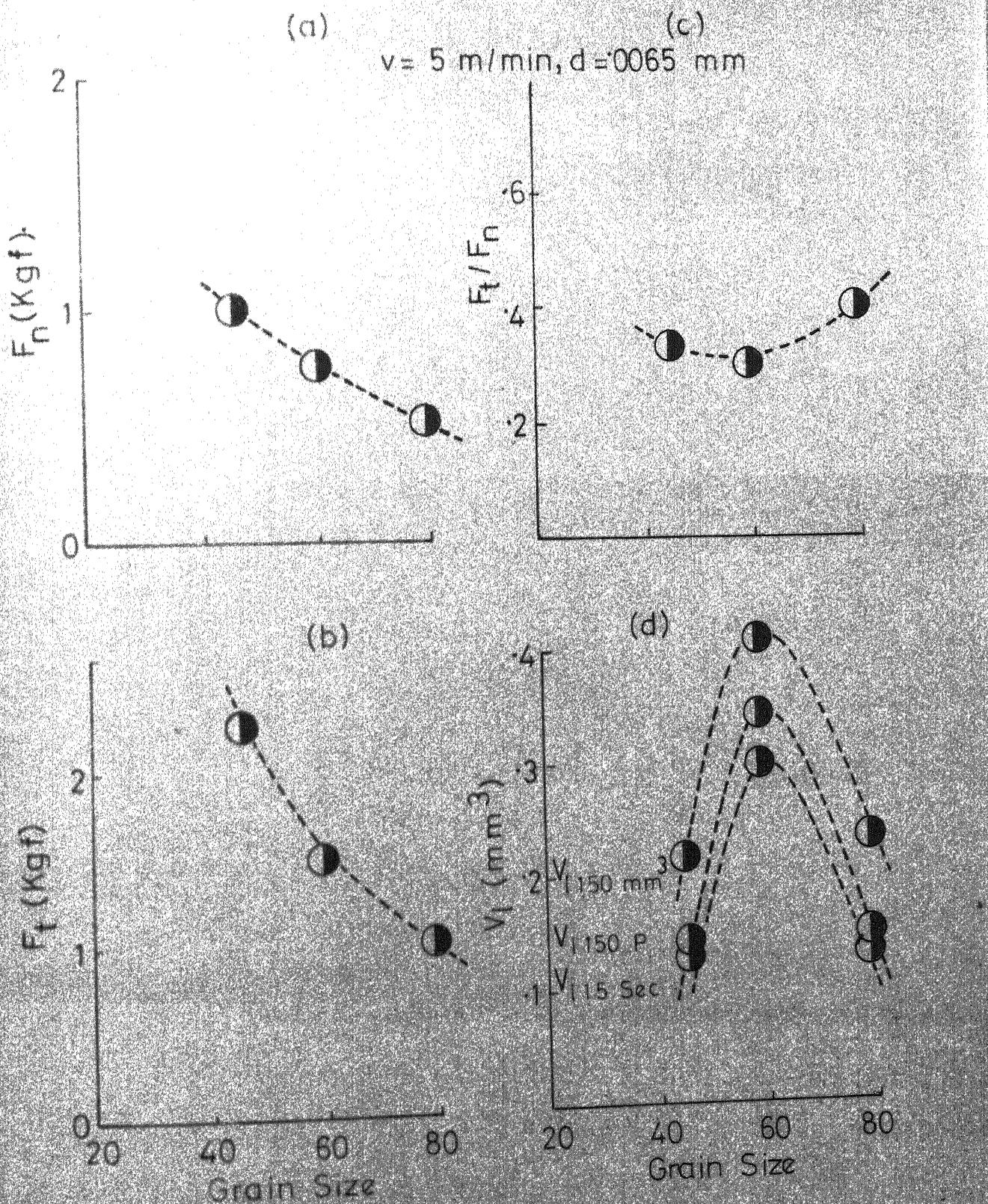
Fig. 435 Effects Of Grain Size On (a) F_t, (b) F_n, (c) Grinding Coeff· (d) Loading Parameters For Brass (38 A Wheel)
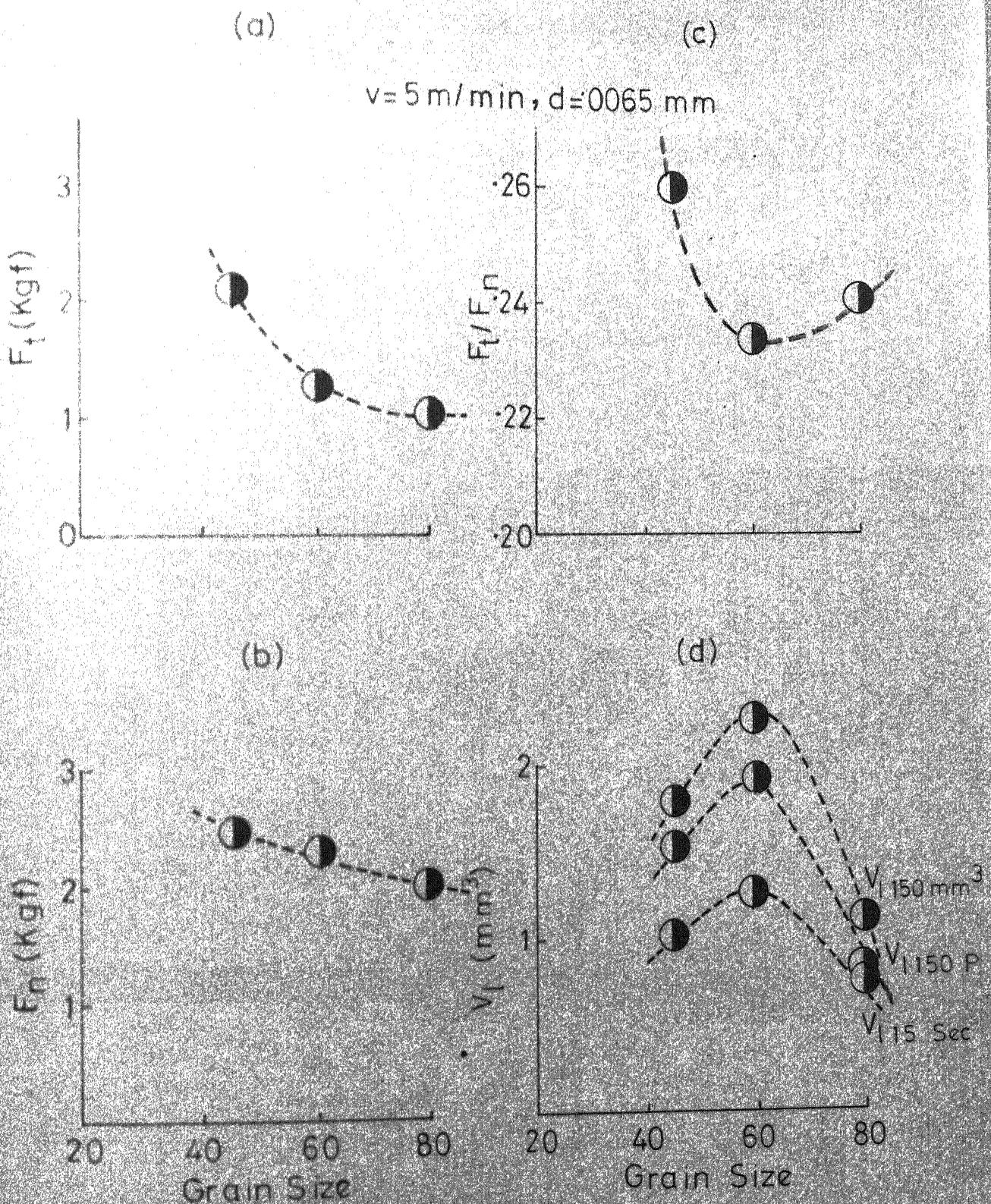
Fig 4·36 Effect Of Grain Size On (c) Grinding Coeff. (d) Loading Parameters For Mild Steel (38 A Wheel)

(a)

V_I (m m²)

38 A 60 K 5 V B E
v = 5 m / min
d = 0065 mm

(b)

V_I (mm³)

Forces (Kgf)

V_r (mm³)
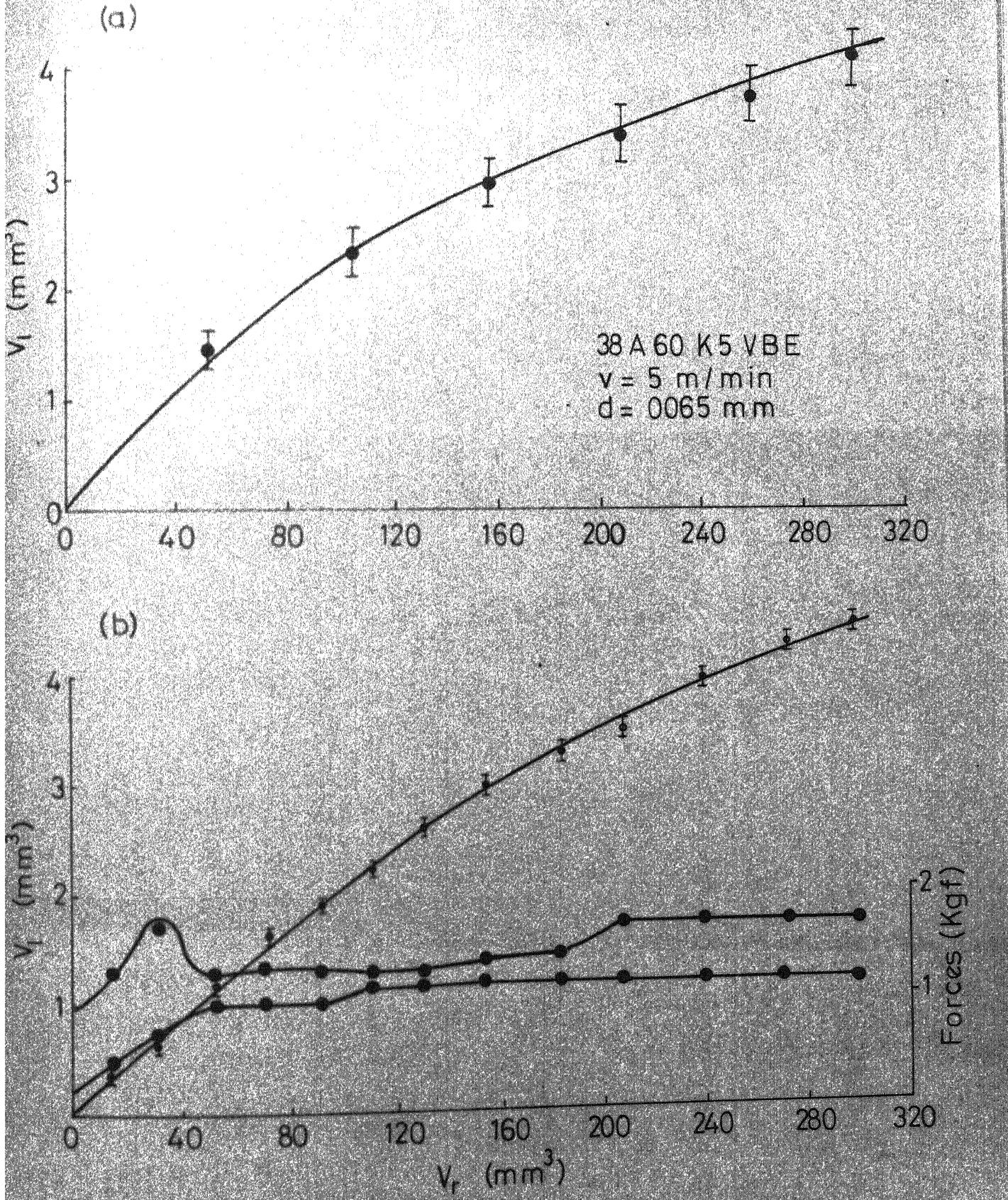
Fig. 4·37   Comparison Of Loading Curves For
(a) Van de Graaf, (b) BARC Irradiated
Mild Steel Samples
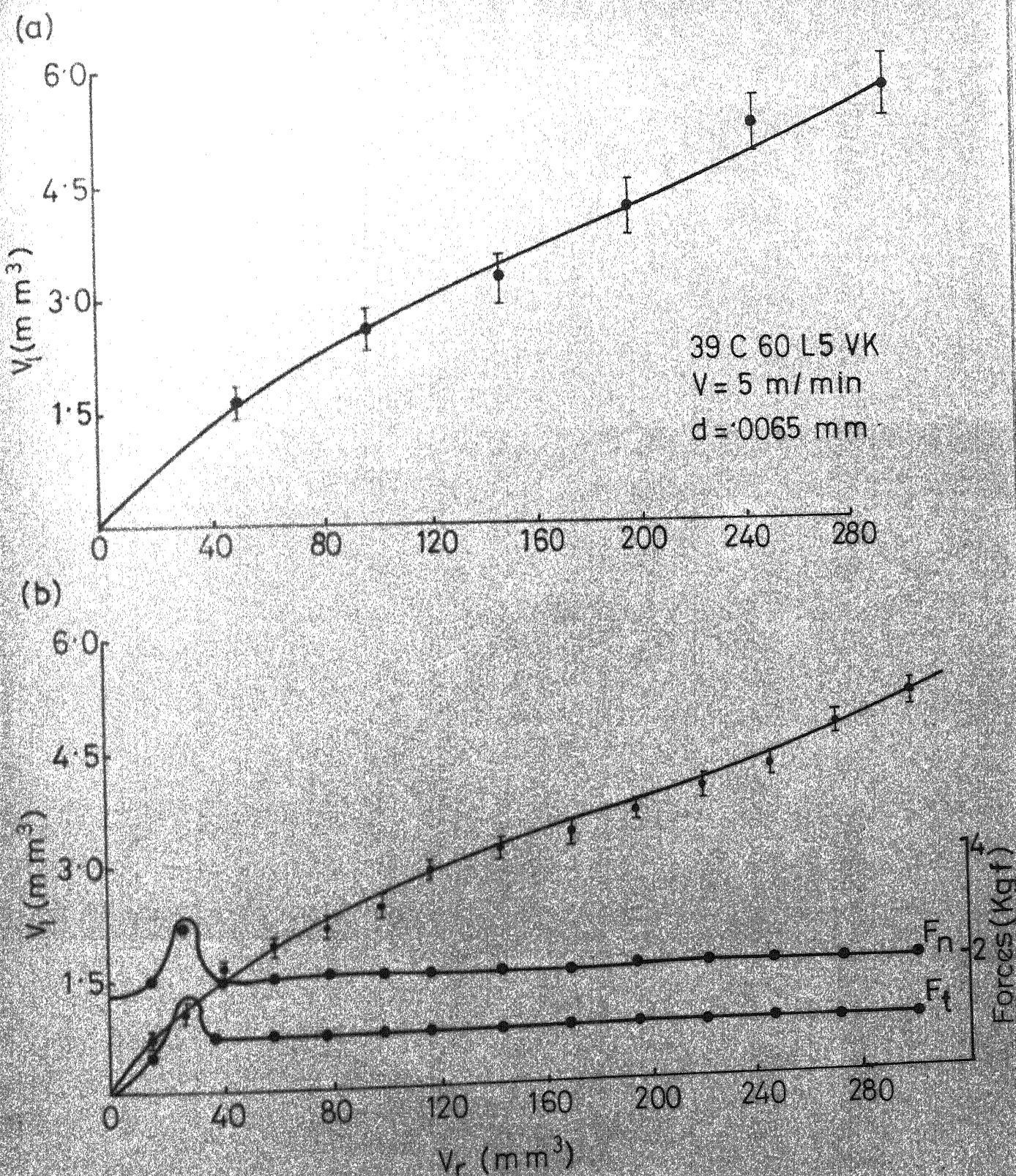
Fig. 4·38 Comparison Of Loading Curves For (a) Van De Graaf (b) BARC Irradiated Brass Samples

(a)

V_l (m m^3)

40

20

20 40 60 80 100 120 140

38 A 60 K 5 V B E
V = 4 m/min
d = 0065 m m

(b)

V_l (m m^3)

40

20

0

20 40 60 80 100 120 140

V_r (m m^3)

Forces (Kgf)

F_n

F_t
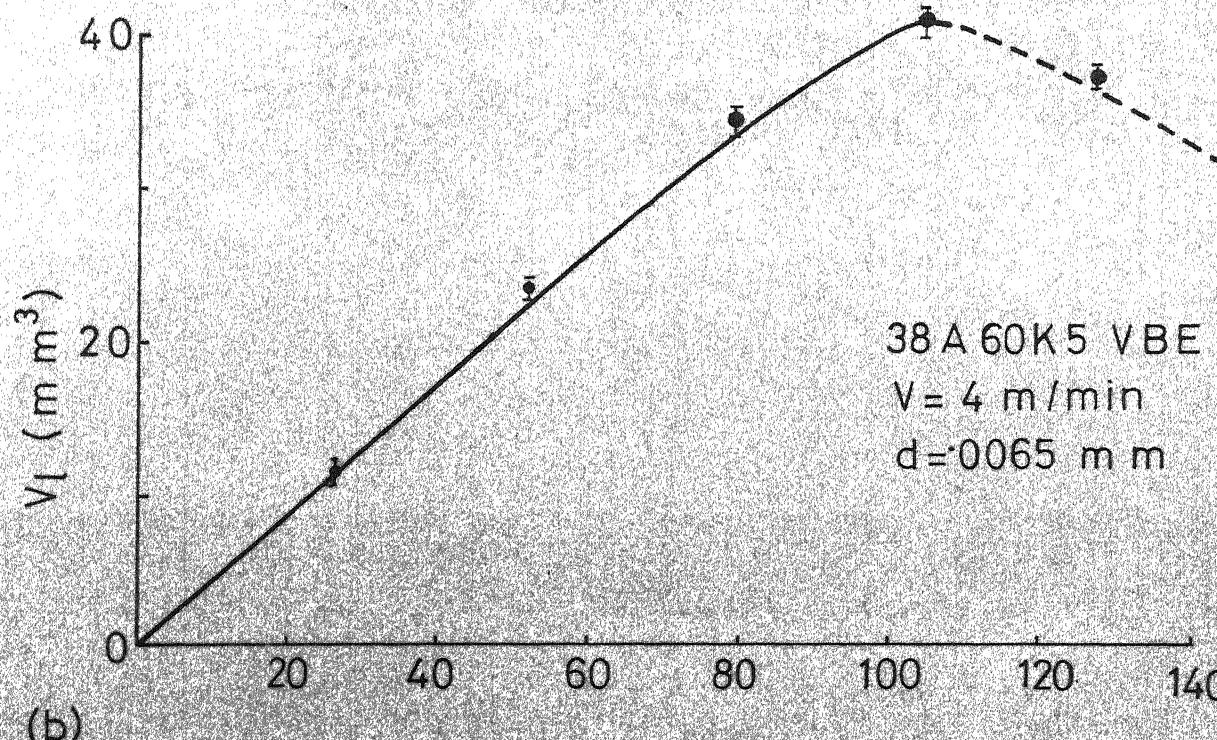
Fig. 4.39   Comparison Of Loading Curves (a)
Van de Graaf (b) BARC Irradiated
Aluminium Samples
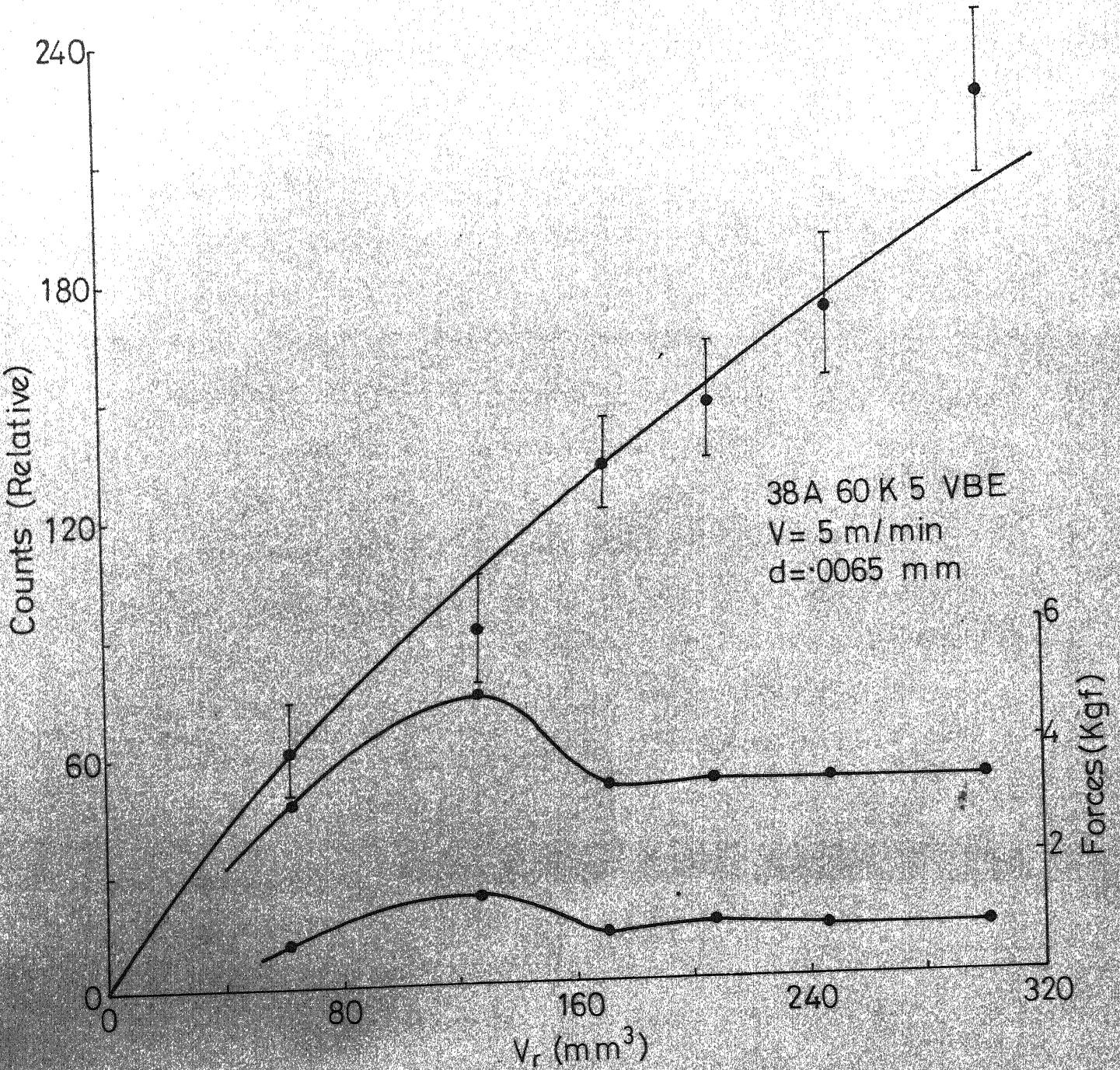
Fig. 4·40 Loading Curve For Van de Graaf Irradiated Hardened HSS Sample

CHAPTER V

CONCLUSIONS AND SCOPE FOR FURTHER WORK

5.1 Conclusions:

Using radiotracer techniques, wheel loading studies have been carried out under dry, plunge-cut grinding conditions for steel, brass and aluminium workpieces with both alumina and silicon carbide wheels.
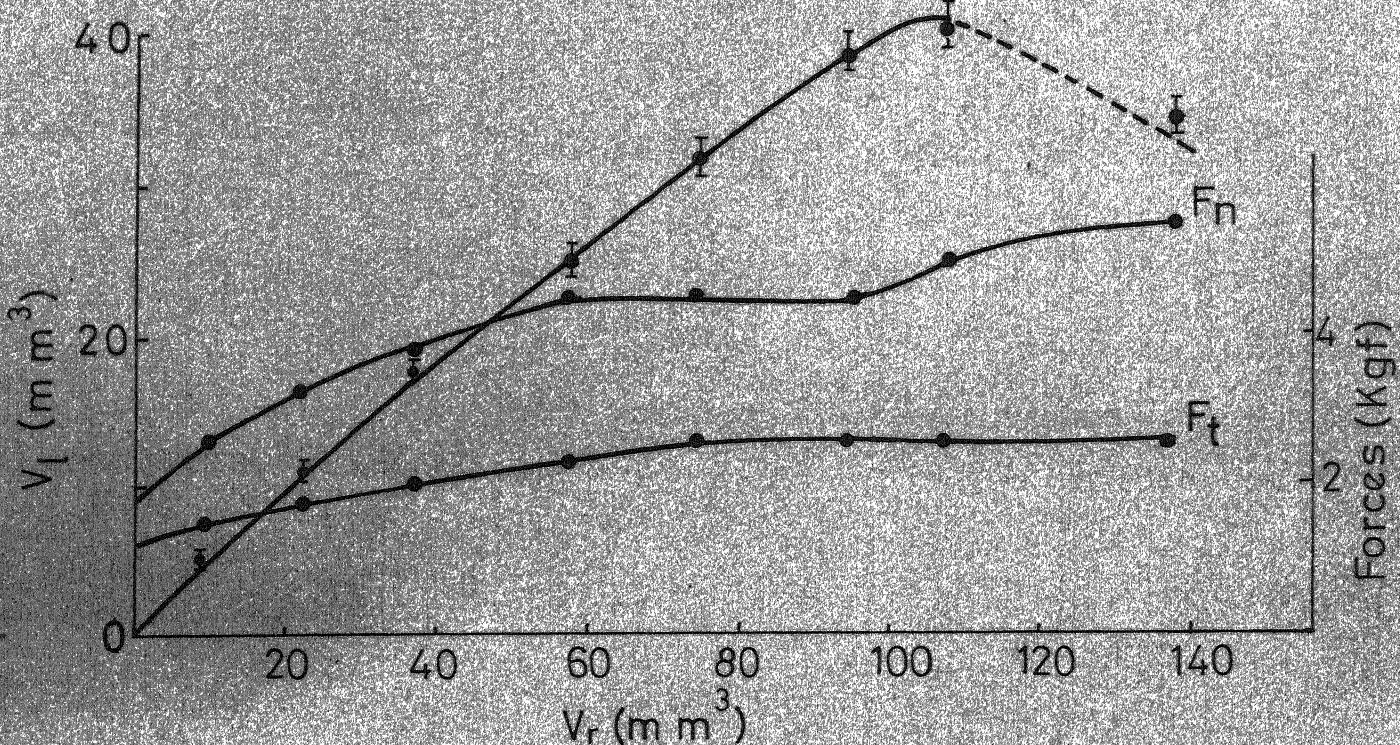
For most of the experiments, thermal neutron irradiated work specimens were used. However, a few experiments were conducted with 14 MeV neutron irradiated workpieces of hardened HSS, mild steel, brass and aluminium to establish that, for each of these materials, alternative radiotracer generation methods can be applied for loading studies. Absolute results were deduced in all experiments by the extrapolation method [9].

For the steel and brass workpieces, it was observed that the amount of loaded material increases rapidly at first and then at a slower, but steady, rate. In the case of aluminium, on the other hand, there was rapid increase of the loaded volume to a very much higher value and an approach to 'saturation' at relatively low volume removal

($\sim$ 100 mm^3). The formation of burrs on the sides of the workpiece did cause higher (5 - 10 %) loading results to be obtained, but the basic nature of the loading curves remained unaffected for the various work/wheel combinations investigated.

In studying the variation of wheel loading with grinding conditions, three different types of criteria were considered at points well removed from the initial transient loading region. These corresponded to a fixed volume removed, a fixed number of passes and a constant grinding time. By considering the scatter in the plots of the three types of loading parameters against various grinding variables, it was observed that the constant grinding time criterion yields the most consistent results.

For the range of table speed (v) and down feed (d) values considered, wheel loading was ~~generally~~ found to increase ~~consistently~~ with both variables for all the work/wheel combinations studied. The sensitivity was higher for aluminium than for brass or mild steel.

The variation of wheel loading with combinations of v and d, viz. material removal rate (α v.d) and chip thickness (α v$^{1/2}$ d$^{1/4}$), was also considered. A smoother variation was indicated with chip thickness. If this is so - and more comprehensive data is required to establish the

result - one should be able to achieve a higher material removal rate, for a given degree of loading, by selecting a lower v and a higher d. It is such considerations, of course, that make the empirical study of wheel loading phenomena meaningful.

Simultaneous measurements of normal (F_n) and tangential (F_t) force components during the present experiments indicated that the factors which cause higher grinding forces also induce greater loading. Results for the variation of loading with grinding coefficient (F_t/F_n) were inconclusive, except in the case of aluminium for which it was observed that higher loading values correspond to lower grinding coefficient.

Experiments with three different grain sizes of alumina wheel (viz. 46, 60 and 80) were conducted for both brass and mild steel. Both F_n and F_t were observed to decrease with grain size, with grinding coefficient indicating a slight dip at 60 grain size. This somewhat contradicts the results reported by Pandey, et al. [15]. The wheel loading was found to be maximum for 60 grain size, in the case of both work materials.

Comparisons of loading curves, obtained with thermal and 14 MeV neutron activated workpieces, confirmed the absence of any systematic errors in the use of alternative

radiotracers for loading studies with steels, brass and aluminium.

5.2 Scope for Further Work:

Wheel loading characteristics have been presently studied for different work/wheel combinations. The interpretation of data, such as that presently obtained, would be more fruitful if other variables, such as chatter **vibration**, surface finish and wheel wear, could be related to wheel loading through simultaneous measurements.

The present experiments were all conducted under dry grinding conditions. The effect of cutting fluids on loading should be studied using the presently applied techhiques.

Another factor which may be expected to have significant effect on wheel loading is the dressing sequence. The effects of dressing depth of cut and cross feed should be separately investigated.

As grinding is now widely employed for stock removal from blanks, it would be useful to conduct loading studies for materials such as cast iron, cast steel, forged steel, etc. This follows from the basic requirement that the material removal rate should be maximum for a given degree of wheel loading, so that the unproductive time spent in truing and dressing is minimal.

REFERENCES

1. Pacitti, V. and Rubenstein C., 'The Influence of the
    Dressing Depth-of-cut-on the Performance of a Single-
    point-diamond-dressed Alumina Grinding Wheel',
    Int. J. Mach. Tool Des. Res.,Vol. 12 (1972) p. 267.

2. Reichenbach, G.S. et al. 'The Role of Chip-thickness
    in Grinding', Trans. ASME (May 1956) p. 847.

3. Shudolz, L.H., et al. 'A Method of Measuring Metallic
    Wheel Loading Characteristics', Mechanical Engg., Vol. 72
    (1950) p. 963.

4. Khudobin, V.V., 'Cutting Fluid and its Effects on
    Grinding Wheel Clogging', Machines and Tooling,
    Vol. XL, No. IX (1969), p. 54.

5. Pandey, P.C. et al., 'Clogging of Grinding Wheels',
    Proc. 5th AIMTDR Conf., Roorkee (1972), p. 31.

6. Sata, T. et al, 'In-Process Measurement of the Grinding
    Process and its Applications', New Developments in
    Grinding, Carnegie Press (1972), p. 752.

7. Suto, T. et al, 'Behaviors of Loading on a Grinding
    Wheel', Bull. Japan Soc. Prec. Engg., Vol. 9, No. 3
    (1975), p. 89.

8. Yamamoto, A., and Maeda, V., 'Magnetic Methods for
    In-Process Measurement of Abrasive Tools', Bull. Japan
    Soc. Prec. Engg., Vol. 8, No. 3 (1974).

9. Gohad, A.G., 'Radiotracer Techniques for Studies of
    the Loading Phenomenon in Grinding', M.Tech. Thesis,
    IIT Kanpur, 1976.

10. Gohad, A.G., Private Communication.

11. Stehn, J.R., et.al., 'Neutron Cross Sections', BNL-325,
    Second Edition, 1965.

12. Lederer, C.M., et al., 'Tables of Isotopes', Sixth Edition, John Wiley and Sons, 1967.

13. Krishnamony, S., and Raghunath, V.M., 'Handbook of ~~Nuclear~~ Physics Data', Report No. BARC/I-55, 1969.
    Health

14. Bygrove, W., Treado, P., and Lambert, J., 'Accelerator Nuclear Physics', High Voltage Engg. Corporation, USA, 1970.

15. Kumar, A. and Pandey, P.C., 'Effects of Wheel Clogging on Grinding Parameters', Proc. 7th AIMTDR Conf., Coimbatore (1976), p. 293.